12-2015

EFFECTS OF GROWTH FACTOR SUPPLEMENTATION AND ENVIRONMENTAL CONDITIONS ON HUMAN ADIPOSE-DERIVED STEM CELL DIFFERENTIATION TOWARDS UROTHELIAL LINEAGE

James Turner
Clemson University, jpturne@g.clemson.edu

EFFECTS OF GROWTH FACTOR SUPPLEMENTATION AND ENVIRONMENTAL CONDITIONS ON HUMAN ADIPOSE-DERIVED STEM CELL DIFFERENTIATION TOWARDS UROTHELIAL LINEAGE

A Dissertation
Presented to
the Graduate School of
Clemson University

In Partial Fulfillment
of the Requirements for the Degree
Doctor of Philosophy
Bioengineering

---

by
James Pierpont Turner
December 2015

Accepted by:
Dr. Jiro Nagatomi, Committee Chair
Dr. Ken Webb
Dr. Richard Visconti
Dr. Todd Purves

ABSTRACT

In recent years, tissue engineering of the bladder has undergone many technological advances. Autologous urothelial cells have been used in animal models and have shown increased performance for ureteral reconstruction compared to unseeded grafts. However, since patients may lack a reliable source of native urothelial cells due to the nature of their specific bladder disease, autologous cells are not an ideal source clinically, and an alternate cell source must be explored. Adipose derived stem cells (ADSCs) are an attractive cell source for such regenerative medicine applications as they have been extensively studied for their multipotential differentiation, immunosuppressive properties, ease of harvest, and relative abundance. The present doctoral thesis investigates the effect of growth factors present in defined keratinocyte serum-free medium (KSFM), all-trans retinoic acid (ATRA), and environmental conditions on ADSCs to explore their efficacy as a potential donor source for urothelial tissue regeneration.

Using serum-free conditions, hADSCs were exposed to defined KSFM and ATRA over a 21-day culture period, and effects on morphology and phenotype marker expression were examined. The results indicated that hADSCs differentiated towards urothelial-like cell lineage without co-culturing or serum-containing medium after 14 days of culture in defined KSFM, while the effect of ATRA supplementation was limited to morphology changes and not on expression of markers tested. Furthermore, a fibronectin/gelatin layer-by-layer coating technique was used to develop a multilayer

tissue construct with both undifferentiated and differentiated hADSCs (cultured using defined KSFM) and UROtsa cells to investigate cell morphology, protein expression, and dextran permeability across the multilayer construct. In hADSCs, cell aggregation occurred in differentiated and coated samples over 24 hours of culture in Transwell® inserts. Fibronectin/gelatin coating technique applied to both UROtsa cells and growth membrane resulted in a multilayer with expression of CK-17, CK-20, UPIb, and ZO-1 urothelial protein markers and less aggregation compared to hADSC. Dextran permeability results after 24 hours indicated diffusion of 4 and 70 kDa dextran across cell constructs with no differences between cell types. Lastly, a tension bioreactor system capable of applying constant tension on cell-seeded tissue engineering constructs was calibrated. Mechanical conditioning may play a role in development of functional tissue in vitro to increase overall strength and compliance of tissue engineered constructs. In the present study, the bioreactor was tested with three materials (parafilm, PCUU, and T1107 hybrid hydrogel) to demonstrate its capability to apply desired loading parameters based on user settings and to record force/distance vs. time profiles.

In summary, the results provide novel evidence that, through a combination of physical and chemical factors, hADSCs differentiate towards urothelial-like lineage under defined KSFM culture after 14 days. Fibronectin/gelatin cell and Transwell® membrane coating promotes *in vitro* formation of urothelial-like multilayer constructs using UROtsa cells. A tension bioreactor system has been calibrated to apply controlled mechanical force stimuli on soft biomaterials intended to reproduce the *in vivo* bladder filling for functional tissue engineering. The knowledge gained from the present study

will serve as foundation for future studies focusing on multilineage and functional bladder tissue engineering using adipose-derived stem cells for the treatment of bladder disorders.

DEDICATION

I would like to dedicate this dissertation to my parents who has given me never-ending support to help me through my endeavors. Also, I would like to dedicate this to my wife, Evaline. For your patience, love, and the smile that uplifted me through the most difficult times.

ACKNOWLEDGMENTS

I would like to extend my sincerest appreciation to my advisor, Dr. Jiro Nagatomi, for his support, guidance, and patience during my graduate career at Clemson. With your assistance, my expertise and knowledge of tissue engineering grew from almost nil to something of which I am very proud. I would also like to thank my committee members, Dr. Ken Webb, Dr. Richard Visconti, and Dr. Todd Purves, who provided valuable insights during the foundation of this project.

My fellow lab members have provided me with an incredible amount of support – both with respect to research and companionship. I would like to extend my deepest gratitude to Dr. Lindsey Sanders, Dr. Brittany Lindburg, Dr. Kevin Champaigne, and Dr. Srikanth Sivaraman. For their direct contributions to my research, I would like to extend a special thanks to my undergraduate students for their hard work and dedication – Julianne Jett, Sayaka Reed, and Tyler Matt. Additional thanks goes out to Maria Torres, Cassie Gregory, and Chad McMahan for troubleshooting me through every unexpected twist and turn in research.

And finally, to my bioengineering colleagues who have provided me with tremendous and never-ending support over the years, I am forever grateful.

TABLE OF CONTENTS

Page

Table of Contents (Continued)

Page

LIST OF TABLES

LIST OF FIGURES

List of Figures (Continued)

List of Figures (Continued)

Figure Page

CHAPTER ONE

INTRODUCTION AND BACKGROUND

1.1. Clinical Relevance

Approximately 400 million people worldwide suffer from bladder diseases ranging from congenital abnormalities to bladder cancer, which can negatively affect the uroepithelium of the urinary system [1]. Additionally, bladder perforation during transurethral resection, ureteroscopic surgery, or extraction of urethral stents can cause damage to the uroepithelial lining. Current widely used clinical approaches in uroepithelial regeneration include grafting of gastrointestinal or buccal tissue for bladder augmentation or urethroplasty [1]. Inherently, functional gastrointestinal mucosa does not provide the proper barrier function typical of uroepithelium. Due to this mismatch in properties, post-surgical complications such as electrolyte imbalance, urolithiasis, tract infection, mucous secretion, and malignancy develop due to tissue incompatibility in the urinary system [2-4]. As such, there have been many attempts in tissue engineering, both using synthetically- and naturally-derived methods, to find alternatives to bladder repair while maintaining similar compliance to native bladder tissue. However, it is also critical to also understand and develop methodology for regeneration of a functional uroepithelium, which is key to the future success of urinary tissue engineering. The following sections below will discuss bladder anatomy and physiology, the importance of the uroepithelium, and current methods in tissue engineering to address dysfunctional bladder tissue.

1.2. Urinary Anatomy and Physiology

The urinary system is critical to the regulation of the body's metabolic processes, electrolyte levels, and removal of wastes through urination. A properly functioning urinary system relies on a coordinated signaling process that contracts and relaxes the bladder voluntarily during voiding and filling respectively. During filling processes, urine travels from the renal pelvis of the kidneys through the ureters after an extensive filtration process and empties into the urinary bladder. The established view in literature is that bladder stretch during filling causes stimulation of mechano-sensitive Aδ-fibers, which in turn signals the parasympathetic nervous system and indicates bladder fullness to the brain [5]. New perspectives on bladder sensation have indicated that the uroepithelium, also commonly referred to as urothelium, may have a role in bladder sensory function rather than being solely a passive tight epithelial barrier [6-12]. Presence of primary afferent neurons and efferent nerve fibers localized near the urothelium provide evidence of a urothelial-associated signaling network that regulates bladder function and sensory signaling [13]. Details on the physiology of each organ are outlined below.

1.2.1. Urinary Bladder

The bladder is a hollow muscular organ that lies within the pelvic cavity, and directly contacts the uterus and vagina in females and the rectum in males. The urinary bladder serves as a distensible reservoir for urine collection from a pair of kidneys connected by ureters.

The two main functions of the urinary bladder are to store urine that is generated in the kidney and to void when necessary. During the storage phase, electrolytes are exchanged in the urine due to passive and active ion transport occurring at the inner uroepithelial layer [14]. As the bladder fills, the organ expands and begins to push against other organs in the pelvic cavity. The uroepithelium structure is restructured as the bladder fills and changes from a transitional epithelial multilayer to a monolayer while apical umbrella cells change to a squamous morphology [13]. Although there is no exact consensus, the maximum bladder capacity is approximately 600 milliliters, while bladder fullness sensation can occur around 150 milliliters with discomfort at 300 milliliters. At this point, signals from sacral preganglionic neurons cause a rise in intravesical pressure, the external urethral sphincter to release, and contractions in the bladder wall in synchrony to allow for voiding [13].

1.2.2. Ureters

The ureters are on average 25 cm long in adults and extend from the renal pelvis of the kidneys and empty into the urinary bladder. The ureters join the urinary bladder through the posterior wall by curving towards the center and entering at a slight angle. Underneath the inner lining of uroepithelium and lamina propria layers, smooth muscle fibers fill the intermediate muscularis layer and contribute to the peristaltic function. The outer adventitia layer contains blood and lymphatic vessels, nerves, and the connective tissue that keeps the ureters from dislocating.

The urine is transported through the ureters through a combination of several effects including peristaltic contractions of the muscle layer, hydrostatic pressure, and

natural flow by gravity. As the urinary bladder fills, the expansion of the bladder wall closes the oblique openings of the ureters and prevents backflow of urine. The speed of the peristaltic waves beginning at the renal pelvis corresponds to the rate of urine formation within the kidneys. An increase in wave frequency corresponds to an increase in renal function and urine production.

1.2.3 Urethra

The primary function of the urethra, the terminal drainage outlet for the urinary system, is to allow urine to be passed out of the urinary bladder. The urethra differs considerably between genders. In females, the urethra extends only about 4 cm and exits between the clitoris and vaginal opening. The urethra contains a mucosal layer consisting of the lamina propria and an epithelial layer that differs along the urethral lining. The uroepithelium continues from the urinary bladder and covers the proximal portion of the urethra. Further along the urethra towards the outlet, the epithelium varies from stratified columnar or pseudostratified columnar to stratified squamous epithelium. The muscularis continues from the bladder and consists of circularly arranged smooth muscle fibers [19].

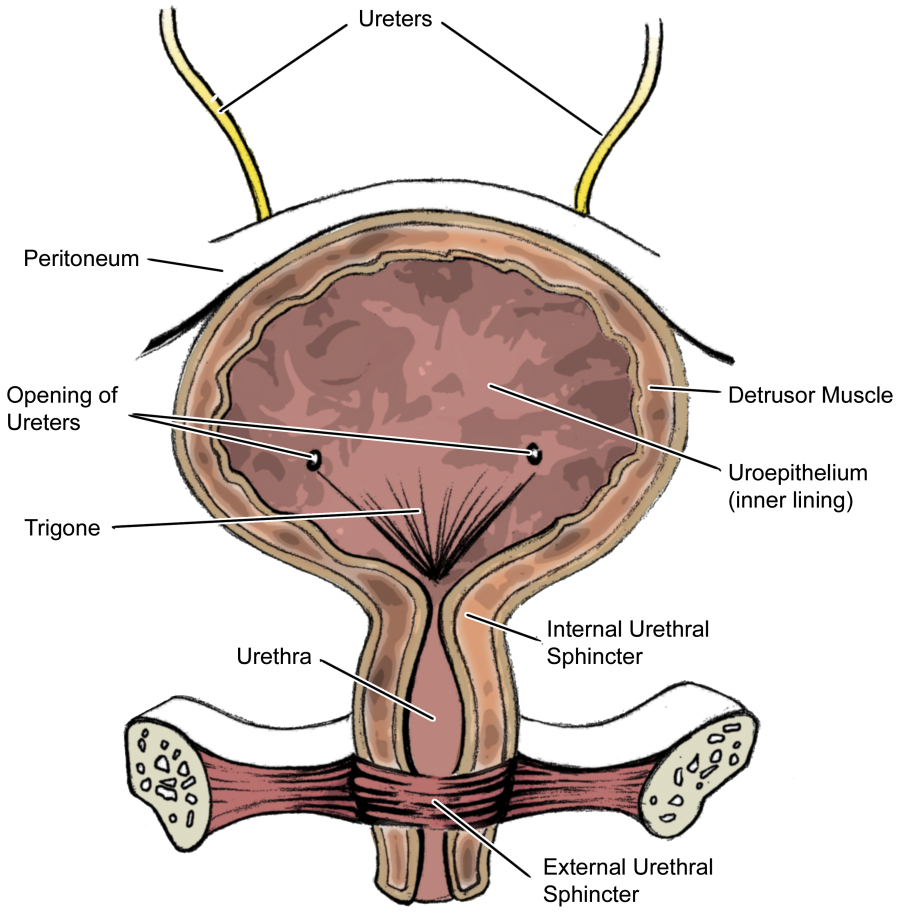

Figure 1.1: A cross section of the urinary bladder. Urine is deposited into the bladder from the ureters in small openings in the rear. As the bladder fills, the ureters are sealed due to the expansion of the bladder wall preventing any backflow. The external urethral sphincter is a voluntary muscle that allows control of urine voiding.

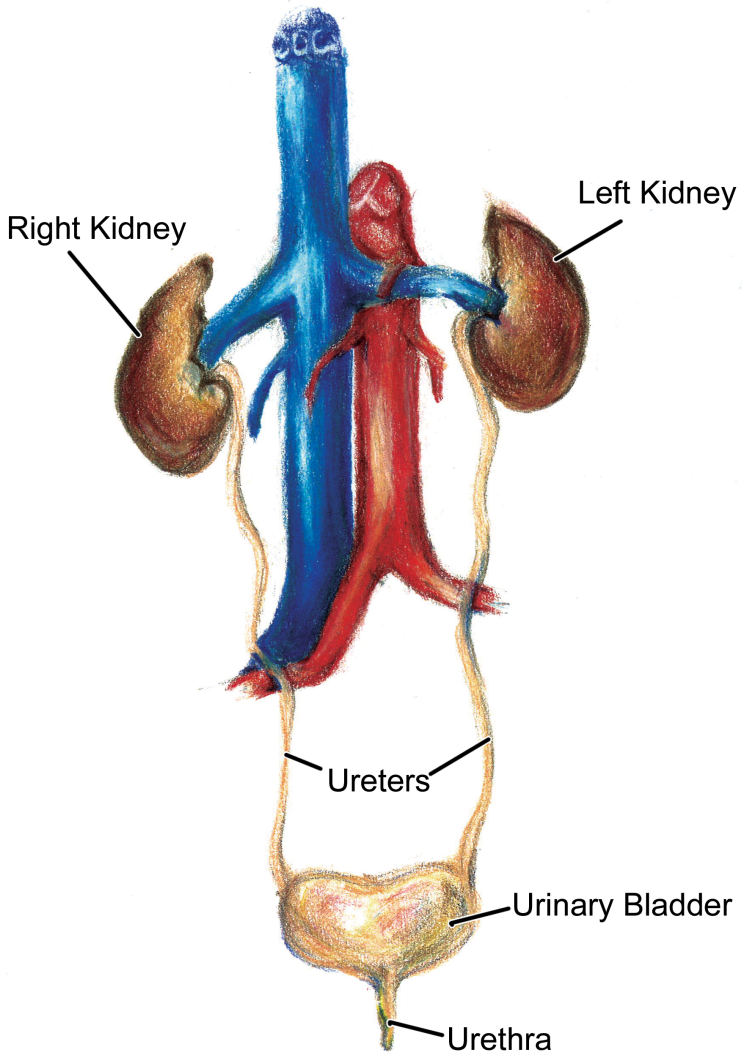

Figure 1.2: An overview of the urinary system. Urine is produced in the kidneys and passed through the renal pelvis into the ureters. The urine is stored in the urinary bladder for a period of time before passing through the urethra. The length of the urethra varies based on gender.

In males, not only urine, but also semen is also discharged through the urethra. The male urethra is approximately 20 cm long and follows a different path from the female urethra. The male urethra is divided into three regions. The prostatic urethra is the portion of the urethra that passes through the prostate. A milky secretion from the prostate (consisting of citric acid, proteolytic enzymes, acid phosphatase, and seminalplasmin as an antibiotic) is carried into the urethra through ducts in this region. Additionally, the vas deferens and seminal glands open into the prostatic urethra. The next and shortest portion, known as the intermediate urethra passes through the deep muscle of the perineum. Around this portion, skeletal muscle fibers are aligned in a circular fashion and form the external urethral sphincter muscle. The longest portion of the male urethra passes through the penis and is known as the spongy urethra. Similar to the changes in the female urethral mucosa, the uroepithelial layer continues from the urinary bladder and changes to stratified columnar epithelium in the intermediate urethra and most of the spongy urethra.

1.2.4. Urinary Tissue Physiology

The bladder wall tissue consists of three main layers. Starting from the interior, the layers consist of the uroepithelium, the lamina propria, and the detrusor. The latter two will be briefly discussed, followed by an in-depth review of the uroepithelium.

Lamina Propria

The lamina propria is separated from the uroepithelium by the basal lamina, and acts as barrier between the epithelium and smooth muscle layer of the bladder. It is mainly composed of connective tissue made up of collagen, laminin, and elastin. Within

the lamina propria, one can find sensory and motor neurons along with lymphatic and blood vessels. The presence of unmyelinated nerves in the tissue indicate that damage to the lamina propria could potentially lead to disruption in normal electrical response due to mechanical strain in the bladder [15] The classical view is that the nerves present in the lamina propria respond to stretch in the bladder [16, 17], while recent studies have demonstrated that the signaling molecules produced in the uroepithelial layer could also interact with these nerves. When the bladder fills, tension is transferred between the lamina propria and the detrusor layers at different ranges of capacity during bladder filling [18]. Though the structural mechanisms on how this occurs are not well-defined, it appears that this transfer is what gives the bladder its unique compliant properties.

Detrusor

Smooth muscle bundles form an interlaced weave spreading in all directions of the detrusor layer. Collagen (Type I and III), laminin, osteopontin, and hyaluronic acid is present and integrated with the smooth muscle fibers [19]. Fibronectin and collagen types I, III, and IV are produced by the bladder smooth muscle cells [20]. The detrusor muscle also extends towards the urethra forming an internal urethral sphincter allowing for retention of urine until voiding. Lack of collagen type I in this region has been shown to increased stress urinary incontinence in females [21].

Uroepithelium

The uroepithelium, or urothelium, is a highly specialized transitional epithelial tissue with three distinct layers of cells identified as the basal, intermediate, and umbrella cells. The umbrella cell layer allows for active sodium ion transport and a barrier

minimizing passive transport of molecules at the interface between the urine and underlying smooth muscle tissue layers, while the basal and intermediate layer provides progenitor cells for the umbrella layer. The urothelium covers the inner lumen of the bladder, the ureters, upper urethra, and the renal pelvis. The presence of tight junctions and specialized apical membrane lipids contribute to the umbrella cells' ability to prohibit free movement of ions and solutes from the urine to the underlying tissue layers [14]. The apical membrane of the umbrella cells consists of plaque regions in between hinges. The plaque regions appear to be asymmetric, due to the outer leaflet being thicker than the inner leaflet. This asymmetry arises because of a highly crystalline structure formed by asymmetric unit membrane (AUM) particles composed mainly of uroplakins (UP) including UPIa, UPIb, UPII, UPIIIa, and UPIIIb. A glycosaminoglycan (GAGs) based barrier composed primarily of chondroitin and heparan sulfate also contribute to the protection of the tissue from the toxicity of the urine [19].

What causes the sensation of fullness in the bladder? The mechanisms controlling and signaling the afferent nerves in the bladder are still not fully resolved. Recent studies have shown evidence that the uroepithelium releases diffusible molecules such as adenosine triphosphate (ATP), acetylcholine (ACh), nitric oxide (NO), and prostaglandins which may interact with receptors in the afferent axons. For example, ATP molecules released from urothelium in response to bladder fullness act on P2X3 receptors located in the suburothelial afferent nerve plexus [22]. It is suspected that epithelial sodium channels (ENaC) are responsible for detection of the mechanical stimuli in the uroepithelium as blocking these channels with amiloride suppresses ATP

release [10, 23]. The afferent signals are carried through myelinated Ad-fibers found in the lamina propria to the neuronal somata located in the dorsal root ganglia at S2–S4 and T11–L2 spinal segmental levels.

Urination, or micturition, involves afferent signaling pathways that derive from the same region of the spinal cord as bladder sensation. The excitation of the efferent pathways for bladder wall contractions begin from the intermediolateral column of the S_2–S_4 spinal cord via ATP/ACh release. Nerves that terminate at the base of the bladder and urethra contain enzymes called nitric oxide synthase. Nitric oxide synthase enzymes create NO in order to relax the urethral muscle. Motoneurons from Onuf's nucleus of the anterior horn in the S_2–S_4 spinal cord terminate at the striated sphincter muscle and release ACh to act on nicotinic receptors and relax the muscle [22]. This gives voluntary control to hold back urine in cases when urination is unwanted.

1.3 Hydrogel Applications in Urologic Tissue

1.3.1. Kidney

The high demand for donor kidneys severely limits transplantation as an option for patients suffering from acute kidney injury (AKI), previously known as acute renal failure [24]. For this reason, stem cell therapy has been explored in recent years to provide an alternative solution to AKI [25, 26] although the debate remains on which cells are actually capable of restoring kidney function. In a study using rat models of AKI, hydrogels were shown to assist in stem cell seeding and viability. More specifically, a thermosensitive chitosan chloride hydrogel was used to deliver adipose-derived stem cells (ADSCs) to an ischemia-induced kidney [27]. When compared to cells injected with

PBS, significantly less apoptosis and increased cell proliferation of the ones seeded with the hydrogel was observed. Moreover, renal function, measured using the serum levels of creatinine and blood urea nitrogen, improved over a 28-day period with concentrations returning near the normal baseline in the kidneys that received the stem cell seeded with hydrogels. Cell retention within the hydrogel matrix is likely the key mechanism that contributes to the success of the implanted material. Without a substrate for cell adhesion, the cells are susceptible to impaired adhesion due to reactive oxygen species (ROS), which can lead to up to 90% cell death within the first week. In addition to providing a substrate for growth, the chitosan chloride hydrogel has anti-oxidative properties, which may curb the interaction of ROS. With the increased retention of cells, the start of angiogenesis and renal cell proliferation may occur earlier with the use of hydrogel scaffolds. With the apparent difficulty of applying free-floating cells to a targeted site *in vivo,* hydrogels will perhaps find success as a cell scaffold for renal tissue engineering, though there may be many hurdles in finding a cell candidate that will accurately behave as functional renal cells.

An approach to consider for renal tissue regeneration is the response of the host tissue to the natural or synthetic hydrogel materials that might be used for cell scaffolds. In an attempt to restore renal function degenerated by chronic kidney disease, several formulations of hydrogels were used to deliver cells in a rodent model and the host response to the hydrogel material was evaluated [28]. Gelatin beads, cross-linked hyaluronic acid (HA), combination HA/gelatin, polycaprolactone (PCL), and poly(lactic-*co*-glycolic acid) (PLGA) were combined with selected regenerative renal cells to

enhance regeneration and promote formation of functional renal tissue. While implantation of acellular gelatin and HA in the renal parenchyma resulted in a minimal immune response after 4 weeks, both PCL and PLGA initiated a severe immune response and promoted little native cell spreading. Only the gelatin-containing hydrogels were able to support cell attachment and spreading *in vitro*. Hyaluronic acid hydrogels did not provide any binding sites, and cells remained in a spheroid shape. Although the authors claim neo-kidney formation *in vivo* in rodents after one week post-implantation, the results of long-term studies are yet to be reported at this time [28].

Laparoscopic renal surgery is arguably the best treatment for renal cell carcinoma since its introduction in 1991 [29]. Since then, the development of surgical technique and equipment for laparoscopic partial nephrectomy (LPN) has provided similar benefits preserving renal function. However, this technique is not without its challenges especially because control of bleeding requires a great deal of skill from the surgeon. While conventional approaches include suturing and use of hemostatic gauze, hydrogel-based tissue sealants have also been explored as a replacement [30]. When compared to a fibrin sealant (Tisseel; Baxter) and intracorporeal suturing in a porcine model, the PEG-based CoSeal hydrogel (Baxter) was found to be a poor substitute for the fibrin glue noting that the hydrogel could not adhere well to the renal parenchyma [31]. More specifically, one animal in the CoSeal group suffered significant blood loss during surgery and was sacrificed after 8 days due to sepsis. Furthermore, all 3 kidneys with the CoSeal hydrogel suffered from urinary leakage in acute follow-up studies (after 3 days) and 1 of 4 in chronic follow-up studies (after 6 weeks). CoSeal also encountered bowel adhesion at the

site of application, which could lead to further complications in the gastrointestinal tract. Another study, however, demonstrated success using CoSeal in a porcine model though a care must be taken in interpretation as the organ section removed, hydrogel application method, and control of blood loss were different in these two studies [32]. Another hydrogel that was considered for its feasibility was a biodegradable PEG-lactide hydrogel photopolymerized by high intensity xenon light [33]. Although hemostasis was achieved, the necessity for additional tools in the operating room prevents it from being convenient especially for laparoscopic surgery. The contrasting results in these studies could be seen as evidence that factors beyond the hydrogel contribute to the success of the surgery.

A review of 1347 LPN cases in the United States and Europe conducted in 2005 revealed that most (n=1042) cases used a variety of different hemostatic agents and/or tissue sealants including gelatin matrix thrombin tissue sealant (FloSeal; Baxter), fibrin glue (Tisseel; Baxter), bovine serum albumin–based adhesive (BioGlue; CryoLife), and cyanoacrylate glue (Glubran; General Enterprise Marketing) [34]. Ultimately, the study found that the number of cases requiring transfusion due to blood loss and urine leakage were very low (2.6% and 1.9% respectively). However, it should be noted that many other factors play a role such as improved surgical technique and the use of other methods outside of tissue sealants such as suture bolstering that would improve these rates. It appears that hydrogels have not yet reached a point where they would have significant benefits over established tissue sealants in the operating room.

1.3.2. Ureters

Ureteral stents are used to preserve urinary drainage from the kidneys under situations where patency may be compromised. Common problems associated with stent usage include stent migration, infection, encrustation, and urothelial hyperplasia. The use of hydrogels in ureteral stent applications has been shown as an antibacterial coating to prevent infection, to enhance lubricity, and prevent encrustation [35-37]. When compared to uncoated control, proprietary hydrogel-coated Boston Scientific Percuflex® ureteral stents dipped in solutions of ciprofloxacin, gentamycin, or cefazolin exhibited an increase in bacterial inhibition activity following *in vitro* assays with activity lasting for more than two weeks in some specimens [35]. Specifically, ciprofloxacin provided the best results up to 15 days after application while gentamycin was only able to maintain bacterial inhibition for 3 days. Although the actual results may vary for different drugs, this study demonstrated that stents coated with a hydrophilic hydrogel could be simply dipped in an antibiotic solution prior to implant to provide protection against infection. Similarly, poly(vinyl pyrollidone) (PVP) hydrogel coating of ureteral stents in a similar manner exhibited decreased bacterial growth of *E. faecalis*, but not *E. coli*, compared to uncoated samples [36]. However, as a lubricant, PVP can decrease friction between implant and tissue and prevent complications due to trauma and irritation during removal. PVP-coated stents also exhibited a significant reduction of hydroxyapatite encrustation on the surface compared to the silicone-coating, which was previously the choice method for prevention of encrustation. Despite the promising results and potential benefits, hydrogel applications in the ureters are currently limited to coatings for stents to prevent

encrustation or bacterial growth. Additional biocompatibility studies and *in vivo* studies are necessary for further conclusions to be made and hydrogel-coated stents are moved into clinical trials. Fortunately, developments in the field of cardiovascular stents can often be applied in urological applications, and many ideas can be shared and adapted between the two fields.

1.3.3. Bladder

As with the kidney, one potential area of application for hydrogels is bladder tissue engineering. The difficulty of successfully engineering replacement bladder tissue can be attributed to the complexity of mimicking the bladder's unique mechanical properties. Currently, there is little published work with hydrogel compound usage for bladder tissue engineering, and the field remains largely unexplored. While there are some publications on hydrogels using bladder smooth muscle cells (SMCs), there is currently very little on hydrogels associated with uroepithelial tissue engineering, though some other approaches without hydrogels have been considered.

Collectively, bladder diseases affect approximately 400 million people worldwide with approximately 35 million affected in the United States with costs of $16 billion annually [38]. Several congenital abnormalities such as epispadias or bladder extrophy, or developed diseases such as bladder cancer or interstitial cystitis call for surgical intervention and tissue substitution. Typically, gastrointestinal segments are used for tissue transplantation or augmentation [39, 40]. However, due to inherent physiological distinctions between intestinal tissue (absorptive) and bladder tissue (excretive, barrier function), long term complications can include urolithiasis, increased mucous production,

and bladder malignancy [41]. Moreover, a shift from a contractile to a synthetic phenotype in bladder SMCs has been associated with scar tissue formation, which, in turn, create a stiffer matrix unable to expand to accommodate the change in volume. Due to the myriad of complications associated with grafting of gastrointestinal segments, tissue engineering with hydrogel matrices has emerged as a potential option for restoring and regenerating the bladder.

A particular challenge in developing tissue *in vitro* is determining how to retain the normal, contractile phenotype of native bladder SMCs. A 3D hydrogel culture system based on poly(ethylene glycol) (PEG) cross-linked with bioactive matrix metalloproteinase (MMP) peptides has been examined for its effect on preserving the contractile phenotype of bladder SMCs and differentiation of mesenchymal stem cells (MSCs) into SMCs in vitro [42]. MSCs cultured in the MMP-modified PEG hydrogel exhibited a spread cell morphology and extracellular matrix (ECM) production while cell proliferation was much slower as compared to those in conventional 2D cultures. Moreover, a 1.7-fold increase in αSMA and 4.4-fold increase in myosin expression were observed in SMCs encapsulated in the PEG hydrogel compared to 2D cultures. In contrast, THY-1, a positive marker for the synthetic phenotype, was significantly downregulated in 3D culture suggesting a contractile phenotype. MSCs from human bone marrow cultured in the PEG 3D system exhibited significant upregulation of smooth muscle markers with slight downregulation of stem cell markers. These results suggest successful differentiation of stem cells towards a contractile smooth muscle phenotype, and that the use of an easily tunable hydrogel matrix is a valuable tool to guide

differentiation or retain phenotypes characteristic of the native bladder smooth muscle cells.

Another method for creating controllable biomaterials comes in the emerging field of "bioprinting". Cells encapsulated in various hydrogel compounds are printed onto a cell culture dish or hydrogel substrate through an inkjet printer. Although the technology offers an attractive option for tissue engineering, it has met several undesired limitations. For example, inkjet systems [43] cannot accommodate a viscous hydrogel scaffold where clogging of the print head becomes an issue. Cell viability and functionality may also be a concern considering the high velocity and spray of the print head [44]. As an alternative, a valve-based droplet generator was used to print bladder SMC encapsulated within type-I collagen gel, and cell viability and proliferation were observed over a five day period [45]. Moreover, after a 51-day culture, a thin (100-400 μm) SMC tissue patch was created with high uniformity throughout although the cells are smaller in diameter compared to native bladder and show little alignment along any particular axis possibly due to the absence of cyclic loading that is typically exerted on native bladder tissue [46]. Furthermore, collagen as the sole component of the bioprinted hydrogel makes for a mechanically weak hydrogel.

Much work has been done on the use of natural and synthetic polymeric biomaterials to provide a mechanically sound scaffold with properties similar to bladder tissue. Some of this work goes beyond the use of hydrogels with common synthetic polymers used in tissue engineering such as poly(glycolic acid) (PGA), poly(lactic acid), and poly(ε-caprolactone) [47]. Synthetic polymers are beneficial in some cases since they

can be fabricated on a larger scale and have controllable mechanical properties. However, they lack inherent biological activity and generally suffer from biological incompatibility [48]. Hydrogels would likely benefit by pairing with a more mechanically stronger material. One application in particular explores the use of two sheets of compressed collagen gel with poly(lactic acid-co-ε-caprolactone) (PLAC) embedded in between [49]. The collagen-PLAC material was easier to handle and was able to be sutured without significant shrinkage unlike its collagen-only counterpart. As such, the combination of 1) materials to promote cell growth and spreading, such as the bioprinting method, with 2) polymers capable of mimicking the bladder compliance may prove to be a viable route. One downside of this method, however, is the potential for release of toxic components from the synthetic polymer as it degrades [50, 51]. In the collagen-PLAC material, it was noted that a delayed immune response occurred that corresponded with the degradation time of PLAC [49].

One challenge to overcome for bladder tissue engineering is developing a material that properly mimics, or at least incorporates well with, the native bladder tissue. Unfortunately at this point, hydrogels alone are too mechanically weak, and many studies turn to more compliant materials like synthetic polymers or decellularized grafts [48].

One noteworthy endeavor of uroepithelial regeneration did not rely on direct hydrogel application, but used cultured cell sheets on polymer-coated thermosensitive dishes based on the poly(*N*-isopropylacrylamide) (PIPAAm) hydrogel. The polymer is bonded to a tissue culture dish using electron beam irradiation creating a slightly hydrophobic surface at 37°C. On the surface, urothelial cells were cultured for three

weeks. After the culture period, the culture dishes are brought below the lower critical solution temperature (LCST) of 32°C, the surface becomes hydrophilic, and the cells spontaneously detach in one contiguous sheet after approximately 30 minutes. Histological sectioning of the cell sheets revealed both monolayered and multilayered sections. Electron microscopy supported the claim that the uroepithelial cells retained umbrella, intermediate, and basal cell morphology [52]. These uroepithelial cell sheets were used in a subsequent canine study in conjunction with demucosalized gastric flaps. Briefly, eight dogs had uroepithelial cells removed by partial cystectomy, which were cultured for a three-week period on the PIPAAm-coated culture dish. After this period, the dogs underwent surgery to have a section of stomach tissue removed and demucosalized. Cell sheets were then seeded and attached to the submucosal surface of the gastric flap, which was placed in a protective latex pouch and returned to the abdominal cavity. After another three weeks, the dogs were sacrificed, and the gastric flaps were examined. Of the eight dogs, five of them had viable regenerated uroepithelial layers covering a majority of the gastric flap surface. There was a change in the morphology of the superficial layer of cells. The remaining three dogs had severe hematomas on the gastric flap, which could possibly be attributed to the cell's exposure to xenogenic material during the culture phase [53].

Approaching cell culturing from this standpoint offers the advantage of producing a cohesive tissue. Other cell harvesting methods using enzymatic treatment cleaves cell-to-cell junctions and association with the extracellular matrix reducing cell function. However, this method of culture is also very lengthy and requires near maximum

confluence to form a unified cell sheet. Additionally, the detachment upon temperature decrease occurs slowly over 30 minutes, which can lead to a decrease in cell viability. Several methods have been explored to improve viability and handling of the cell sheet [54].

In most cases of bladder cell carcinoma, early stages of the tumor formation appear in the uroepithelial layer, and treatment normally consists of transurethral resection of the tumor with high rates of success. Unfortunately, there are also high rates of tumor recurrence, and anti-cancer drugs delivery are commonly administered postoperatively to suppress this. However limitations arise when the drug is delivered orally. Additionally, large doses would have to be administered systemically in hopes of having a small portion reach the bladder, and thus increasing risks for side effects. Intravesical delivery of the drug by catheter provides a method for local release, yet this technique is not without its disadvantages. Low permeability of the uroepithelium prevents drug uptake, filling of the bladder during catheterization dilutes the drug concentration at the target site, and voiding of urine will carry the drug out of the bladder [55]. Hydrogels may provide a potential solution to prevent repeat catheterization and drug delivery. Ideally, a hydrogel compound loaded with drugs would be able to withstand bladder filling without being washed away too quickly.

Recent studies have explored various types of thermosensitive hydrogel compounds that are liquid at room temperature but undergo gelation at body temperature to improve retention of locally delivered drugs. For example, a FITC dye was used to model drug elution from a tri-block copolymer hydrogel consisting of PEG-PLGA-PEG.

The hydrogel was shown to hold FITC dye significantly better than free FITC injected into the bladder in rat models [56]. Urinary cystitis was also induced using an intraperitoneal injection of cyclophosphamide in some rats. This chemically induced cystitis is marked by increased micturition frequency, development of ulcers, hemorrhages, and erosion. Rats were divided into control groups containing saline, hydrogel, and misoprostol, a therapeutic drug for gastric and duodenal ulcers. The treatment group was injected with a hydrogel and misoprostol compound. The frequency of voiding significantly decreased in rats treated with the drug-loaded hydrogel compared to either the drug or the hydrogel delivered alone. Another similar study explored poly(*N*-isopropylacrylamide) (PNIPAM) grafted with hyaluronic acid (HA) and gelatin [57]. Cisplatin, a drug for the treatment of bladder cancer [58, 59], was added to the compound and drug diffusion and effects on the uroepithelium were observed in rat models. The study found slower release of the hydrogel-encapsulated drug compared to drug dissolved in aqueous solution and minimal disruption of the uroepithelial layer where the hydrogel was applied.

Another bladder pathological condition that hydrogels might also offer benefits is interstitial cystitis (IC), which is a condition characterized by a disruption or increase in the permeability of the uroepithelial layer causing irritation of the smooth muscle tissue [60, 61]. The lack of knowledge in the etiology of IC prevents significant progress on the best method of treatment, and most current methods only attempt to treat the symptoms [62]. Some avenues of treatment have turned to glycosaminoglycans (GAG) such as hyaluronic acid, heparin, pentosan sulfate, and chondroitin sulfate to alleviate the pain of

patients suffering from IC [63-67]. Since the mechanisms of IC are not well understood, it was speculated that GAGs administered intravesically are providing relief by replacing the damaged bladder lining. However, research on the mechanisms of how GAGs could adhere to the glycocalyx and interact with the bladder is also lacking. Nonetheless, one recent study examined intravesical instillation of hyaluronic acid and chondroitin sulfate administered weekly for the first 2 months and then every 2 weeks for 6 months [67]. Based on subjective surveys, all patients reported improvement in urinary urgency and bladder pain. A reduction in the times voided and an increase in the volume of urine per voiding were seen post-treatment.

The applications of hydrogels in the bladder have been improving over recent years, but still have much more to go. Though the mechanical strength of hydrogels may not be on par with native tissue yet, they do fare well as a supplement material for application that require longer-term diffusion or degradation like drug delivery or cell encapsulation. Additionally, discoveries in the etiology of interstitial cystitis may lead to more uses of natural hydrogels combined with supplemented medicine to not only relieve symptomatic pain, but to cure the condition altogether.

1.3.4. Urethra

Stress urinary incontinence (SUI) affects approximately 35% of females over the age of 18 and 45% over the age of 60 hampering their quality of life [68]. Economic costs associated with SUI, which is estimated to be $27 billion dollars annually, includes the purchase of disposable products, laundry costs, injuries resulting from rushing to the

bathroom, complications from treatment, requirement of caretakers, and lost time from work [69].

Currently the standards of treatment for SUI include pelvic floor exercise to strengthen the muscles surrounding the vagina and urethra and assist in retaining voluntary control. While surgery to implant suburethral slings made of polypropylene mesh is an option, potential complications and pain associated this procedure deter some patients. Hydrogel bulking agents are gaining popularly as an alternative for treatment of SUI and its effectiveness and safety were examined in a study on 514 elderly women who were each treated with one of four different bulking agents between 1999 and 2012 [70]. The commercially available bulking agents compared in this study were Contigen®, Zuidex®, Tegress®, and Bulkamid® made from cross-linked bovine collagen, hyaluronic acid/dextranomer copolymer, ethylene vinyl alcohol, and polyacrylamide hydrogel, respectively. The treatment for intrinsic sphincter deficiency is performed by periurethral injection of the hydrogel material into the submucosa to thicken the urethral wall. It is believed that bulking agents work by increasing the central filler volume, which lengthens the sarcomeres in the sphincter muscle and strengthens it [71]. Although the study found significant improvement in maximum urethral closure pressure and reduction in urine leakage, survey taken during the study revealed that patients still feared urine leakage and continued to take the same precautions prior to the treatment. Since the currently available bulking agents only provide a temporary fix to retain continence, and repeat injections are necessary over a period of time, recent work has explored the use of a composite hydrogel polyethylene glycol and carboxymethyl cellulose as a bulking

agent for the urethra sphincter. Allowing for little swelling or shrinkage, this particular hydrogel formulation can potentially become a more permanent option. However, additional work is necessary in order to reduce the inflammatory response and urethral degradation before use in humans can be considered [72]. Though bulking agent treatments are considered relatively safe, risks exist for urinary tract infection, urethral erosion and prolapse, and diverticula formation, which can require additional treatments with added costs. With the variability in responses to the bulking agents from patients [70], it remains to be seen whether a highly successful hydrogel compound will be developed that does not lead to severe complications and eliminates the need for repeat injections.

In addition to the use as a bulking agent, hydrogels may also contribute to the regeneration of dysfunctional urethra. While current surgical methods rely on implantation of tubes created from buccal mucosa or foreskin tissue, hydrogels may be used instead for treatment of conditions such as hypospadias and urethral stricture. Hypospadias is a congenital defect found in approximately 1 in 300 male births [6] that is characterized by development of the urinary meatus (opening of the urethra where the urine exits) along the shaft of the penis rather than at the glans. One particular study explored the feasibility of high-density collagen gel tubes seeded with rabbit bladder smooth muscle cells for urethral regeneration in rabbit models [74]. At one and three months after implantation, urethrograms revealed that lumen calibers of acellular grafts were 62.69% ± 18.1% and 42.4% ± 34.3% compared to native control urethra, respectively. In contrast, the lumen calibers of seeded grafts were 45.7% ± 43.62% at one

month and 96.6% ± 12.5% at three months. The observations that host cell ingrowth occurred in both acellular and seeded scaffolds suggest that use of the acellular scaffold will eliminate the time necessary to harvest and expand smooth muscle cells for seeding and the collagen gel approach may potentially improve short- and long-term complications over current surgical methods. In surgical cases where radical urethral repair or replacement is not necessary, glues or sealants are used to repair damaged tissues. Urethrocutaneous fistula is a post-operative complication of hypospadias repair, and its incidence can be as high as 20% [75]. The use of fibrin glue as a sealant applied along the suture lines during hypospadias repair has been shown to diminish occurrence rate of complications from 53% to 20% [76]. Fibrin glue can also be used to promote wound healing in many cases urethroplasty, such as those previously described, and to assist with bulbar urethroplasty using buccal mucosa grafts [77,78].

Various types of hydrogels are used not only in urethral reconstruction, but also as a coating material for devices that come in contact with the tissue. In both ureteral stents and urethral catheters, problems with infection, lubricity, and encrustation can occur. Several stents and catheters are on the market using proprietary hydrogel coatings such as LubriLAST™, HydroPlus™, the BIOCATH® and LUBRI-SIL® Foley catheter. However, these hydrogels are all advertised to improve only patient comfort by providing adequate lubrication. Further improvements in hydrogels used for stents and catheters will likely be found through developments that prevent bacterial growth and encrustation. For urethral catheters made from segmented polyurethane, surface modifications are used to reduce the complications such as bacterial colonization, urethral trauma, catheter

obstruction, encrustation, and infection [36, 79-81]. The adhesion and growth of bacteria around the catheter site arises from the protein adsorption cascade [82]. Furthermore, irritation and inflammation due to the friction between the catheter and the urethral lining can exacerbate the complications mentioned. Particularly, one study compared the protein reduction and lubrication properties of a chitosan/poly(vinyl alcohol) (PVA) hydrogel with LubriLAST™, a general solution currently used to create a lubricated surface for several devices including urinary catheters. Long-chain chitosan provides a flexible network for entanglement of PVA that is designed to elute from the chitosan network upon swelling. These particular components were chosen for their antimicrobial capabilities (chitosan) and reduction of protein adsorption and cell adhesion (PVA). Results of the study showed significantly less protein adsorption on the chitosan/PVA-coated catheters compared to uncoated and LubriLAST™ coated samples. Additionally, antibacterial tests measuring areas of bacterial inhibition were performed and large antiseptic regions were demonstrated around the chitosan/PVA-coated samples when incubated with *S. aureus*, *P. aeruginosa*, and *E. coli* [83].

1.4. Tissue Engineering of Bladder

1.4.1. Importance of a functional urothelial layer

The urothelium accomplishes this through high-resistant tight junctions, glycan layer, and specialized protein and lipid composition present in the umbrella, or uppermost, cell layer. There is evidence that the uroepithelium also plays a role in the control of active transport of molecules, ions, and water across the mucosal surface of the bladder. Active release of neurotransmitters such as adenosine triphosphate (ATP),

acetylcholine, and adenosine from the urothelial layer to various nerve processes in the underlying tissue may play a role in the sensation of bladder fullness [14]. It is hypothesized that interruption of the urothelial layer and the sensory functions associated with it leads to bladder dysfunction and certain bladder diseases such as interstitial cystitis [84]. Current clinical methods explore the use of buccal mucosa or segments of the gastrointestinal tract as donor tissue for diseased bladder, however contact of the foreign tissue can contribute to complications such as urolithiasis, increase mucus production, malignancy, infection, and metabolic disturbances for the patient [41, 85-87]. Ultimately, it would be desirable to produce transplantable tissue that would be capable of handling the *in vivo* conditions of the urinary tract.

1.4.2. Adipose-derived stem cells for therapeutic benefits

Throughout the lifespan of a person, the adipose tissue on their body can undergo drastic changes in volume. In some cases, small increases in the lipid amount in each adipocyte contribute to small volume fluctuations while larger increases remodel the adipose tissue through production of new adipocytes. Research has shown that progenitor cells and stem cells within the adipose tissue contribute to the radical remodeling that can occur within the adipose vasculature. One population of cells that have been isolated from adipose tissue has been termed as adipose derived stem cells (ADSCs). In literature, there have been several names for the cell population including adipose-derived adult stem cells (ADAS), processed lipoaspirate cells (PLA), and adipose tissue-derived stromal cells.

ADSCs have been extensively studied for their multipotent differentiation potential, and the prospects for their use in tissue regeneration have been proposed for a variety of different applications. Mesenchyme-derived adult stem cells (MSCs) such as ADSCs and bone marrow-derived stem cells (BMSCs) provide an alternative to the hotly debated embryonic stem cells while still having a similar differentiation potential. BMSCs are capable of differentiation into adipocytes, chondrocytes, osteoblasts, and myoblasts [88-93] with *in vitro* studies. Practically, however, harvesting BMSCs can cause pain and morbidity at the extraction site, and expected low cell yields necessitate an *ex vivo* expansion, which is costly and time consuming in itself. Instead, ADSCs may provide an alternative source for adult stem cells with a higher cell yield per harvest, lower pain and discomfort for the patient, and relative ease of harvest [94]. ADSCs are extracted through an established method in which human raw lipoaspirate from such liposuction procedures is processed to yield an adult stem cell population [95]. The same group showed that the ADSCs within this processed lipoaspirate possess the capacity to differentiate into adipose, bone, cartilage, and muscle. Furthermore, there has been research showing the capability of ADSCs to differentiate towards skeletal muscle [96-98], cardiac muscle [99-101], neuronal cells [102-104], hematopoietic cells [105], endothelial cells [106], and hepatocytes [107].

Another reason that ADSCs are an attractive cell source for stem cell-based tissue engineering is due to their immunomodulatory capabilities. These characteristics were first studied in autologous mesenchymal stem cells due to their wide usage in therapeutic treatment for various diseases such as urinary incontinence and erectile dysfunction,

though a number of studies explored the potential for allogeneic and xenogeneic transplantation [108, 109]. The first studies that explored the immunosuppressive properties of the ADSCs were shown in their ability to prevent a mixed lymphocyte reaction – though it is not clear whether or not this requires direct cell-cell contact [110-112]. Literature has shown that immunosuppression occurs not through cell-cell contact, but rather through the secretion of soluble factors such as prostaglandin E2, indoleamine 2,3 dioxygenase and leukemia inhibitory factor [112-115]. In studies where those specific soluble factors were inhibited, the response demonstrated a neutralization of the immunomodulatory effect of the ADSCs [113-115]. Though there are many strict guidelines that are yet to be thoroughly established in stem cell therapy, the immunosuppressive capabilities demonstrated put ADSCs at the forefront of therapeutic options. With allotransplant, there is potential to establish a stem cell bank in which ADSCs can be differentiated, stored, and delivered when necessary without having to harvest autologous tissue and undergo an extensive culture and expansion period.

1.4.3. Adipose-derived stem cells for epithelial differentiation

Since the ultimate goal of this research is to derive uroepithelial cells from ADSCs, we are interested in the epithelial potential of this cell population. Several previous studies have sought an answer to whether or not cell types originating from the mesenchyme – such as BSMCs or ADSCs – are capable of differentiation towards epithelial lineages using soluble factors in media. Previously, BMSCs have been shown to be capable of in vitro differentiation towards epithelial-like lineage using varying differentiation modalities including growth factors, conditioned media, co-culture, a

biomimetic environment, or a combination of these methods [116-119]. One particular study speculated that retinoids would be capable of stimulating epithelial differentiation in ADSCs due to its anti-proliferative and effect on differentiation in various tissue types [120]. The results from the study demonstrate an increase in cytokeratin 18 – a highly conserved keratin important in cell polarization and typical of simple epithelial (such as in intestine or kidney) – in both protein and mRNA expression after exposure to 5 μM all-trans retinoic acid (ATRA) after 10 days. Conversely, there was a decrease in the expression of vimentin – a mesenchymal marker [121]. Aside from ATRA, epidermal growth factor (EGF), keratinocyte growth factor (KGF), and hepatocyte growth factor (HGF) have all been implicated to induce a change in expression of ADSCs in vitro [122-124]. One study aimed to use the listed growth factors in various concentrations to determine their combinatorial effects in an air-liquid interface created with a Transwell® membrane [179]. The study found the highest upregulation of cytokeratin 19 (CK-19) mRNA expression with the addition of ATRA, hydrocortisone, EGF, HGF, and KGF and similar trends with protein expression of CK-19, cytokeratin 13 (CK-13), and involucrin – another terminal epithelial marker. Though positive results were shown of epithelial differentiation of these rabbit ADSCs, it is unclear if uroepithelial differentiation was achieved due to the lack of detection for urothelial specific markers. Furthermore, the necessity of the air-liquid interface as a culturing method was not tested and would ultimately act as a chokepoint to culture a large number of cells effectively.

CHAPTER TWO

RATIONALE AND SPECIFIC AIMS

2.1. Rationale

Various urological treatment approaches such as transurethral resection, bladder cancer, and ureteroscopic surgery can cause damage to the urothelial lining tissues. Current gold standard in bladder tissue regeneration, however, are limited to gastrointestinal or buccal tissue augmentation, which can lead to severe consequences such as urolithiasis, electrolyte imbalance, tract infection, and mucus production [85]. Currently, no suitable method exists, particularly in cases of bladder cancer, to restore the urothelial layer from a non-urothelial cell source. Due to the nature of bladder cancer pathology, the use of native urothelial cells is severely restricted in cases of bladder cancer and disease [18] despite their successes with tissue regeneration *in vitro* [133, 134, 146] and *in vivo* [53, 149, 150, 169]. The long-term goal of the present study is to develop a therapeutic system using defined keratinocyte serum-free media to consistently differentiate human adipose-derived stem cells (hADSCs) towards a urothelial lineage, which can be used to promote repair and restoration of a functional uroepithelial lining. Human ADSCs are a desirable cell source due to their ease of harvest and propagation, and evidence of immuno-modulatory properties allowing for allogeneic or even xenogeneic transplantation without use of immunosuppressants (Lin CS, Stem Cells and Development. 2012; 21: 2770-78). Thus far, attempts in differentiating ADSCs towards urothelial and epithelial lineages included the use of co-culturing and conditioned media, which relied on multiple cell sources and have provided unreliable and inconsistent

results [136-139]. In order to translate the successes obtained in cell culture studies to a more physiologically relevant growth environment, research continues to investigate development of three-dimensional tissue-engineered constructs to replicate bladder physiology [7-9]. Hydrogels have also been explored in tissue regeneration as a method to deliver cells, provide essential growth factors, and control cell growth at a target site [132]. The use of adult stem cells continues to be a challenge in replicating urothelial physiology, as it is not a straightforward task to mimic complex characteristics such as urothelial impermeability and rapid changes in the urothelial umbrella layer associated with bladder compliance and distention, which is especially the case for cells not initially suited for such purposes.

2.2. Specific Aims

In pursuit of our research goals, human ADSCs were cultured in various culture conditions to test the effects of defined keratinocyte serum-free media and all-trans retinoic acid (ATRA) on cell differentiation. After prescribed time periods, cell differentiation towards a urothelial cell lineage was assessed through morphological imaging, reverse transcription and polymerase chain reaction (RT-PCR) for mRNA expression of urothelial and stem cell markers, and translation of such markers to protein expression via western blotting and immunofluorescence studies. Furthermore, some preliminary studies were conducted on investigating the cellular response in 3D matrix using collagen, PMBV/PVA hydrogel, and fibronectin/gelatin layer-by-layer method. The dissertation is dividing into the follow aim sections as follows:

1. Evaluating the effects of defined keratinocyte serum-free media on mRNA gene and protein expression of hADSCs towards a urothelial lineage via reverse-transcription and polymerase chain-reaction, western blotting, and immunofluoresence.
2. Evaluating the effects of a fibronectin/gelatin layer-by-layer coating on morphology and urothelial marker expression of urothelial-like cells in a three-dimensional microenvironment.
3. Development of a tension bioreactor system for the application of static stretch in a viscoelastic environment susceptible to creep behavior.

Upon completion of these aims, we expect to illuminate the key components in developing a reliable and consistent differentiation method for hADSCs towards urothelial lineage. Furthermore, we hope to advance the research in development of a functional urothelial multilayer *in vitro* using non-native cell sources for stem cell therapies.

CHAPTER THREE

EFFECTS OF KERATINOCYTE-SERUM FREE MEDIA ON UROTHELIAL PHENOTYPIC EXPRESSION IN ADIPOSE DERIVED STEM CELLS

3.1. Introduction

Various congenital and adult bladder diseases require approximately 60,000 surgical interventions annually in the US [140-142] and many of the procedures can permanently damage the urothelial tissue along the urinary tract. Current standard approaches substitute damaged urothelial tissue with gastrointestinal or buccal mucosa, or in cases of bladder cancer, abnormal urothelium is removed in a transurethral resection procedure leaving the underlying layers exposed to the urine [85]. In both cases, the urine contacting the smooth muscle layer leads to unwanted complications such as electrolyte imbalance, urolithiasis, tract infections and mucus production [41, 87]. It is critical to develop a methodology for clinical use to restore the urothelium especially from a non-urothelial cell source.

Although tissue engineering of the bladder has received much attention [143-145], use of synthetic or natural scaffolds to repair dysfunctional urologic tissue has seen limited success compared to conventional treatment [146]. For example, naturally derived materials such as submucosa of bladder or small intestine, collagen in various forms, or alginate gel have been used to facilitate incorporation of the implanted cells and elicit a biological response conducive to formation of neo tissue [144]. Synthetic polymeric biomaterials such as polyglycolic acid (PGA), poly-L-lactic acid (PLA), or poly(lactic-co-glycolic acid) (PLGA) or a hybrid of naturally and synthetically derived materials

have also been used. The advantage of synthetic materials is their scalability, quick and reproducible production, and mechanically tunable properties [52, 147, 148]. However, more studies are focused on materials for regenerating smooth muscle tissue and not on the urothelial layer. Shiroyanagi et al. reported that using canine urothelial cells seeded onto thermally sensitive polymer surfaces coated with poly(*N*-isopropylacrylamide) (PIPAAm) formed thin, stratified cell sheets retaining urothelial phenotypic markers after three weeks post-harvest [52]. In a follow-up study, the cell sheets were grafted onto demucosalized gastric flaps and implanted into the stomach of a canine model with similar morphological traits to native urothelial tissue, though regenerated urothelium lacked urothelial-specific uroplakin markers [53]. Additionally, autologous cells have been used for ureteral reconstruction [149] and urethral defect repair [150, 151] in animal models to prevent restenosis compared to tissue constructs without use of natively-derived urothelial cells. Though the results are promising, seeding with autologous urothelial cells from a diseased donor site is ill-advised due to the nature of bladder cancer pathogenesis [152]. As such, alternate and reliable sources for cells must be considered. In this study, we explore the potential for adipose derived stem cells as an alternative cell source to differentiate into urothelial-like cells for bladder regeneration.

Adipose derived stem cells (ADSCs) are adult stem cells extracted from raw lipoaspirate [153] and have been extensively studied for their multipotential differentiation into various lineages such as adipocytes, chondrocytes, osteoblasts, and myoblasts [153, 154]. Although bone marrow-derived stem cells (BMSCs) are capable of similar differentiation, harvesting BMSCs can cause pain and morbidity at the extraction

site, and expected low cell yields necessitate an *ex vivo* expansion, which is more costly and time consuming compared to harvesting of ADSCs [94, 153, 154]. Furthermore, ADSCs have been shown to exhibit immunosuppressive properties possibly and can decrease alloreactivity when implanted [110, 155]. For these reasons, ADSCs are an attractive cell source for regenerative medicine applications and we chose to use them in the present study.

Others have attempted the urothelial differentiation of ADSCs using various approaches including media supplementation with all-trans retinoic acid (ATRA) [121], co-culturing with or conditioned media from additional cell lines [136-139]. Although discrepancies in interpretation for the specific cause of urothelial phenotype upregulation exist between results, these studies indicate evidence of an association between urothelium-associated marker expression and soluble factors in the growth media. Furthermore, another drawback in these studies is the xenogeneic use of bovine-derived products, where the undefined chemical profile of fetal bovine serum lends itself to less control over the differentiation process [156]. In search of alternatives to bovine-derived products and supplemental cell lines for cell differentiation, we hypothesized that consistent differentiation towards urothelial lineage could be achieved in hADSCs using defined keratinocyte serum-free media (supplemented with epidermal growth factor) because it has been used to retain phenotype in human urothelial cell culture [157-159]. The present study explored the effects of defined keratinocyte serum-free media and ATRA on differentiation of ADSCs into urothelial lineage. Specifically, the morphology and cell viability was observed via phase-contrast and fluorescence staining, and mRNA

and protein expression profile were examined using reverse transcription, polymerase chain reaction, western blotting, and immunofluorescence techniques.

3.2. Materials and Methods

Cell culture.

Human adipose derived stem cells (hADSCs) were purchased from Lonza (PT-5006) and expanded in low D-glucose (1000 mg/L) DMEM (Life Technologies) supplemented with 10% fetal bovine serum (FBS, Fisher), 1% GlutaMAX (Life Technologies), and 1% antibiotic/antimycotic solution (AB/AM; Life Technologies). For differentiation towards urothelial lineage, hADSCs at approximately $2.5x10^5$ cells/cm^2 were cultured in defined keratinocyte serum-free media with the growth supplement kit provided by the manufacturer (fibroblast growth factor (FGF), epidermal growth factor (EGF), and insulin; Life Technologies) and 1% AB/AM in the presence or absence of 5 μM all-trans retinoic acid (ATRA, Sigma) for 7, 14, and 21 days. HADSC between passages 3 and 7 were used in all experiments of the present study. UROtsa cells, an immortalized normal human urothelial cell line (kindly donated by the laboratory of Dr. Naoki Yoshimura, Department of Urology, University of Pittsburgh), were cultured in DMEM supplemented with 5% FBS, 1% AB/AM solution, and without GlutaMAX. For a co-culture experiment, rat bladder smooth muscle cells (rBSMCs) were harvested as described previously [160] and the cells under passage 10 were used as a feeder layer. In separate experiments, human ADSCs were pre-labeled with Celltracker Red CMPTX (Molecular Probes), encapsulated in a collagen gel (2 mg/ml type I collagen, MP

Biomedicals; DMEM, 10% FBS), and cultured in DMEM or defined KSFM with 2% FBS in presence or absence of the rBSMC feeder layer for 7 days.

Reverse transcription / polymerase chain reaction

At the end of the prescribed time periods, total RNA was collected from the cells using Qiagen RNeasy Mini Kit according to the manufacturer's instructions (Qiagen) and quantified using Thermo Scientific Nanodrop 2000c UV-Vis Spectrophotometer. Complementary DNA (cDNA) was synthesized from 2 μg of total RNA using the MMLV-RT reverse transcriptase in the RETROscript® Kit (Life Technologies). The resulting cDNA was amplified in the polymerase chain reaction using the HotStarTaq DNA polymerase in the QuantiTect SYBR Green PCR Kit and a Rotor-Gene (RG-3000, Corbett Research) Thermal Cycler. Custom primers (Table 3.1) were used to assess expression levels of cytokeratin 17 and 20 (CK-17, CK-20) for epithelial cell differentiation, uroplakins Ib and II (UPIb, UPII) for urothelial cell differentiation, and CD90 and CD105 for mesenchymal stem cell markers. Glyceraldehyde-3-phosphate dehydrogenase (GAPDH) was used as the endogenous control. For the PCR cycles, the DNA denaturation step was set at 95°C followed by primer annealing at 55°C and primer extension at 72°C for 40 cycles. Gene expression levels of differentiated cells were analyzed and compared to those of the control hADSC using the comparative delta Ct method. Statistical analysis of RT-PCR results was conducted using a one-sample student's t-test to compare the mean Ct values of control and experimental groups. A statistical significance was defined as p-value ≤ 0.05.

Gene	GenBank ID	Sequence (5'–3')
Cytokeratin 17	NM_000422.2	F: CCGCACCAAGTTTGAGACAG R: TTCAGGTAGGCCAGCTCCTC
Cytokeratin 20	NM_019010.2	F: TGGATTTCAGTCGCAGAAGC R: CATAAACGCTGGGTGTCGTC
Uroplakin Ib	NM_006952.3	F: TTGCTGTGGCGTAAATGGTC R: GCCTCCAGGTTGAGAGGTTC
Uroplakin II	NM_006760.3	F: GCCCTTGATCCTGATTCTGC R: ACCAGCAGGCTCTCCGTTAG
CD90	NM_006288.3	F:AGAGCCTCCGTCTGGACTGC R:GAGCGGTATGTGTGCTCAGG
CD105	NM_001114753.2	F:AGCTGACTCTCCAGGCATCC R:GCCTGGATTTGTAGGCCAAG
GAPDH	M32599	F: ACCACAGTCCATGCCATCAC R: TCCACCACCCTGTTGCTGTA

Table 3.1: Gene name and nucleotide sequence of the primers.

Cell Immunofluorescence and Morphological Imaging

Cells were fixed using a 4% paraformaldehyde solution for 20 minutes and washed thoroughly using PBS. Blocking solution (PBS with 2% goat serum albumin with added dilute Triton X-100) was added and cells were permeabilized at room temperature for 30 minutes before they were incubated with mouse monoclonal anti-cytokeratin 17 (CK-17, Sigma, C9179), goat polyclonal anti-cytokeratin 20 (CK-20, Santa Cruz Biotechnology, SC-17113), or goat polyclonal anti-uroplakin Ib (UPIb, SCBT, SC-15174) at 4°C overnight. All primary antibodies were used at a 1:100 dilution in PBS. For detection of membrane-bound UPIb, Triton X-100 was omitted from the blocking solution. Following primary antibody conjugation, species-specific fluorescently labeled (FITC or Alexa Fluor 488) secondary antibody was added at a 1:1000 dilution in PBS and incubated at room temperature for one hour. Cell nuclei were then stained with 300

nM DAPI in PBS for 5 minutes followed by dehydration using ethanol. For general morphological examination, phase contrast images of hADSCs under different media conditions and UROtsa cells grown in DMEM were compared after 10 days. Additionally, actin filaments in hADSCs and UROtsa cells in two-dimensional cultures were probed with rhodamine phalloidin and imaged to examine cell morphology after 10 days. For co-culture experiments, cell viability in hADSCs and rBSMCs were detected using Live/Dead assay (Molecular Probes) and detection of CK-17 presence via immunofluorescence was performed. All images were taken on a Nikon epifluorescence microscope (TE-2000S) and a Hamamatsu digital camera (C4742-95).

Western Blot

At the end of the culture period, cells were washed using ice-cold PBS and lysed using Radio Immuno Precipitation Assay (RIPA) buffer consisting of 150 mM sodium chloride, 1.0% Triton X-100, 0.5% sodium deoxycholate, 0.1% SDS, 50 mM Tris at pH 8.0 and a protease inhibitor cocktail (Abcam). After centrifugation of the lysates to pellet the insoluble materials, supernatant was collected and concentration of protein sample was determined using a Bradford protein assay (Pierce). Proteins and a standard ladder (Life, LC5800) were separated on a 4-15% gradient polyacrylamide gel (Bio-Rad). Proteins on the gel were then transferred via wet electroblotting (tank transfer) to Immun-blot® PVDF membrane (Bio-Rad) in transfer buffer solution. Membranes were blocked using 2% nonfat dry milk (NFDM) in 50 mM Tris buffer (pH 8.0). The proteins of interest were detected with the following primary antibodies at a 1:500 dilution in 1% NFDM with Tris buffer at 4°C overnight: mouse monoclonal anti-CK17, goat polyclonal

anti-CK20, goat polyclonal anti-UPIb, and mouse monoclonal anti-GAPDH (Life, AM4300) and species-specific HRP-conjugated secondary antibodies at 1:5000 dilution in 1% NFDM with Tris buffer. Protein bands on the membranes were imaged using chemi-luminesccence and analyzed using ChemiDoc™ XRS+ Molecular Imager with ImageLab software (BioRad).

3.3. Results

Morphological changes of hADSCs

Images of hADSCs after rhodamine phalloidin staining provide evidence that cells grown in DMEM alone exhibit an elongated spindle-like morphology typical of mesenchyme-derived stem cells (Figure 3.1.A). After 10 days of culture in defined KSFM, hADSC exhibited the small cobblestone-like morphology with a reduction of elongated actin filament expression (Figure 3.1.C) similar to the positive control, UROtsa cells (Figure 3.1.B). When hADSCs were grown in the presence of 5 μM ATRA, cells displayed contact growth inhibition and formed a monolayer typical of epithelial cells in 10 days (Figure 3.1.D and 3.1.E). Phase contrast imaging provided further evidence that hADSCs cultured in defined KSFM exhibited cell morphology similar to that of UROtsa cells (Figure 3.2).

Expression of urothelial and stem cell marker mRNA

The results of real time RT-PCR provided evidence that mRNA expression for one of the urothelial cell markers tested, CK-17, by hADSC exposed to what media was significantly ($p < 0.01$) lower when compared to that of undifferentiated hADSCs maintained under DMEM control media at all time points tested (Figure 3.3). In contrast,

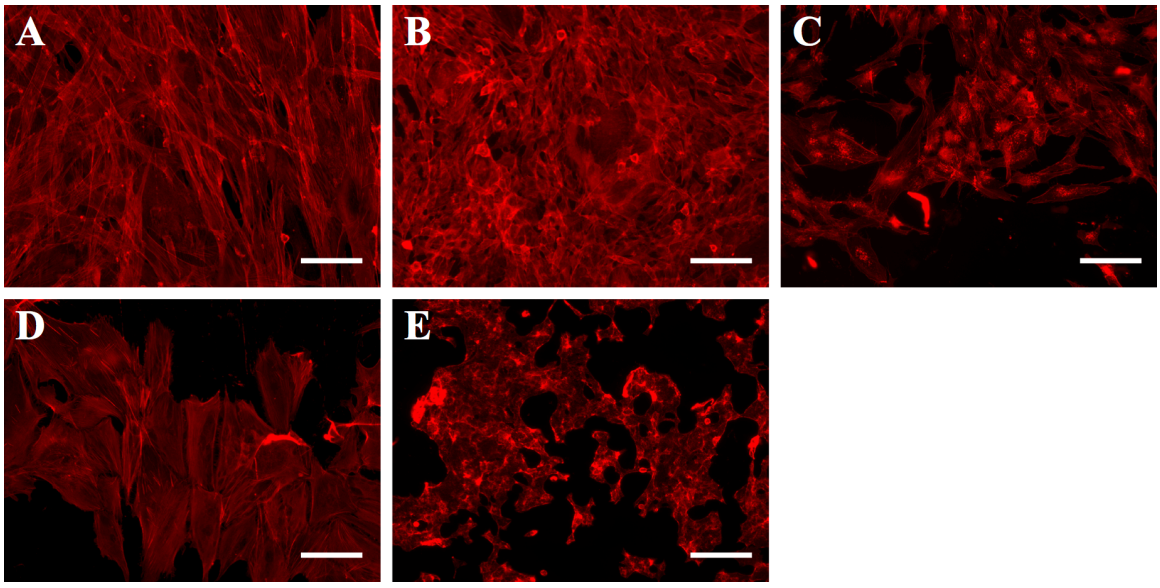

Figure 3.1: Fluorescence imaging of hADSCs with rhodamine phalloidin staining for F-actin filaments. Undifferentiated hADSCs (A) exhibit an elongated morphology. Culturing hADSCs in defined KSFM for 10 days (B) shifted cells towards a smaller cobblestone-like with reduction of internal actin, while the addition of 5 µM ATRA to the media caused hADSCs to retain actin filaments (C). hADSCs cultured in DMEM with 5 µM ATRA (D) displayed spread morphology with actin filaments. UROtsa cells were used as positive control for comparison (E). Scale bars = 100 µm

CK-20 mRNA expression in hADSC cultured in KSFM increased approximately ten-fold compared to the undifferentiated state after one week and continued to increase over two and three weeks of culture. Moreover, significant increases in UPIb mRNA expression occurred in cells cultured under both KSFM and KSFM with 5 µM ATRA, with the highest upregulation after 21 days in KSFM with 5 µM ATRA. Finally, hADSC cultured

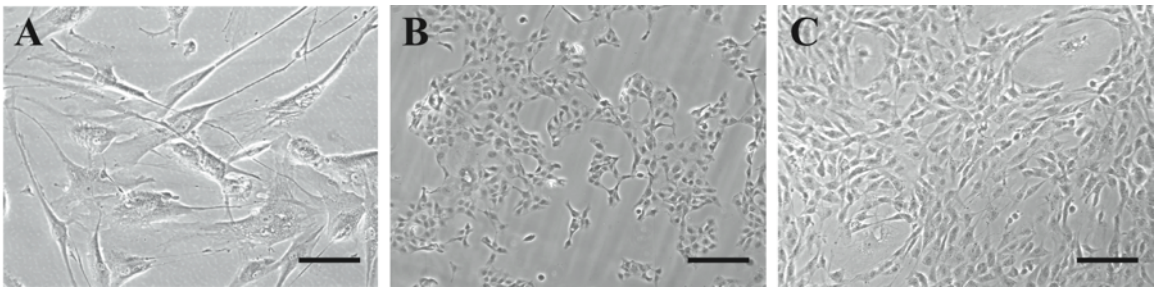

Figure 3.2: Phase contrast imaging of hADSCs. Undifferentiated hADSCs (A) exhibit an elongated morphology with long cell extensions. In contrast, UROtsa cells (B) display a smaller cobblestone-like morphology and appear to form colonies of cells. After 10 days in incubation with defined KSFM, hADSC morphology appears to shift towards urothelial-like cells (C). Scale bars = 100 μm.

in KSFM exhibited significant ($p < 0.01$) downregulation of CD90 and CD105 markers after 2 weeks indicating differentiation away from the stem cell characteristics.

Urothelial cell marker protein expression in hADSCs

Western blot analysis revealed that greater expression of CK-20 was present in hADSCs cultured in KSFM for up to 21 days compared to cells cultured in all other media (Figure 3.4). However, neither CK-17 nor UPIb expression was detected in any of the groups by the western blot analysis. Additionally, it was concluded that transmembrane markers could not be visualized using the prescribed protein isolation procedure for western blotting due to the circumstance that protein aggregation was occurring during the denaturation process (not pictured). To verify the changes in protein expression seen by western blotting, immunofluorescence staining of hADSC was performed for 7, 14, and 21 days (Figure 3.5-3.7). The results of immunostaining demonstrated that expression of

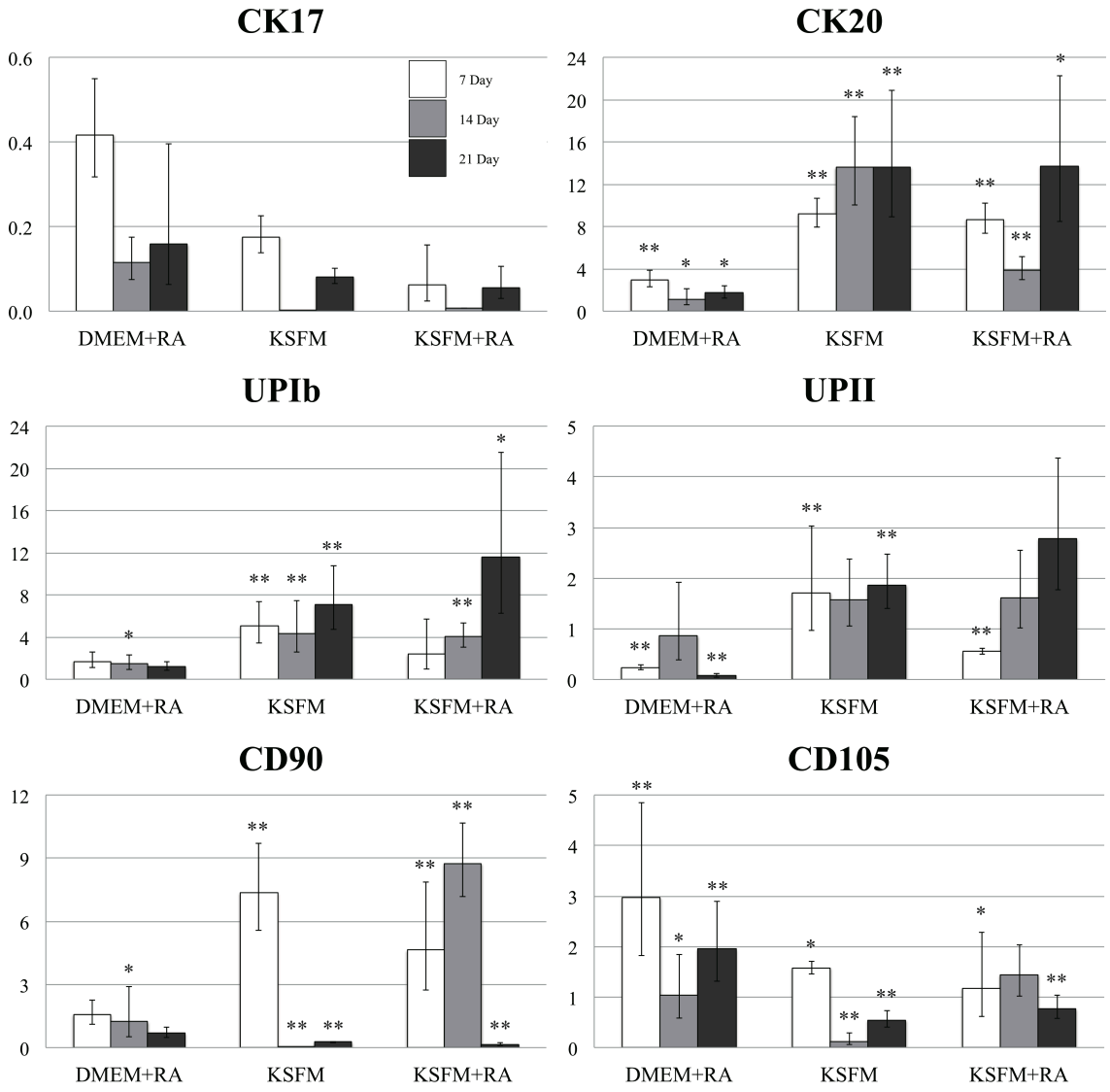

Figure 3.3: Relative expression ratios of mRNA markers in hADSCs under media conditions after 7, 14, and 21 days. Error bars indicate ± 2 S.D. Stars indicate significant difference in expression compared to control undifferentiated hADSCs (normalized with R.E.R. of 1) using one-sample student's t-test (*: p-value < 0.05; **: p-value < 0.01). All values for CK17 are significantly different with values of $p < 0.01$.

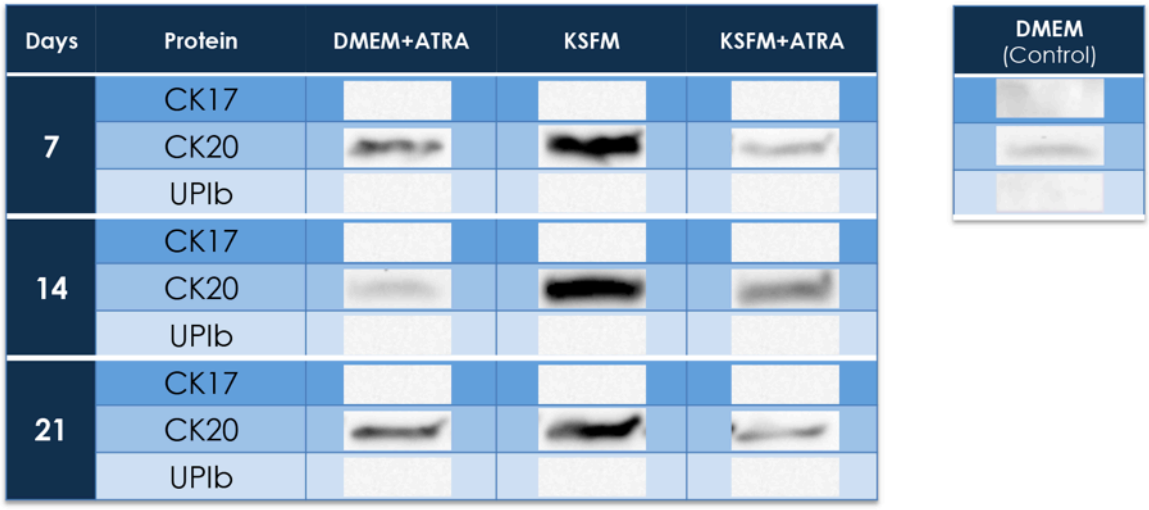

Figure 3.4: Images of western blots to detect protein expression in hADSCs under indicated media conditions after 7, 14, and 21 days. Expression of all three markers was notably absent from undifferentiated hADSCs cultured in control DMEM media. UPIb expression was also absent from each group.

CK-20 with the characteristic appearance of cytoskeletal intermediate-filaments was present strongly in hADSCs incubated in defined KSFM with or without ATRA. In addition, UPIb expression was detected as early as 7 days in cells cultured in defined KSFM with and without 5 µM ATRA. However, CK-17 expression was absent in hADSC cultured under all supplementation conditions tested in the present study.

Phenotype and Viability in Smooth Muscle Cell Co-culture.

Human ADSCs encapsulated within a collagen hydrogel revealed distinct CK-17 expression when supplemented with keratinocyte serum-free media both with and without the presence of a rat BSMC feeder layer (Figure 3.8). This CK-17 expression was not seen with hADSCs seeded under identical condition supplemented with control DMEM. The expression was further visualized in a comparison of CK-17, CK-20, and UPIb expression in hADSCs cultured in both KSFM and DMEM for 7 days. After the prescribed period, fluorescence images indicate that CK-17 protein is expressed solely in hADSCs encapsulated in 3D collagen hydrogel under KSFM culture, while all other proteins are absent in both KSFM and DMEM (Figure 3.9). Additionally, fluorescence images show cell viability of both cell types after Live/Dead assay through the one-week culture period (Figure 3.10).

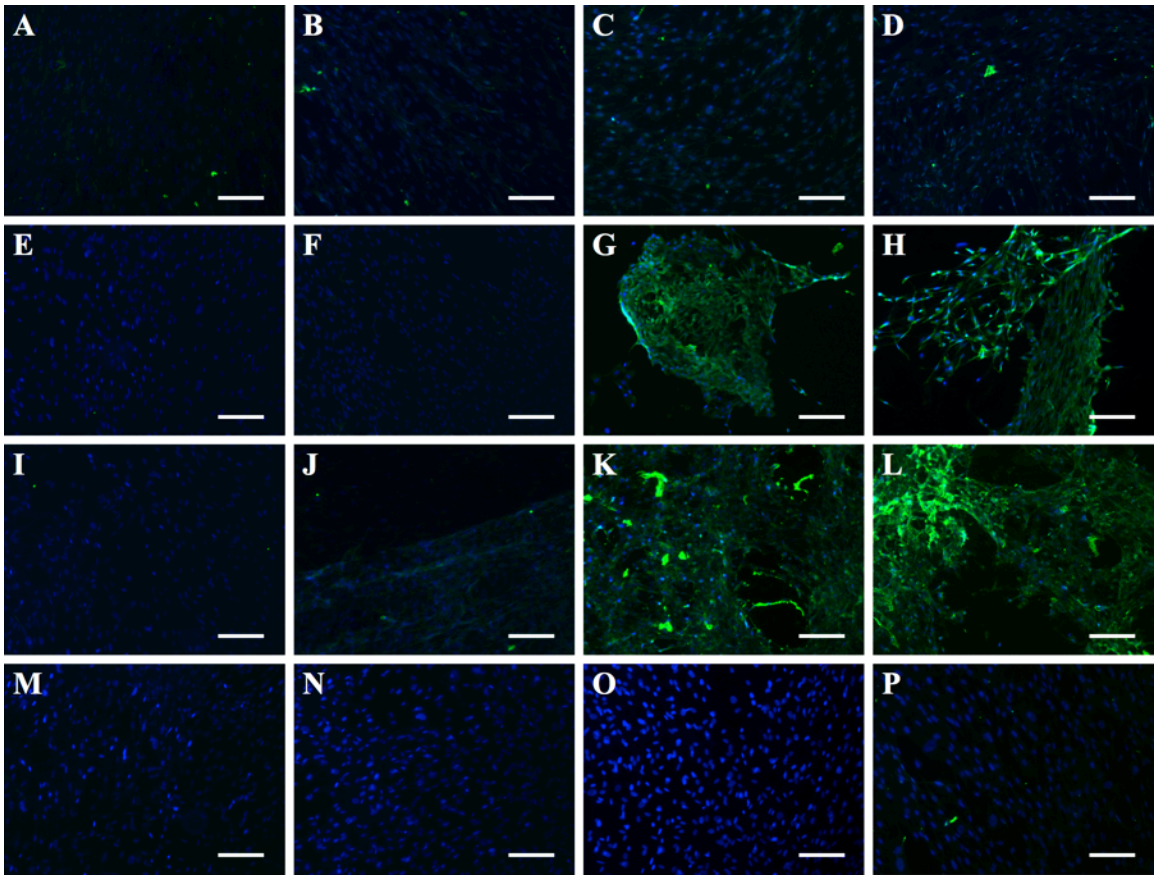

Figure 3.5: Immunofluorescence imaging of hADSCs at 7 days. Undifferentiated hADSCs in control DMEM (A, E, I, M), hADSCs cultured in DMEM with 5 µM ATRA (B, F, J, N), in defined KSFM (C, G, K, O), and defined KSFM with 5 µM ATRA (D, H, L, P) after 7 day differentiation regimen. Green fluorescence is indicative of CK-17 protein expression in the first row (A-D), CK-20 expression in the second row (E-H), and UPIb expression in the third row (I-L). Non-specific binding of second antibody (no primary Ab control) was tested for each cell group with no background staining detected in the fourth row (M-P). Scale bar = 100 µm.

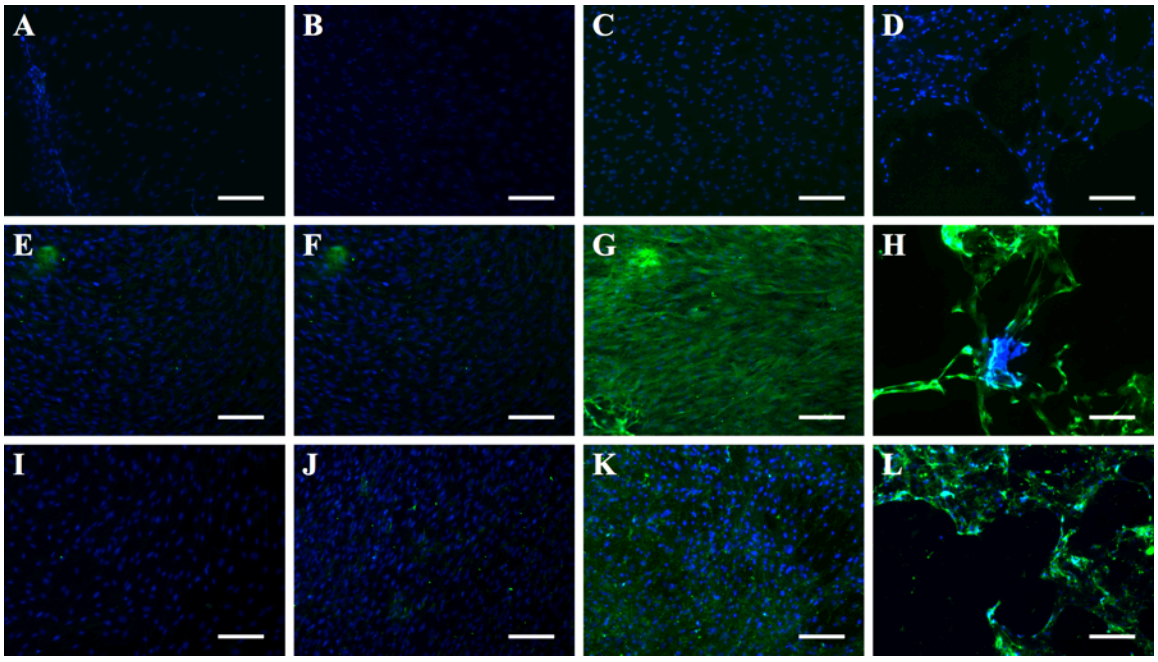

Figure 3.6: Immunofluorescence imaging of hADSCs at 14 days. Undifferentiated hADSCs in control DMEM (A, E, I), hADSCs cultured in DMEM with 5 µM ATRA (B, F, J), in defined KSFM (C, G, K), and defined KSFM with 5 µM ATRA (D, H, L) after 14 day differentiation regimen. Green fluorescence is indicative of CK-17 protein expression in the first row (A-D), CK-20 expression in the second row (E-H), and UPIb expression in the third row (I-L). Scale bar = 100 µm.

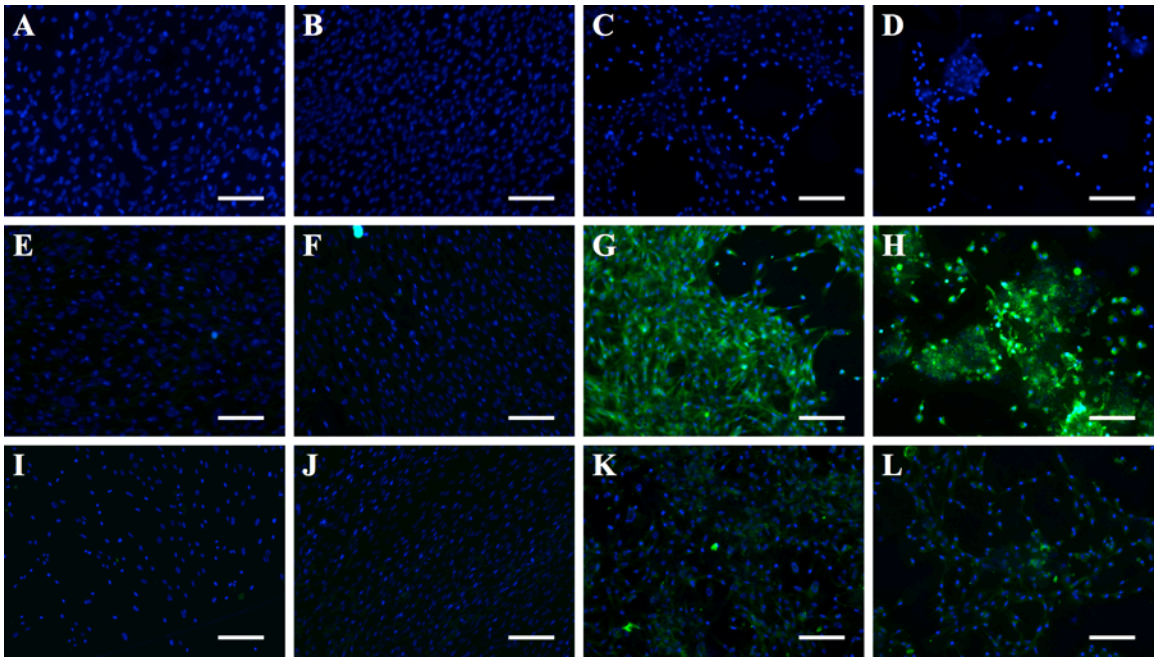

Figure 3.7: Immunofluorescence imaging of hADSCs at 21 days. Undifferentiated hADSCs in control DMEM (A, E, I), hADSCs cultured in DMEM with 5 µM ATRA (B, F, J), in defined KSFM (C, G, K), and defined KSFM with 5 µM ATRA (D, H, L) after 21 day differentiation regimen. Green fluorescence is indicative of CK-17 protein expression in the first row (A-D), CK-20 expression in the second row (E-H), and UPIb expression in the third row (I-L). Scale bar = 100 µm.

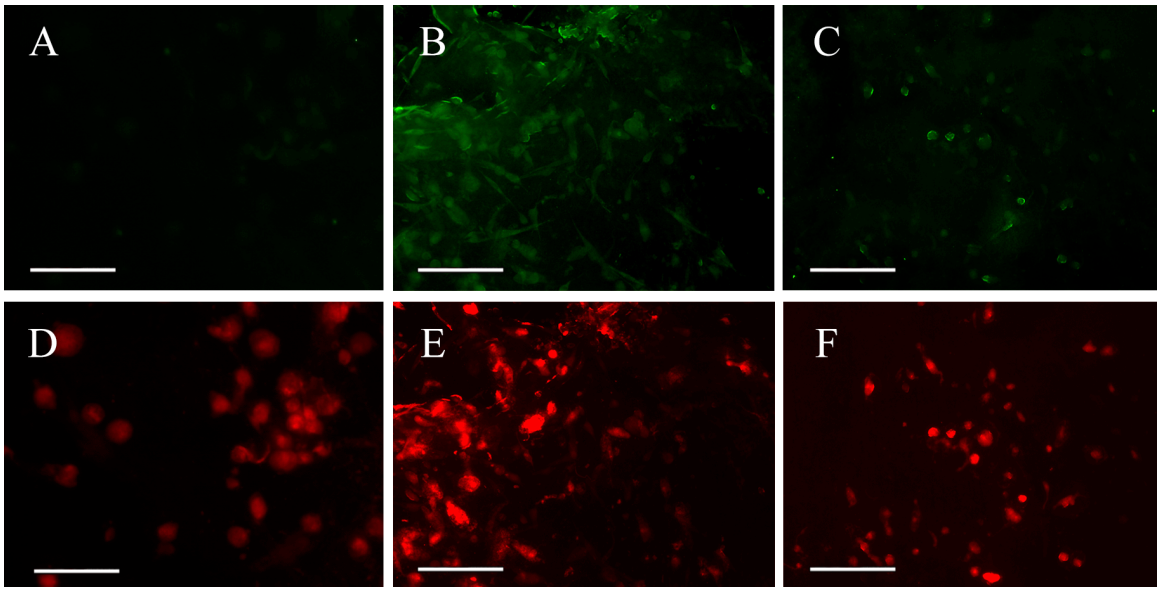

Figure 3.8: Expression of CK-17 in hADSCs within 2 mg/mL collagen type I hydrogel cultured in DMEM (A), in KSFM with rat BSMC layer (B), and in KSFM without rat BSMC layer (C). Additionally, hADSCs were also stained using Celltracker Red to visualize within collagen gel (D-F). Scale bar = 100 μm.

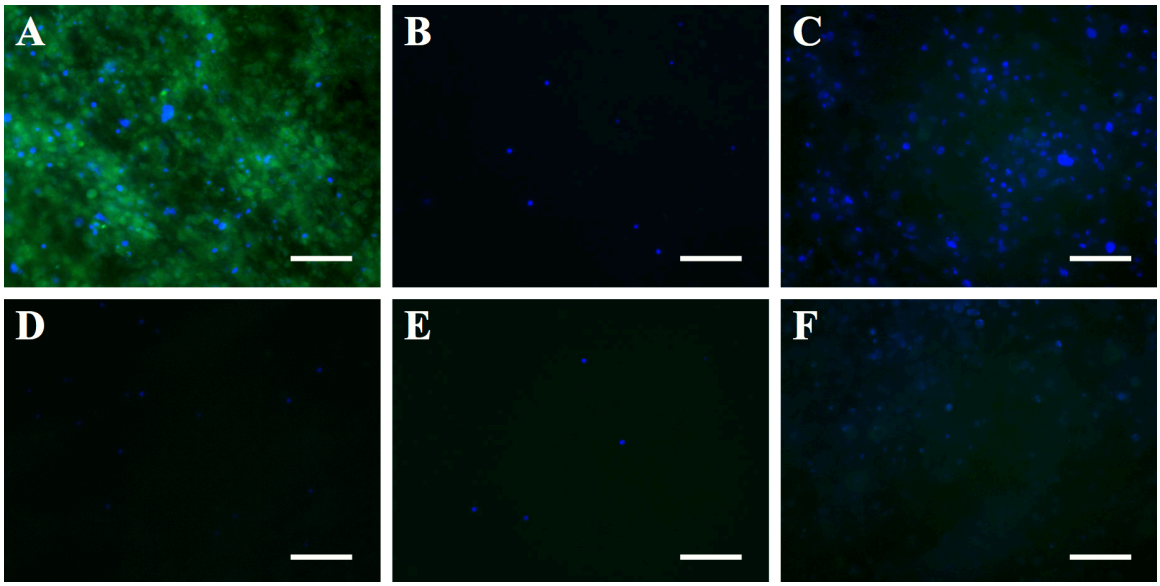

Figure 3.9: Comparison of CK-17, CK-20, and UPIb protein expression in hADSCs in 3D collagen gel culture after 7 days. CK-17 expression was present in hADSCs cultured in KSFM (A), while expression of CK-20 (B) and UPIb (C) were absent. Protein expression was absent in undifferentiated hADSC samples cultured under DMEM. DAPI was used for counterstain of cell nuclei. Scale bar = 100 μm.

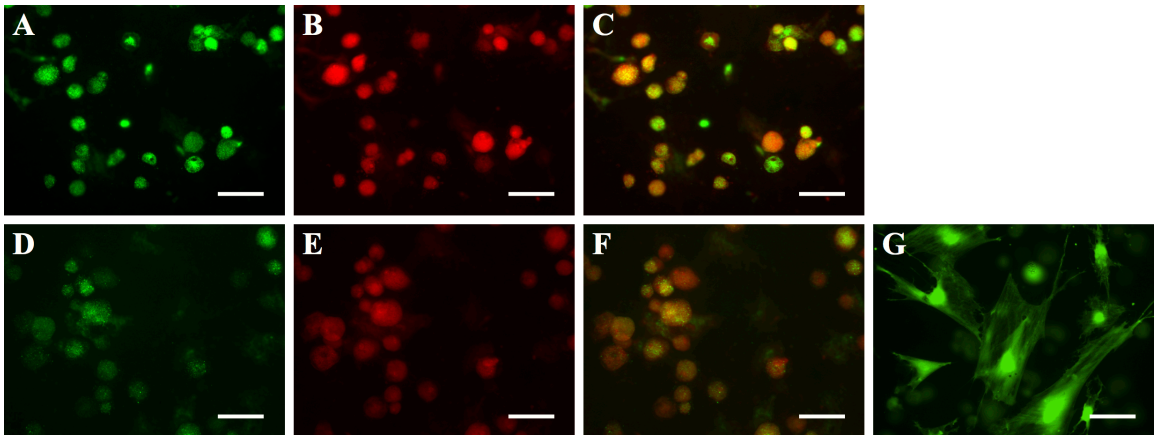

Figure 3.10: Live/Dead assay of hADSCs. Human ADSCs were encapsulated within 2 mg/mL collagen type I hydrogel and cultured in DMEM (A-C) and in KSFM (D-F) with rat BSMC layer (G). Since hADSCs were cultured in Celltracker Red (B, E), dead cells were identified via overlay (C, F) where green and red cells indicated live cells, and red cells indicated dead. Scale bar = 100 μm.

3.4. Discussion

New developments in urinary tissue engineering methodologies have provided potential alternative solutions to the current standard of using gastrointestinal tissue and buccal mucosa with inherent mismatches in biological properties and function. Of these alternative solutions, recent methods in literature have focused on differentiation of mesenchymal-derived adult stem cells, which includes hADSCs, using serum-based media in co-culturing methods or conditioned medium from multiple cell lines and had varied success in terminal transdifferentiation towards urothelial lineage [136-139]. Liu et. al. [137] reported that differentiation of hADSCs towards urothelial lineage as evidenced by urothelial-specific CK-18 and UPIb expression was a result of direct co-culture with human urothelial cells and not of indirect co-culture or conditioned media. However, Shi et. al. reported increased CK-18 and UPIb expression in hADSCs cultured under conditioned medium from human ureter urothelial cell culture [138]. From these studies, the particular mechanisms that drive hADSC differentiation towards urothelial lineage are not clear, though both studies conclude that it may be due to the local environment or secretion of cytokines from the urothelial cells. However, to elucidate the feasibility of hADSCs as alternative cell source for urothelium in clinical translation, it is important to avoid the use of autologous urothelial cells [152] and serum-based media [156]. We show that hADSCs cultured in defined KSFM exhibited an increase in mRNA expression for urothelial-specific markers CK-20, UPIb, and UPII as well as presence of CK-20 and UPIb proteins in hADSCs as early as 7 days and up to 21 days. Furthermore, rhodamine-phalloidin staining (Figure 3.1) and phase-contrast imaging

(Figure 3.2) revealed that hADSCs appear morphologically similar to UROtsa cells in culture. These outcomes were previously obtained only when hADSCs were subjected to direct co-culture or conditioned media with urothelial cell lines [137-139]. The results of the present study suggest that defined KSFM with its soluble chemical factors can be used as a viable alternative method to drive differentiation of hADSCs towards urothelial lineage in lieu of serum-based media previously described in literature.

Urothelial cells in native tissue express cytokeratins of various subsets, which are intermediate filament proteins found within the cytoskeleton [160]. Studies have shown that the expression of cytokeratin types is highly dependent on location within the urothelial layers; CK-17 is expressed only within basal cells, while CK-20 is expressed solely in umbrella cells [160]. This expression profile in cytokeratins is typically used to demarcate the transition from basal to superficial transition in regenerating hyperplastic urothelium [161]. The results of the present study suggest that the expression of cytokeratins may be dictated by the extracellular matrix presence, physical environment surrounding, and presence of KSFM. Specifically, CK-20 mRNA and protein expression significantly increased in hADSCs under both KSFM and KSFM with ATRA conditions compared to control hADSCs. However, we noted the downregulation of CK-17 mRNA and (Figure 3.3) and protein expression (Figure 3.4-3.7) throughout all time points in hADSCs cultured in 2D on conventional TCPS. In contrast, cells encapsulated within collagen gel under KSFM expressed CK-17 (Figure 3.8, 3.9). Because this occurred both in the presence and absence of the BSMC feeder layer under KSFM supplementation, we speculate that the presence of bladder smooth muscle cells does not affect the expression

of CK-17 in hADSCs. Rather, results indicate that growth within 3D collagen matrix and supplementation with KSFM both contribute to the expression of CK-17 in hADSCs, and could possibly indicate that these hADSCs are differentiating towards a basal/intermediate urothelial lineage as opposed to umbrella cell types seen in 2D samples.

ATRA has been previously demonstrated to induce differentiation of adult stem cells toward epithelial lineage [165, 166], which was indicated by increased expression of cytokeratins [121, 166] and a morphology shift towards a monolayer, contact-inhibited growth profile [121]. In the present study, the addition of 5 μM ATRA caused hADSC to exhibit epithelial-like cell morphology (Figure 3.1), which is in agreement with a previous report [121]. However, compared to hADSCs cultured in defined KSFM, gene expression of CK-20 was significantly lower at all time points in hADSCs cultured in both DMEM and KSFM with ATRA (Figure 3.3). Qualitative analysis of western blotting and immunofluorescence results agree with gene expression results as marginal protein expression of CK-20 in hADSCs cultured with both DMEM and KSFM with ATRA (Figure 3.4-3.7) were observed. This result coupled with the high expression of CD90 and CD105 markers indicates greater retention of a stem-cell phenotype and a less pronounced shift towards an umbrella cell urothelial-like phenotype when cultured with ATRA. The results of the present study confirmed that 5 μM ATRA does appear to have an effect on cell morphology in vitro seen previously in literature. However, taken together with gene and protein expression results found in this present study, current evidence suggests that 5 μM ATRA supplemented in either DMEM and KSFM have

negligible effect on hADSC differentiation towards urothelial-specific cell phenotype, but rather may only be promoting epithelial cell differentiation.

Along with the morphology shift (Figure 3.2), another critical morphological difference to note was the actin filament profile between different cell types and culture conditions. Romih et. al. previously suggested that a morphological change in subcellular distribution of actin filaments can be an indication of a shift in differentiation of urothelial cells from basal and intermediate cells towards superficial umbrella cell [167]. In the present study, control hADSCs (Figure 3.1A) and hADSCs in DMEM and KSFM supplemented with ATRA (Figure 3.1D and 3.1E) exhibted a distinct network of bundled actin filaments. In contrast, both UROtsa cells (Figure 3.1B) and hADSCs cultured in defined KSFM alone (Figure 3.1C) exhibited undefined distribution of actin filaments. The similar distribution of actin filaments between UROtsa cells and hADSCs in defined KSFM, which was distinctly different from control and ATRA-supplemented samples, provides additional evidence indicating a morphological change in hADSCs towards a superficial urothelial cell phenotype.

One of the most critical markers of terminal urothelial phenotype is the presence of uroplakins. The uroplakin family of transmembrane proteins arrange into hexagonal asymmetric unit membrane (AUM) particles consisting of an inner (formed by UPIa/UPII heterodimers) and outer ring (formed by UPIb/UPIIIa heterodimers) that make up the majority of the apical membrane plaques of urothelial umbrella cells [53]. These crystalline network formed by uroplakin plaques is thought to contribute to the impermeability of the urothelium and modulation of bladder function [163] and are found

in both superficial and upper intermediate urothelial cell layers of native tissue [164] and primary urothelial cell cultures [53]. In the present study, a significant increase in UPIb expression compared to control was observed for cells cultured in defined KSFM with or without ATRA at the mRNA (Figure 3.3) and protein (Figure 3.5-3.7) levels. A significant increase in mRNA expression of UPII was also detected in hADSC cultured in defined KSFM at 7- and 21-day time points with ATRA and at 14- and 21-day time points without ATRA, though the fold-change in UPII expression was only minor (approximately 2-fold) in these samples. Along with upregulation of cytokeratin markers, these results provide additional evidence of differentiation of hADSCs towards more superficial urothelial populations.

3.5. Conclusion

In summary, exposure of hADSCs to defined KSFM induced differentiation toward a urothelial-like lineage after 14 days in culture. Evidence of morphology shifts and increased phenotypic marker expression has shown for the first time that hADSCs are capable of differentiation towards umbrella cells is possible without co-culturing or serum-containing medium [156]. Although we presented morphological data and significant evidence of differentiation towards urothelial phenotype, further research is necessary to conclusively prove that hADSCs can differentiate towards a *functional* urothelial cell type. This study lays the foundation for use of an alternative cell source with a serum-free differentiation protocol towards the goal of functional urothelial regeneration in 3D culture, which is pivotal in providing a complete solution to repair of damaged bladder. Future research will investigate the efficacy of pre-differentiated

hADSCs to replicate urothelial barrier function via transepithelial resistance measurement and dextran permeability assays and to characterize their interaction with bladder smooth muscle cells using 3D *in vitro* co-culture models.

CHAPTER FOUR

THE FABRICATION OF MULTILAYER UROTHELIAL TISSUE IN VITRO

4.1. Introduction

In pursuit of functional tissue regeneration, studies have turned to implantation of tissue-engineered constructs developed *in vitro* with limited success in replicating bladder physiology [7-9]. Hydrogels have also been explored in tissue regeneration as a method to deliver cells, provide essential growth factors, and control cell growth at a target site [132]. Though some success has been shown in regeneration of the urothelium using native urothelial cells [133, 134], their use and availability is severely restricted in cases of bladder cancer and disease [18]. The use of adult stem cells continues to be a challenge in replicating urothelial physiology, as it is not a straightforward task to mimic complex characteristics such as urothelial impermeability and rapid changes in the urothelial umbrella layer associated with bladder compliance and distention – which is especially the case for cells not initially suited for such purposes.

One particular method to create a multilayer tissue construct uses a layer-by-layer coating technique to deposit a nanoscale extracellular matrix (ECM) on cellular surfaces using fibronectin and gelatin [131]. The addition of fibronectin and gelatin films to the cell surface provides functionalization, the benefits of fibronectin towards promoting cell-adhesion [133], stable cell-cell interactions [134,135], and protection of the cells during multilayer tissue formation [131].

In the present study, we test the effects of culturing a 3D tissue construct with both hADSCs and UROtsa cells tissue using the fibronectin/gelatin coating technique [131]. After performing the layer-by-layer coating technique, the cells are transferred to a Transwell® growth membrane and cultured for 24 hours. Cell morphology and phenotype was studied via H&E staining and immunofluorescence on frozen sections, and dextran permeability assays were performed to examine barrier function of the multilayer tissue construct.

4.2. Materials and Methods

Cell culture.

Human adipose derived stem cells (hADSCs) were purchased from Lonza (PT-5006) and expanded in low D-glucose (1000 mg/L) DMEM (Life Technologies) supplemented with 10% fetal bovine serum (FBS, Fisher), 1% GlutaMAX (Life Technologies). For differentiation towards urothelial lineage, hADSCs at approximately $2.5x10^5$ cells/cm^2 were cultured in defined keratinocyte serum-free media with the growth supplement kit provided by the manufacturer (Life Technologies) for 14 days. hADSC between passages 3 and 7 were used in all experiments of the present study. UROtsa cells, an immortalized normal human urothelial cell line (kindly donated by the laboratory of Dr. Naoki Yoshimura, Department of Urology, University of Pittsburgh), were cultured in DMEM supplemented with 10% FBS, and GlutaMAX. All cells were cultured under standard cell culture conditions (sterile, humidified at 37°C, 5% CO_2)

Fabrication of multilayer cell constructs

In preparation for construct fabrication, bovine fibronectin (Sigma) and gelatin were dissolved in 50 mM Tris-HCl (pH: 7.4) to create a 0.2 mg/mL stock solution. To create multilayered hADSC constructs, undifferentiated (control) and differentiated hADSCs were coated in alternating layers of bovine fibronectin and gelatin via resuspension of cells in 0.04 mg/mL working solution. Cells were washed between each coating step by gentle resuspension in 50 mM Tris-HCl. After cells were coated in alternating layers (5 layers of fibronectin and 4 layers of gelatin), cells were suspended in cell culture media and were seeded in 12-well Transwell® inserts (Corning) coated in one layer of fibronectin (FN-coated). Undifferentiated and differentiated hADSCs without FNG coating were used as control. In a separate experiment, both UROtsa cells and membranes were coated with alternating layers of fibronectin and gelatin (5 layers of fibronectin and 4 layers of gelatin) or single fibronectin layer (FN-coated membrane). To create 8 layers of cells, $8.0x10^5$ hADSCs and $2.0x10^6$ UROtsa cells were required per well, respectively. For 2 layers of cells in hADSCs, $2.0x10^5$ cells were seeded per well. Cells were allowed to culture for 24 hours before further experiments were conducted.

Histology and immunofluorescence of multilayered cellular constructs

After the prescribed culture period, hADSCs and UROtsa cells were fixed on the Transwell® membrane using 10% neutral buffered formalin, followed by infiltration using 30% sucrose for cryoprotection. Samples were removed from the cell culture insert using a scalpel, and embedded in OCT for cryosectioning. Samples were stained with H&E to examine cellular morphology and images were taken using a microscope (Motic BA210) and Canon mounted camera (Canon EOS Rebel SL1). Glycosaminoglycans

(GAGs) were stained with 1% Alcian Blue in 3% acetic acid at pH 2.5 with s248-Nuclear Fast Red 0.1% Kernechtrot (Poly Scientific R&D Corp.) as counterstain following manufacturer's protocol. For immunofluorescence staining, UROtsa samples were subjected to blocking solution (5% non-fat dried milk in PBS) at room temperature for 30 minutes before incubation in mouse monoclonal anti-cytokeratin 17 (CK-17, Sigma, C9179), goat polyclonal anti-cytokeratin 20 (CK-20, Santa Cruz Biotechnology, SC-17113), goat polyclonal anti-uroplakin Ib (UPIb, SCBT, SC-15174), or goat polyclonal anti-ZO1 (Santa Cruz Biotechnology, SC-11111) at 4°C overnight. All primary antibodies were used at a 1:100 dilution in PBS. Following primary antibody conjugation, species-specific fluorescently labeled (FITC or Alexa Fluor 488) secondary antibody was added at a 1:1000 dilution in PBS and incubated at room temperature for one hour. Cell nuclei were then stained with 300 nM DAPI in PBS for 5 minutes. Fluorescence images were taken on a Nikon epifluorescence microscope (TE-2000S) and a Hamamatsu digital camera (C4742-95).

Permeability measurements using fluorescent dextran

The barrier function of hADSC and UROtsa multilayer constructs was determined via measurement of fluorescently labeled dextran molecules in the lower well of the Transwell® culture system. Fluorescein isothiocyanate (FITC) conjugated (4 kDa) and Rhodamine B conjugated (70 kDa) dextran in cell culture medium (2 mg/mL concentration, 300 μL per well) was placed on top of a cellular multilayer cultured in Transwell® inserts, and wells were filled with 1 mL pre-warmed culture medium without tracer to create a liquid interface. Inserts without cells were used as control. Fluorescence

measurements of culture medium (1 mL) taken from the abluminal side of Transwell® inserts at various time points over a 24-hour period using a Biotek Synergy 4 microplate reader at 485 nm and 520 nm excitation wavelengths and 544 nm and 590 nm emission wavelengths for FITC and Rhodamine B, respectively.

Cell Viability Assessment

The viability of UROtsa cells was qualitatively assessed using a Live/Dead assay kit (Life Technologies) and following the manufacturer's instructions. Briefly, culture medium was removed and cells were washed 3 times using PBS before adding ethidium homodimer-1 (4 μM) and calcein AM (2 μM) dye mixture for 5 minutes. The membranes were cut and removed from the Transwell® insert and imaged (Nikon Eclipse TE 2000-S).

4.3. Results

Histology and immunofluorescence of multilayered cellular constructs

H&E stained 8-layered undifferentiated/uncoated hADSCs showed uniform, multilayered distribution (Figure 4.1.A). Conversely, both undifferentiated/coated hADSCs (Figure 4.1.B) and differentiated/uncoated hADSCs (Figure 4.1.C) exhibited aggregation with incomplete multilayering and lack of defined cell-cell adhesion. Cellular detachment from the membrane and severe aggregation was observed in differentiated/coated hADSCs (Figure 4.1.D) groups. Gross examination of the cellular construct showed visible aggregation of cells in undifferentiated/coated hADSCs, differentiated/uncoated hADSCs, and differentiated/coated hADSCs groups after 24

hours. When hADSCs were seeded at lower density (for 2 layers) cell aggregation similar to 8-layer conditions was observed in gross examination (images not shown), which correlated with observations shown in H&E stained sections (Figure 4.2).

UROtsa exhibited uniform cellular distribution and multilayer formation in both coated cells/FNG-coated membrane (Figure 4.3.A) and coated cells/FN-coated membrane (Figure 4.3.B) groups. Uncoated cells on FNG-coated membrane (Figure 4.3.C) displayed a scattered, multilayer morphology with cellular aggregation seen in gross examination of the Transwell® membrane. Uncoated cells on FN-coated membrane displayed some adhesion to the membrane on the basal layer with lack of cell-cell adhesion in superficial layers. Gross examination of all UROtsa cells shows

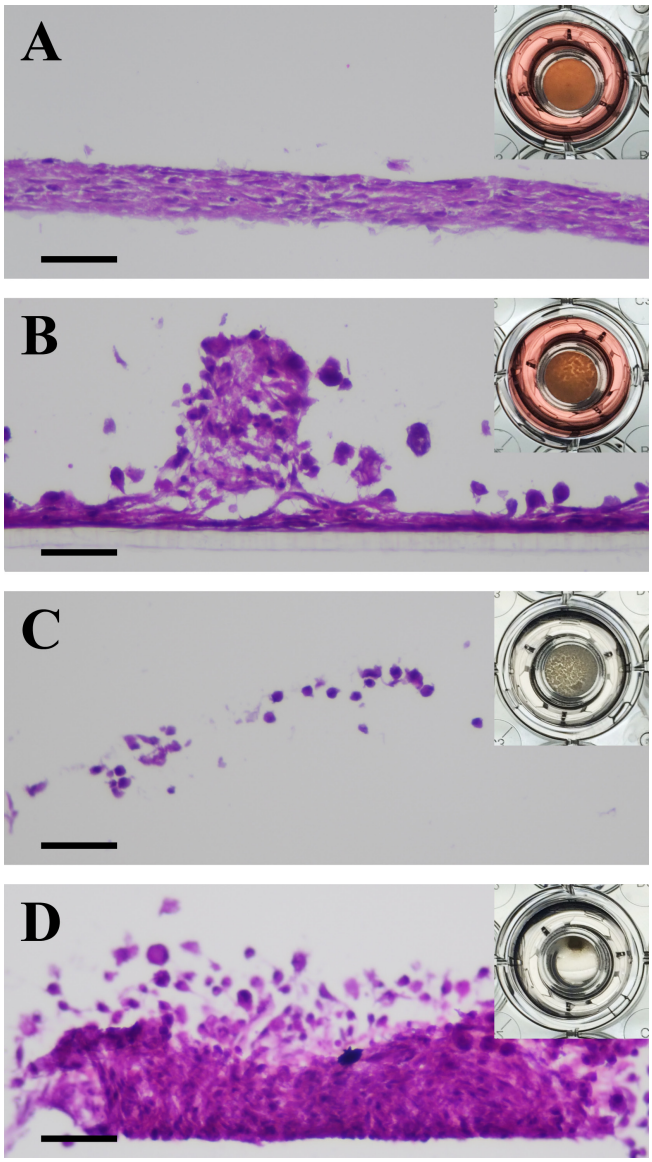

Figure 4.1: Cell morphology of 8-layered hADSC constructs. Frozen sections of fixed differentiated/undifferentiated and coated/uncoated cells on FN-coated Transwell® membranes were stained using H&E. Cellular adhesion to construct was uniform in undifferentiated hADSCs (A). Cell aggregation was apparent in undifferentiated/coated hADSCs (B), differentiated/uncoated hADSCs (C), and differentiated/coated hADSCs (D) Top right images show gross examination of cell aggregation. Scale bar = 100 μm.

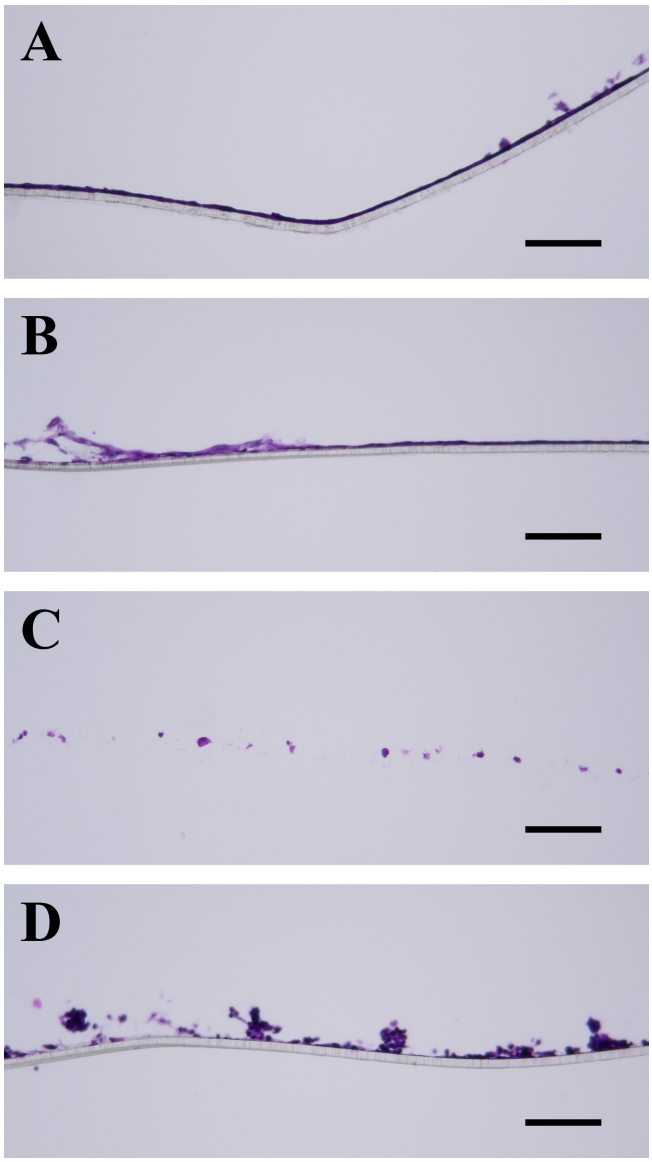

Figure 4.2: Cell morphology of 2-layered hADSC constructs. Frozen sections of fixed differentiated/undifferentiated and coated/uncoated hADSCs on FN-coated Transwell® membranes were stained using H&E. Cellular adhesion to construct was uniform in undifferentiated hADSCs (A). Cell aggregation was apparent in undifferentiated/coated hADSCs (B), differentiated/uncoated hADSCs (C), and differentiated/coated hADSCs (D). Scale bar = 100 μm.

generally homogenous cellular distribution with some aggregation. Alcian blue staining in both hADSC and UROtsa cell multilayers showed absence of GAGs in any samples after 24 hour growth period in Transwell® membrane (Figure 4.4, 4.5)

Fluorescence imaging revealed strong protein expression of CK-17 throughout multilayer construct of UROtsa cells in all samples after 24-hour culture period with no particular localization (Figure 4.6). Distinct CK-20 protein expression was visible in all samples with strong expression localized in superficial layers of UROtsa cells (Figure 4.7). Protein expression of UPIb was present in all samples with no particular localization in any cell layer for coated cells/FNG-coated membrane (Figure 4.8.A). Coated cells/FN-coated membrane (Figure 4.8.B), uncoated cells/FNG-coated membrane (Figure 4.8.C), and uncoated cells/FN-coated membrane (Figure 4.8.D) expressed UPIb though at lesser intensity. For coated cells/FNG-coated membrane (Figure 4.9.A) and coated cells/FN-coated membrane (Figure 4.9.B), protein expression of ZO-1 was well defined and distributed in intracellular junctions. Uncoated cells/FNG-coated membrane (Figure 4.9.C) and uncoated cells/FN-coated membrane (Figure 4.9.D) had less-defined expression of ZO-1 after 24-hour culture in 3D construct.

Cell Viability Assessment

Qualitative assessment of the Live/Dead assay on UROtsa cells performed 24 hours after fibronectin/gelatin coating demonstrated cell viability in both coated and uncoated samples (Figure 4.10). Quantitative assessment via comparison of relative intensity values using ImageJ shows 93.0% and 85.0% live cells in uncoated and coated samples respectively.

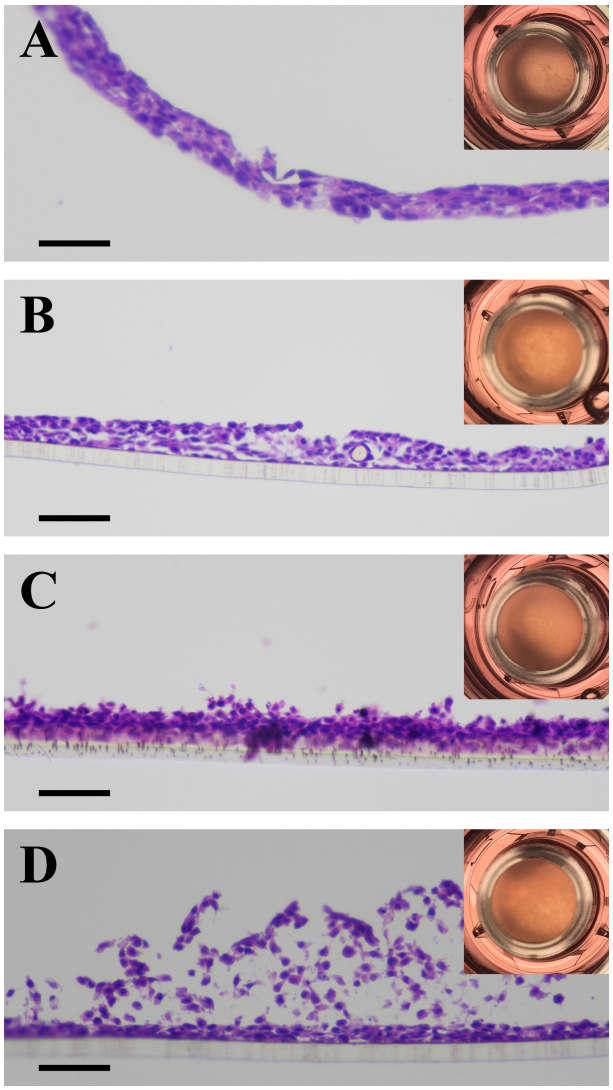

Figure 4.3: Cell morphology of coated and uncoated 8-layered UROtsa constructs. Frozen sections of fixed coated and uncoated UROtsa cells on FN-coated or FNG-coated Transwell® membranes were stained using H&E. Cellular adhesion to construct was uniform in coated cells in both FNG-coated (A) and FN-coated membranes (B). Uncoated cells in FNG-coated (C) and FN-coated membranes (D) displayed a scattered appearance with cellular aggregation. Top right images show gross examination of cell aggregation. Scale bar = 100 μm.

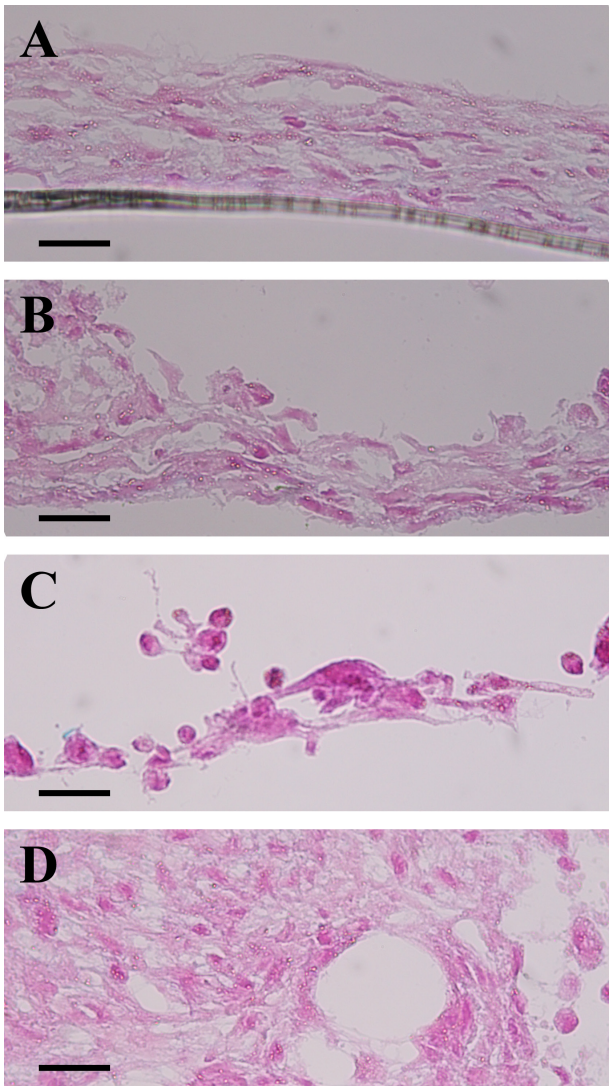

Figure 4.4: Staining for GAG content of 8-layered hADSC constructs. Frozen sections of fixed differentiated/undifferentiated and coated/uncoated cells on FN-coated Transwell® membranes were stained using Alcian blue and counterstained with Nuclear Fast Red. Alcian blue stain did not show presence of GAG content in undifferentiated/uncoated hADSCs (A), undifferentiated/coated hADSCs (B), differentiated/uncoated hADSCs (C), or differentiated/coated hADSCs (D). Scale bar = 50 μm.

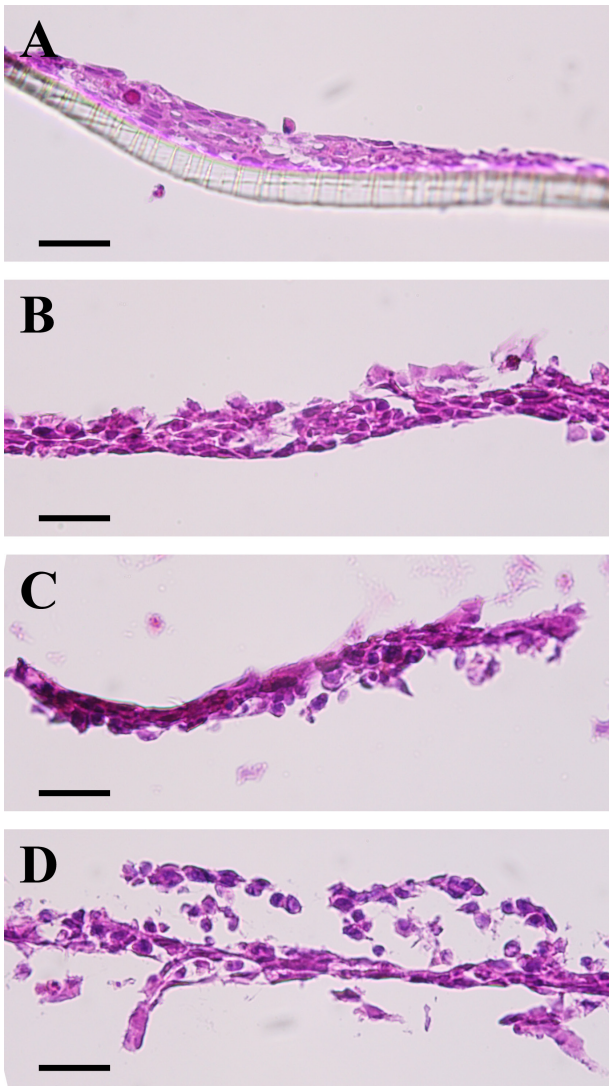

Figure 4.5: Staining for GAG content of 8-layered UROtsa constructs. Frozen sections of fixed coated and uncoated UROtsa cells on FN-coated or FNG-coated Transwell® membranes were stained using Alcian blue and counterstained with Nuclear Fast Red. GAG content was not detected in coated cells on FNG-coated (A) and FN-coated membranes (B), or in uncoated cells in FNG-coated (C) and FN-coated membranes (D). Scale bar = 50 µm.

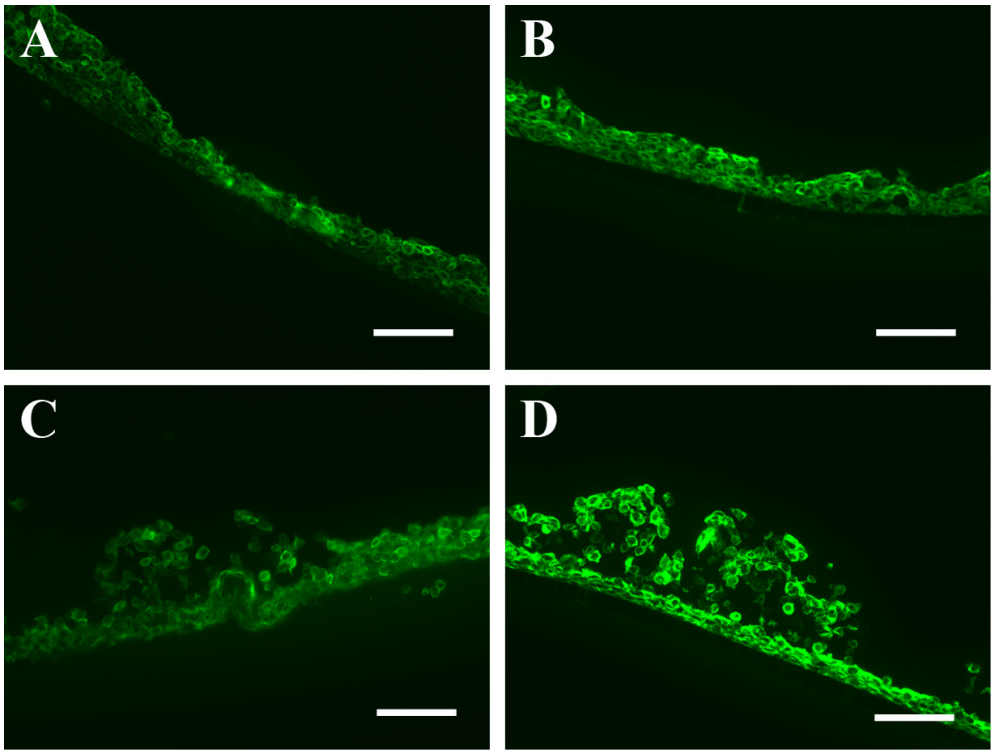

Figure 4.6: Fluorescence imaging for CK-17 in 8-layered UROtsa construct. Frozen sections of fixed coated and uncoated cells on fibronectin-coated or fibronectin/gelatin-coated Transwell® membranes were stained for CK-17 protein. Expression of CK-17 was uniform in all samples: coated cells/FNG-coated membrane (A), coated cells/FN-coated membrane (B), uncoated cells/FNG-coated membrane (C), and uncoated cells/FN-coated membrane (D). Scale bar = 100 μm.

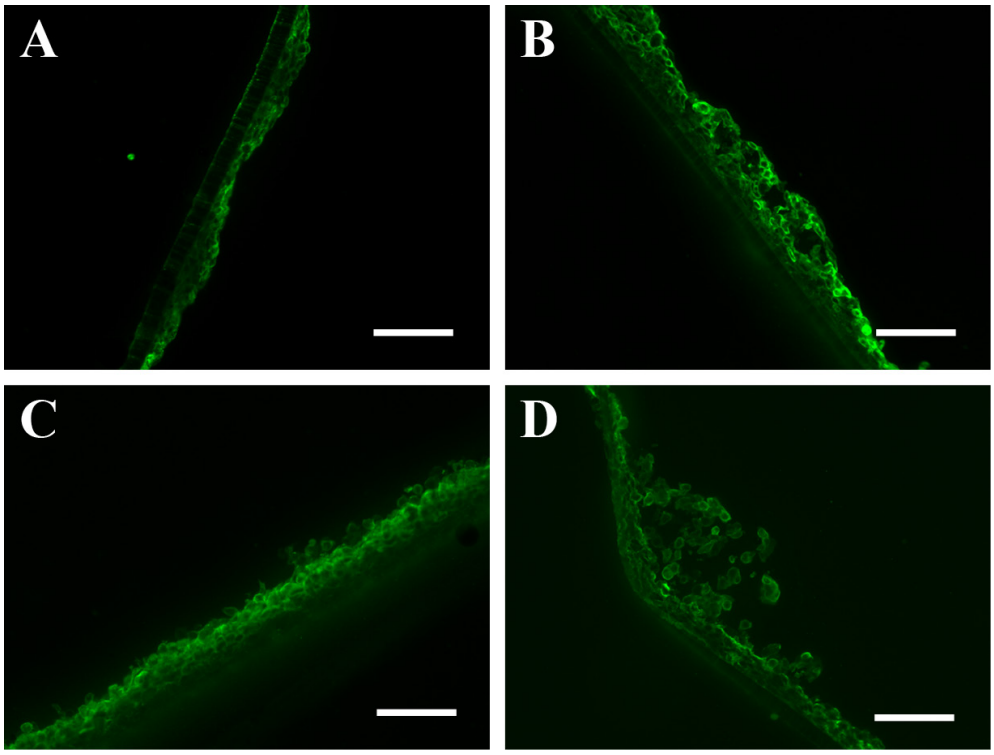

Figure 4.7: Fluorescence imaging for CK-20 in 8-layered UROtsa construct. Frozen sections of fixed coated and uncoated cells on fibronectin-coated or fibronectin/gelatin-coated Transwell® membranes were stained for CK-20 protein. Expression of CK-20 was generally distributed towards luminal side in all samples: coated cells/FNG-coated membrane (A), coated cells/FN-coated membrane (B), uncoated cells/FNG-coated membrane (C), and uncoated cells/FN-coated membrane (D). Scale bar = 100 μm.

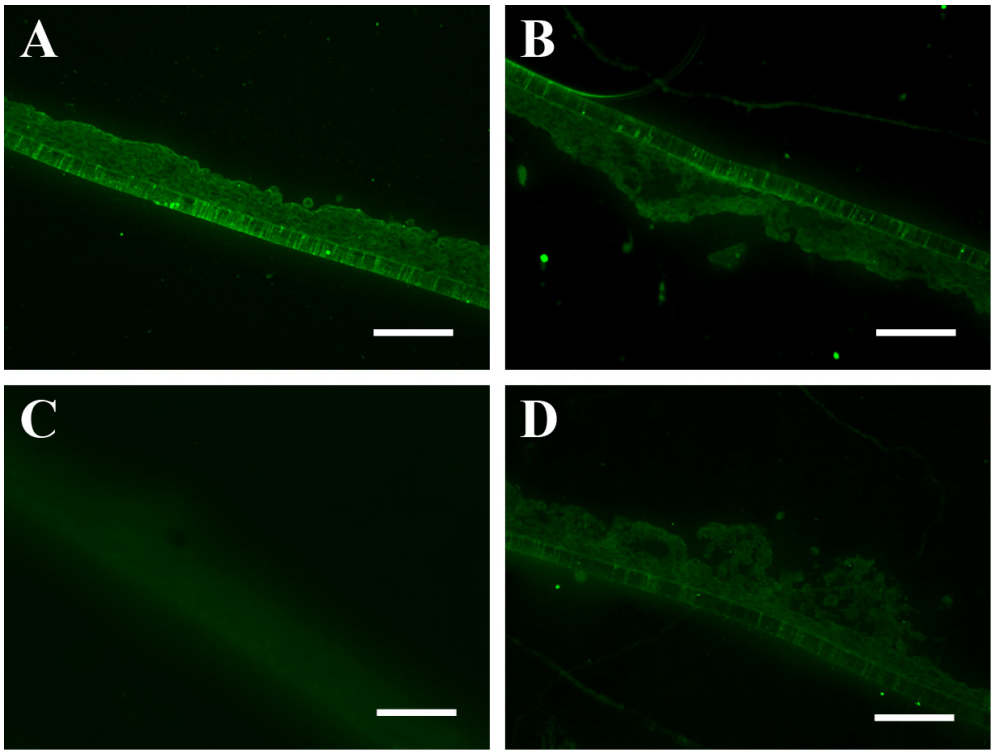

Figure 4.8: Fluorescence imaging for UPIb in 8-layered UROtsa construct. Frozen sections of fixed coated and uncoated cells on FN-coated or FNG-coated Transwell® membranes were stained for UPIb protein. Expression of UPIb was present in all samples, though most expressed in coated cells/FNG-coated membrane (A). Coated cells/FN-coated membrane (B), uncoated cells/FNG-coated membrane (C), and uncoated cells/FN-coated membrane (D) had lower expression qualitatively. Scale bar = 100 μm.

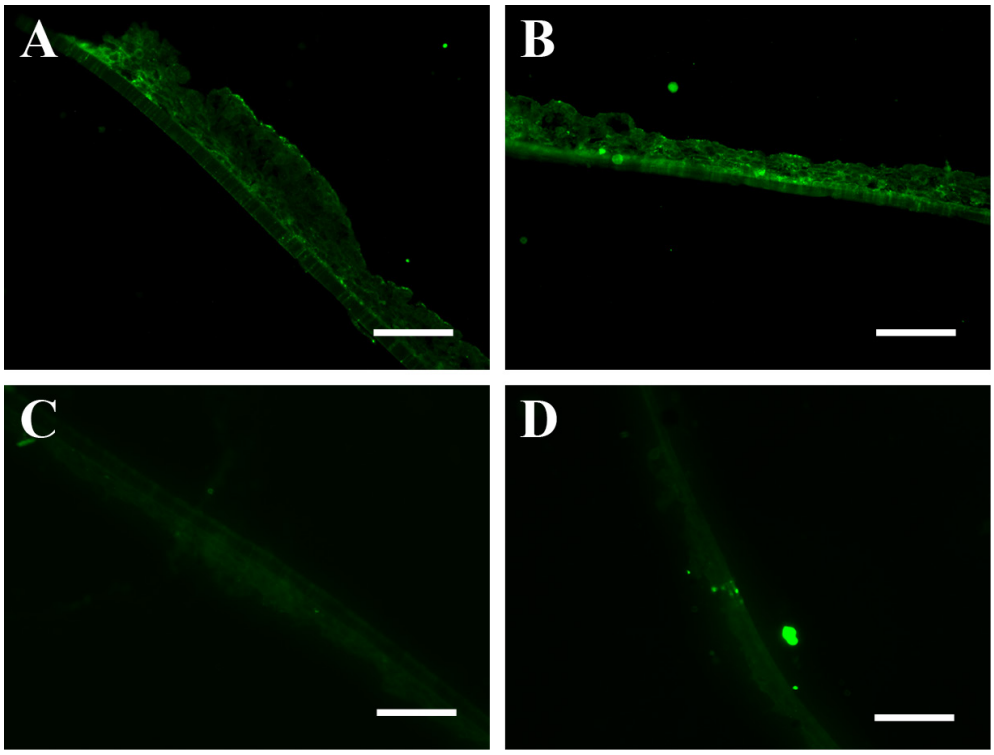

Figure 4.9: Fluorescence imaging for ZO-1 in 8-layered UROtsa construct. Frozen sections of fixed coated and uncoated cells on FN-coated or FNG-coated Transwell® membranes were stained for ZO-1 protein. Expression of ZO-1 was generally distributed in junctions between cells in coated cells/FNG-coated membrane (A) and coated cells/FN-coated membrane (B) samples. Uncoated cells/FNG-coated membrane (C) and uncoated cells/FN-coated membrane (D) had weaker and less-defined expression. Scale bar = 100 μm.

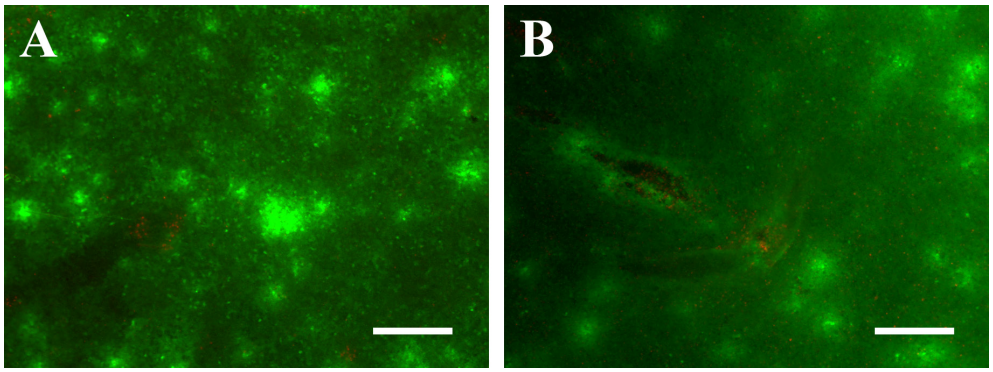

Figure 4.10: Live/Dead Imaging on UROtsa Cells. Imaging of apical surface of coated and uncoated UROtsa cells on FNG-coated Transwell® membranes. Merged image displays live cells stained green and dead cells stained red. Scale bar = 200 μm.

Permeability measurements using fluorescent dextran

Fluorescence measurements of dextran molecules diffused into the lower well of the Transwell® culture system over a 24-hour period showed significantly lower readings in both differentiated/undifferentiated and coated/uncoated hADSCs compared to the blank well samples. Comparison between coated/uncoated and differentiated/ undifferentiated groups after 24 hours showed similar effectiveness in preventing passive diffusion of dextran molecules (Figure 4.11). In UROtsa cells, preliminary results indicate similar trends to that of hADSCs showing differences in dextran permeability between blank samples and cell-seeded samples throughout measurements taken over 24 hours, but no differences between combinations of cell-coating and well-coating samples. Quantitative comparison of fluorescence values for UROtsa groups showed permeability was roughly between 45% and 50% for 4 kDa dextran and between 25% and 30% for 70 kDa dextran compared to the well without seeded cells (Figure 4.12).

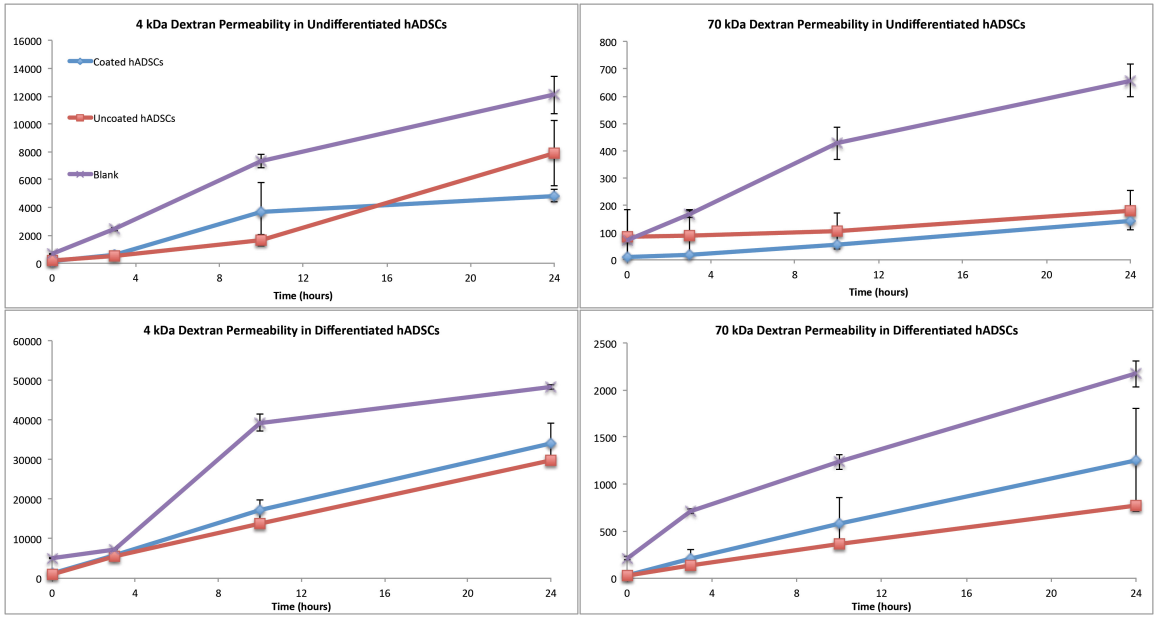

Figure 4.11: Dextran permeability in hADSCs. Fluorescence measurements for 4 kDa FITC-conjugated and 70 kDa Rhodamine B-conjugated dextran permeability taken over 24 hours in undifferentiated (top) and differentiated (bottom). Vertical axis numbers are arbitrary fluorescence values measured at 544 nm and 590 nm emission wavelengths for FITC and Rhodamine B respectively. Error bars indicate ±1 S.D.

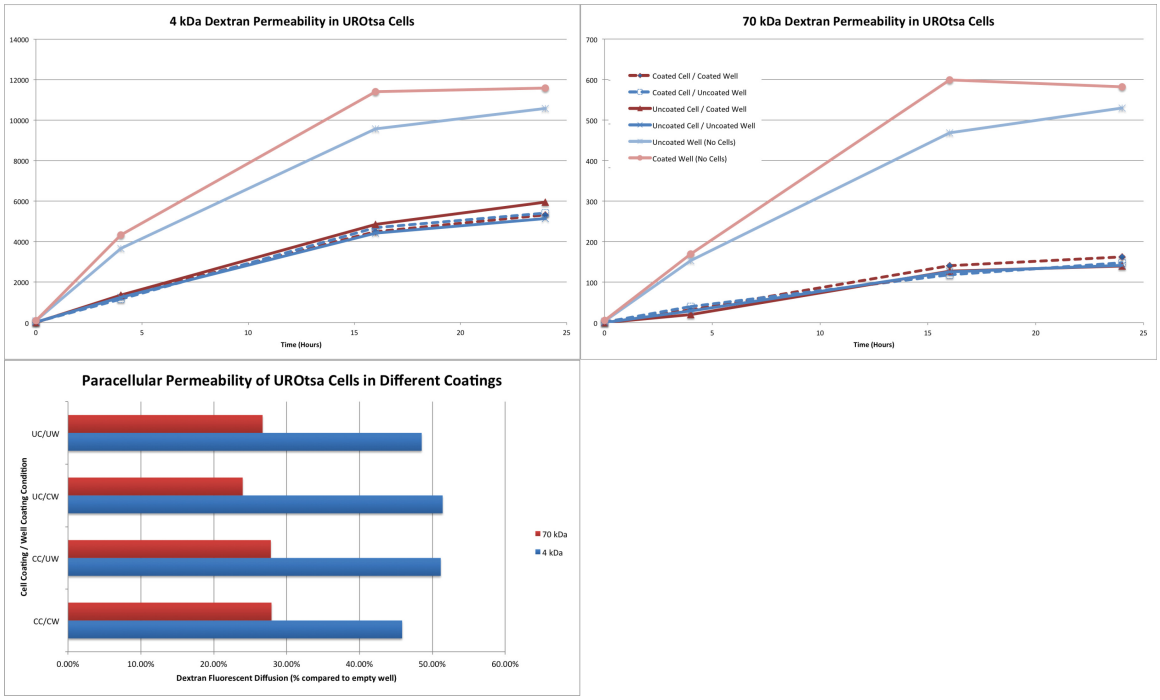

Figure 4.12: Dextran permeability in UROtsa. Fluorescence measurements for 4 kDa FITC-conjugated (top-left) and 70 kDa Rhodamine B-conjugated (top-right) dextran permeability taken over 24 hours. Vertical axis numbers are arbitrary fluorescence values measured at 544 nm and 590 nm emission wavelengths for FITC and Rhodamine B respectively. Permeability percent ratio was compared for 24-hour time point between cell samples under different coating combinations and empty wells (bottom-left).

4.4. Discussion

The objective of the present study is to develop a multilayer culture construct of urothelial cells differentiated from hADSCs for functional tissue regeneration. Previously, several cell culture models have been developed to recreate characteristics of native urothelial tissue [52, 125-127]. Shiroyanagi et al. [51, 52] reported the preparation of transplantable urothelial cell sheets using canine harvested urothelial cells on temperature sensitive PIPAAm-bonded surfaces with stratification obtained using cell culture medium containing FGF-7 and the 3T3 feeder layer method. In the present study, application of a layer-by-layer fibronectin/gelatin coating technique [131] to both UROtsa cells and Transwell® growth membrane resulted in a multilayer tissue construct with some characteristics of native bladder urothelium in both morphology (Figure 4.3) and phenotype (Figure 4.6-4.9). Although cellular multilayers developed in all groups (uncoated cells/FNG-coated cells and FN-coated membrane/FNG-coated membrane), the results of H&E staining indicated well-developed, cohesive urothelial-like tissue with presence of tight junction proteins, ZO-1 only in FNG-coated cells grown on FNG-coated membranes (Figure 4.9).

To explore the feasibility of developing an *in vitro* urothelial cell construct that could mimic native tissue function without the use of autologous urothelial cells [18] and serum-based media [29], we explored 3D tissue culture with urothelial-differentiated hADSCs to determine their functionality *in vitro* as compared to UROtsa cells. Our previous studies demonstrated that hADSCs cultured in defined KSFM could develop urothelial-like morphology and phenotype in 2D cell culture evidenced by an increase in

mRNA expression for urothelial-specific markers CK-20, UPIb, and UPII as well as presence of CK-20 and UPIb proteins. Preliminary results indicated that using the FNG-coating methods have detrimental effects on multilayer formation of the coated and differentiated hADSCs. Specifically, although undifferentiated, uncoated hADSCs display a well-developed multilayer construct (Figure 4.1A), uncoated/differentiated and coated/undifferentiated hADSCs display slight aggregation of the cells after 24hours visible in both the H&E images and gross examination, which could be attributed to preferential cell-cell contact in differentiated hADSCs or adhesion to the fibronectin/gelatin matrix in coated hADSCs. This effect appears to be amplified in the coated/differentiated hADSCs, in which the cells aggregate to form a cluster as seen in the gross examination image (Figure 4.1D). When the procedure was repeated with fewer cells (enough for 2 layers, instead of 8), similar results were obtained as 8-layer samples where a cohesive cellular layer was obtained in undifferentiated/uncoated hADSCs (Figure 4.2A), while scattered growth was seen in the remaining samples (Figure 4.2B-D) showing that the initial seeding density of hADSCs in Transwell® membranes does not necessarily contribute to cellular aggregation.

To explore the effects of the fibronectin/gelatin-coated urothelial cell construct on urothelial-like cells *in vitro*, combinations of uncoated/FNG-coated UROtsa cells and FN-coated/FNG-coated Transwell® membranes were explored. After a 24-hour growth period, cells of all four coating combinations showed multilayer growth with minimal cellular aggregation in gross examination (Figure 4.3). In FNG-coated cell/FNG-coated membrane, good structural stability and homogenous multilayer growth can be clearly

seen in H&E sections with deterioration of such qualities as shown in other groups when omitting the cell and membrane coating. In the uncoated cell/uncoated membrane, cellular detachment can be seen in the apical layers (Figure 4.3D). These results provide evidence that FNG-coating of both cells and the growth membrane may be required for proper development of multilayer tissue construct in urothelial-like cells.

Native urothelial cells express various forms of cytokeratins and uroplakins of various subsets, which contribute to the structural integrity and functionality of the cell [14, 34, 36], and expression of particular protein types is dependent on location within the stratified urothelium. For example, expression of CK-17 can be seen in basal and intermediate cells, while CK-20 and uroplakins subtypes are typically expressed in superficial cells of native tissue [34, 38]. In our previous study (Chapter 3), results suggested that the influence of the ECM and physical environment might determine the differential expression of cytokeratins and uroplakins in cell culture. All samples from the present study showed expression of CK-17 in all layers of the multilayer construct after 24-hour culture in Transwell® membranes. Furthermore, stronger expression of CK-20 in superficial cells can be seen compared to basal cells in all samples except the uncoated-cell/FN-coated membrane sample providing evidence that multilayer differentiation begins to occurs within 24-hours. Expression of UPIb appears throughout all layers of the multilayer construct with the lack of stratification in these results possibly due to the short culture time in 3D and the presence of uroplakins in all UROtsa cells during 2D cell culture. Overall, it appears that the extracellular matrix provided by the fibronectin/gelatin cell and membrane coating provides the necessary

microenvironment for UROtsa cells to develop a 3D multilayer construct and express urothelial-specific protein markers.

A critical function of the urothelial layer is to provide a barrier between the urine and the underlying smooth muscle tissue. In addition to the uroplakins preventing passive diffusion via apical membrane plaques on the umbrella cell surface, separation of the urine and underlying smooth muscle layer is also regulated by the presence of tight junction proteins such as occludin and ZO-1 [14]. Expression of ZO-1 in the cells with FNG-coated cells, and lack thereof in uncoated cells, indicate that presence of the ECM coating promotes cell-cell adhesion and tight junction formation within 24-hours. Dextran diffusion experiments [128, 129] were conducted to determine relative permeability through the multilayer tissue samples. Briefly, FITC-conjugated dextran at 4 kDa and Rhodamine B-conjugated dextran at 70 kDa were used to determine transcellular (passage through the apical and basolateral membrane of the cell) and paracellular (passage between intercellular spaces) permeability, respectively. For both UROtsa and 8-layer hADSC cells, preliminary results suggest that the presence of the cells reduce transport of dextran compared to Transwell® membranes without seeded cells. However, different FNG-coating conditions or cell differentiation states did not appear to have an effect on permeability. Although not clearly visible in the histological examination, single-layered cells were present in areas of the Transwell® insert that appear to show little to no aggregation upon gross examination. Cells and ECM present in these areas may contribute to the slower diffusion of fluorescent dextran across the Transwell® membrane over time. Along with evidence of cellular aggregation in examination of the

multilayer morphology, these results suggest that certain essential components for epithelial development, such as cell number or provision of growth factors, or maturation time is lacking to create a well-developed tissue construct capable of providing a barrier function without cellular aggregation. According to a study by Janssen et al., one possibility is the lack of glycosaminoglycan (GAG) presence, particularly chondroitin sulfate, on the surface of the multilayer tissue construct, which has been shown to reduce urothelial permeability in native human and porcine bladder [130]. From the results of the Alcian blue stain, evidence indicates that neither hADSCs nor UROtsa are producing GAGs in the multilayer construct after 24 hours. The time course for cells to begin self-production of GAGs in the present model are currently unclear, however the lack of GAG content may provide another explanation for the incomplete barrier function.

4.5. Conclusion

Preliminary results show that when layer-by-layer FNG coating was applied aggregation of differentiated hADSCs begins to occur within 24 hours of cell culture. UROtsa results suggest that coating of the Transwell® membrane prior to cell seeding could be an important factor in preventing cellular aggregation. Furthermore, dextran permeability results suggest that although there is slowing in the dextran diffusion rate across the membrane due to cellular presence in both hADSCs and UROtsa cells, a zero-diffusion rate of dextran molecules would be necessary to demonstrate barrier function closer to what is seen in the native bladder. Although presence of ZO-1 proteins in UROtsa suggests some extent of cell-cell tight junction formation, permeability results indicate that barrier function is not fully developed in multilayer tissue constructs.

Addition of GAG supplement to culture during the seeding process on the apical surface of the tissue construct, like seen in native tissue, may provide the necessary component to initially assist the barrier against solute diffusion through the membrane prior to self-production of GAGs by the cells.

CHAPTER FIVE

STATIC TENSION BIOREACTOR FOR BLADDER TISSUE ENGINEERING APPLICATIONS

5.1. Introduction

The primary objective for tissue engineered grafts and scaffolds in urology has undergone a paradigm shift over recent years. Research has moved more from a top-down to a bottom-up approach – rather than providing a basic urine reservoir, but instead exploring the use of synthetic and natural polymers to design materials that imitate the compliance of the native urologic tissue [143]. In a clinical trial performed by Atala et al., PGA composite grafts were seeded with autologous cells and wrapped in omentum prior to implantation in 7 patients. In a 5-year follow up, histological data revealed the formation of urothelial and smooth muscle layers, but patients suffered from lack of bladder compliance, low urine capacity, and the need for intermittent catheterization [169]. Further research would be necessary to better illuminate the mechanisms that are key in functional bladder restoration.

Starting *in utero*, the bladder undergoes filling, storage, and urination cycles that are important for the physiological development of the urinary bladder. This cycling process causes stimulation in and ultimately leads to replication of bladder smooth muscle cells [173]. One approach seeks to couple mechanical stimulation for physical conditioning with *in vitro* tissue maturation in a process termed functional tissue engineering. Growing evidence suggests that conditioning tissues with normal mechanical stimulation leads to better cellular growth, graft survival, and proper gene

expression and cellular bioactivity [174]. On a cellular level, mechanical forces in the growth environment of urothelial and bladder smooth muscle cells are critical for retention of native cell physiology. Roby et al. demonstrated that sustained tension on bladder smooth muscle cells increase expression of α-SMC indicative of the contractile smooth muscle phenotype [170]. Another report in the literature demonstrates that mechanical stretch may play a role in Ca2+ influx and ATP release in primary urothelial cell culture [171]. In response to these studies, a bioreactor system capable of applying constant tension on tissue engineering constructs in a cyclic loading, holding, and unloading profile was developed for replication of bladder filling cycles in typical cell culture environments.

5.2. Materials and Methods

Device Design & Construction

The tension-controlled bioreactor (Figure 5.1), which had been designed and assembled previously in our laboratory [175], was modified and calibrated. Briefly, the setup contains two channels capable of linear uniaxial stretch on small specimens with stepper motors (21H4AA-2.5-907, Haydon Kerk Motion Solutions) driven by a chopper drive circuit (Model 40105 #EDL9950, Haydon Kerk Motion Solutions) and powered by a linear power supply (HC24-2.4, Bel Power Solutions). On the opposite end, full bridge thin-beam load cells (LCL-113, Omega) are placed to measure voltage changes due to strain via signal conditioning module (DMD-465, Omega). The stepper motor is controlled through a custom designed LabVIEW (National Instruments) program

allowing for precise control of linear displacement, which simulates tension associated with bladder filling *in vivo*. The LabVIEW program uses a feedback loop mechanism that reads the output force generated by the stretch of the specimen and converts this value into tension. The loading rate and maximum stretch, determined by calculations and estimations of native bladder filling in the literature, can be controlled through the LabVIEW program. The bioreactor is designed to operate in cell culture conditions of humidified, 37°C and 5% CO_2 and device components can be sterilized by UV radiation.

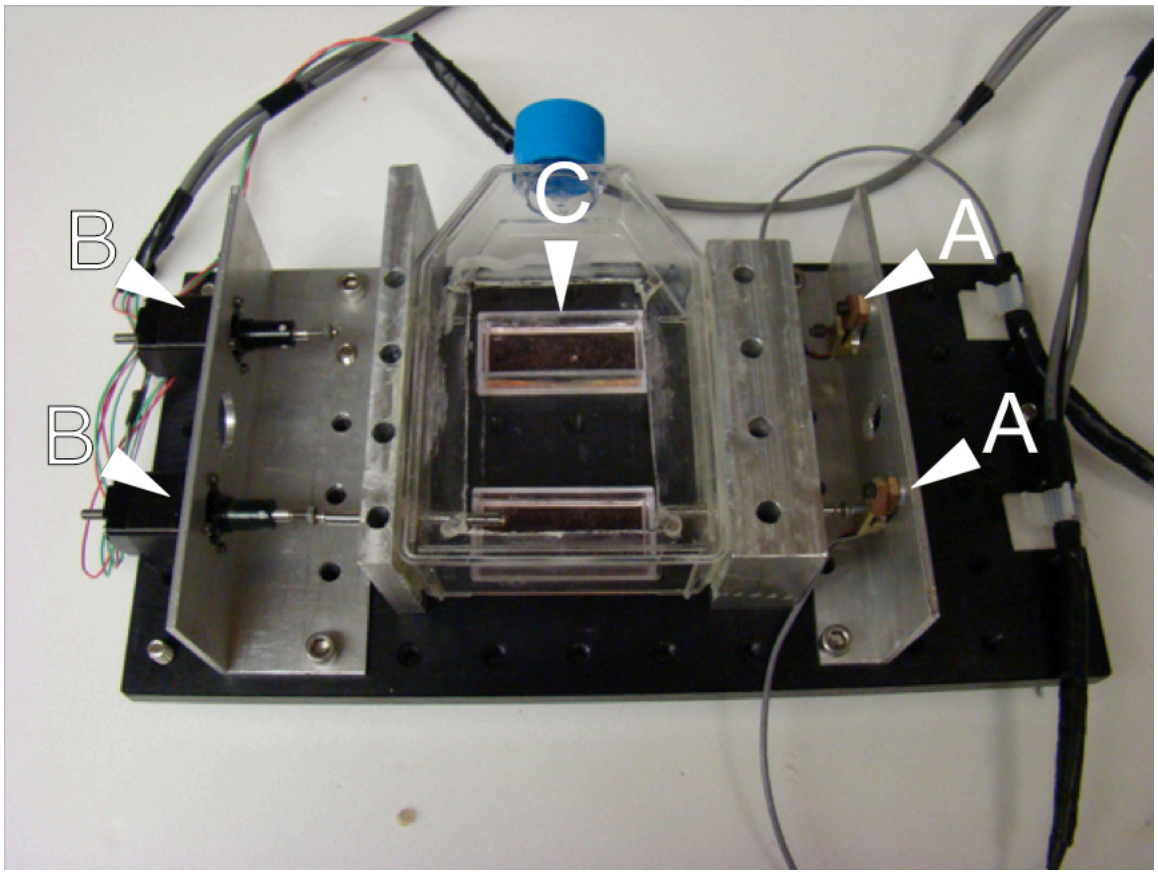

Figure 5.1: The tension bioreactor device. The load cell (A) and linear stepper motor (B) attach linearly to a hydrogel construct made in a Teflon mold with Biovyon wafers and suspended in wells filled with cell culture media or PBS for hydration (C).

LabVIEW Program Design

The LabVIEW program (Figure 5.2) was designed based on state machine architecture to transition to the different stages of cyclic loading using a main loop for the state machine control, and three separate loops for voltage/force measurements, force/distance over time graphing, and load rate calculation (Figure 5.3). The program outline (Figure 5.4) describes the overall logic to determine the current state based on

force calculations converted from voltage readings based on a linear calibration (Appendix 2). Prior to executing the main program for bioreactor control, the sample is attached to the stepper motor and load cell and a separate program is used to manually adjust the stepper motor extension so that the voltage shows negligible tension on the load cell. When the program is executed, the initial state is set in which the user will specify experimental conditions under parameters such as cycle number, load rate, desired force, time target, and voltage offset (Table 5.1). The voltage offset value is entered in order to set the initial force reading to zero. Once the experimental conditions are determined, the program proceeds to the loading state, sending pulse signals to the stepper motor and plots force and distance over time graphs. When the output force reading matches or exceeds the desired force value, the program proceeds to the static state and begins a state-specific timer loop, which runs until the time target value is reached. During this time, if stress relaxation in the hydrogel causes the output force to decrease below the desired force value, the stepper motor will engage to pull the hydrogel. When the time target value is reached, the program proceeds to the unloading state, which will take the calculated displacement value determined from the pulse signals sent to the stepper motor and pulse the stepper motor with the opposite voltage until it returns to the initial displacement. When the motor resets the to the initial displacement position, one cycle is added to a cycle counting loop and the program continues to function until the set cycle number has been reached, at which point the program will cease and allow the user to export the plot data to Microsoft Excel.

Input Parameter	Definition
Cycle Number	Sets the number of full loading, static, and unloading cycles will complete before the program halts
Load Rate	Sets the rate (in mm/sec) at which the loading state will run the stepper motor and apply strain to the hydrogel construct
Desired Force	Sets the minimum force value (in N) during the holding state that will engage the stepper motor if the output force values falls below the desired force value.
Time Target	Sets the time (in sec) spent in the static state to simulate a static strain period at desired force.
Voltage Offset	Offset value for the output voltage to compensate for minor strain initially placed on the load cell due to attachment of the hydrogel in order to zero reading values.

Table 5.1: Definitions of initial state input parameters.

T1107 Hybrid Hydrogel Preparation and Loading

For calibration of the device, model hydrogel tissue constructs were prepared according to an established protocol of our laboratory (REF). The hydrogel was formed by adding Tetronic® T1107 (BASF Corporation) acrylate (117.5 mg/mL) to a collagen type I solution of 6 mg/mL dissolved in 0.02N acetic acid overnight. Additionally, a photo-initiator compound (Irgacure, I-2959, BASF Corporation, 100mg / 1mL ethanol) and hyaluronic acid (MW: 1.5-1.8 MDa, Sigma, 10mg / 1mL H_2O) were added to the mixture with periodic vortexing to ensure homogeneity. The hydrogel was formed in a Teflon mold with a rectangular inset measuring 3cm X 1cm X 0.5cm (Figure 5.5). Two small porous Biovyon wafers (Porvair PLC, Norfolk, UK) were used as anchors for metal pins and to allow for an increased area of attachment. The hydrogel was then removed from the mold and connected to the bioreactor device using small rare earth magnets glued to the pins using epoxy, and suspended in a phosphorous-buffered saline solution.

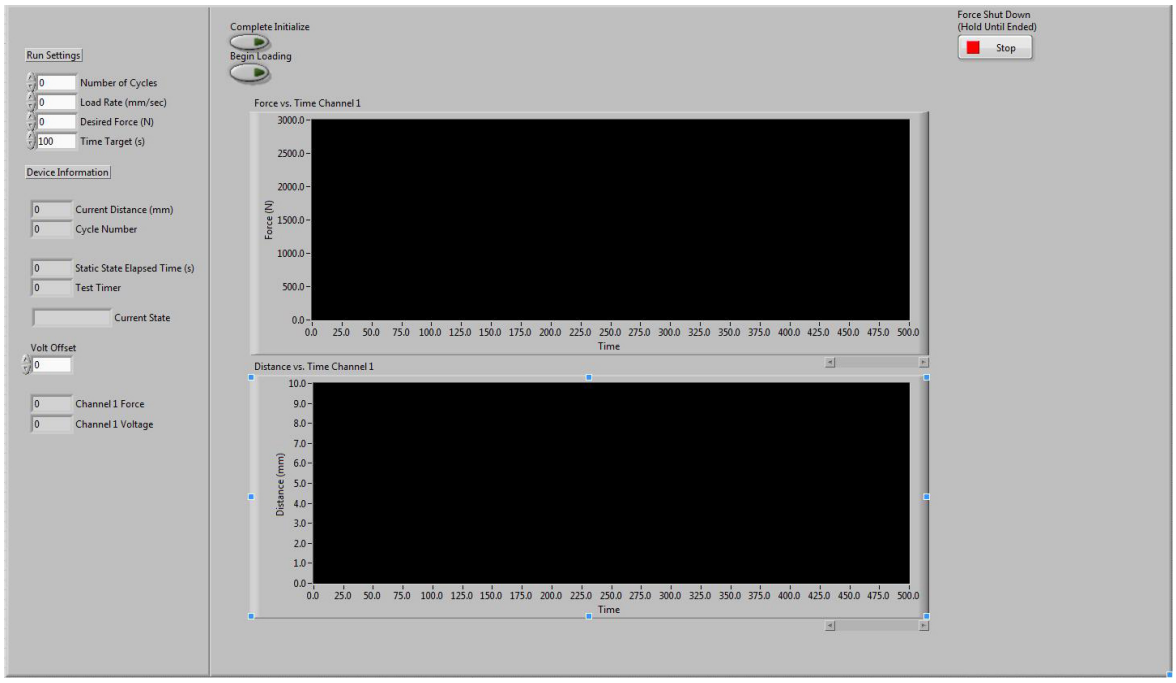

Figure 5.2: Front Panel of Tension Bioreactor Program. The user interface to input initial parameters and read output data during static and cyclic loading experiments.

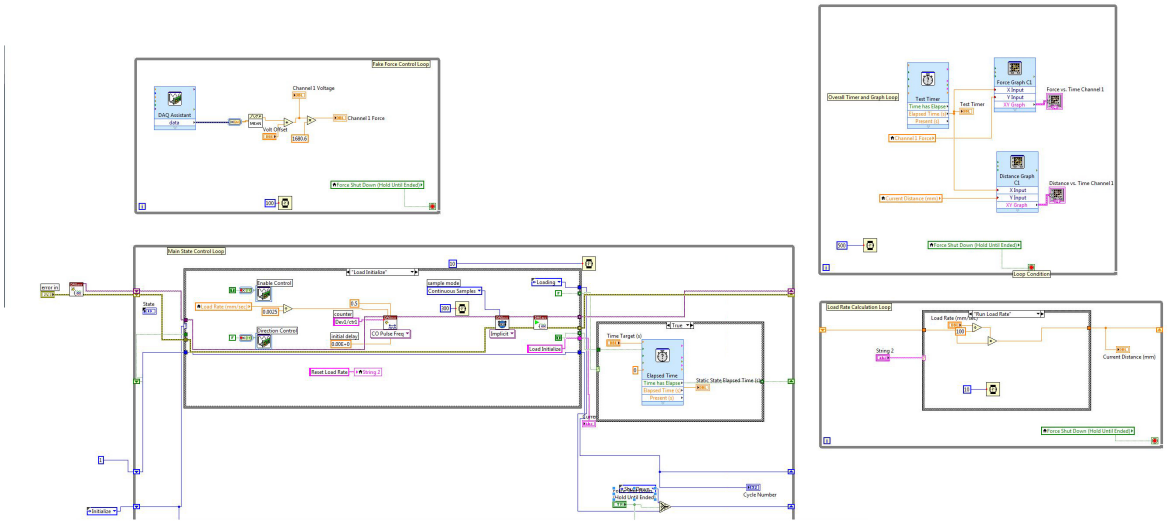

Figure 5.3: Block Diagram of Tension Bioreactor Program. The programming architecture for the state machine design with multiple simultaneous while loops.

The bioreactor was placed into a cell culture incubator at 37°C in a humidified 5% CO_2 atmosphere.

Calibration of Bioreactor

To calibrate the tension bioreactor, three materials, T1107 hybrid hydrogel, Parafilm M (Bemis), and a PCUU scaffold, were used. For each test, the specimen was attached to the connecting rods of the stepper motor and the load cell and motor position was set to a zero strain position. The T1107 hybrid hydrogel was subjected to static tension of 1.0 N for three 600-second cycles with a loading rate of 0.0625 mm/sec. The Parafilm sample was attached directly to the connecting rods and subjected to 4.0 N for one cycle at 0.2 mm/sec. The PCUU scaffold was subjected to 2.5 N for two 1000-second cycles at 0.1 mm/sec.

5.3. Results

Calibration of Tension Bioreactor

The T1107 hybrid hydrogel sample failed under approximately 0.9 N of force and 15 mm of linear displacement (Figure 5.6, 5.7). In contrast, the parafilm maintained the applied force at 4.0 N for the duration of the static while the displacement continued to climb and the test was halted after 90 seconds (Figure 5.8). From the bioreactor output data, a stress/strain curve for Parafilm M was generated (Figure 5.9). Over the two cycles, the PCUU scaffold held a constant force at 2.3 N for the first cycle and at 2.0 N for the second cycle while displacement of the motor was maintained at approximately 9 mm and 6 mm, respectively (Figure 5.10).

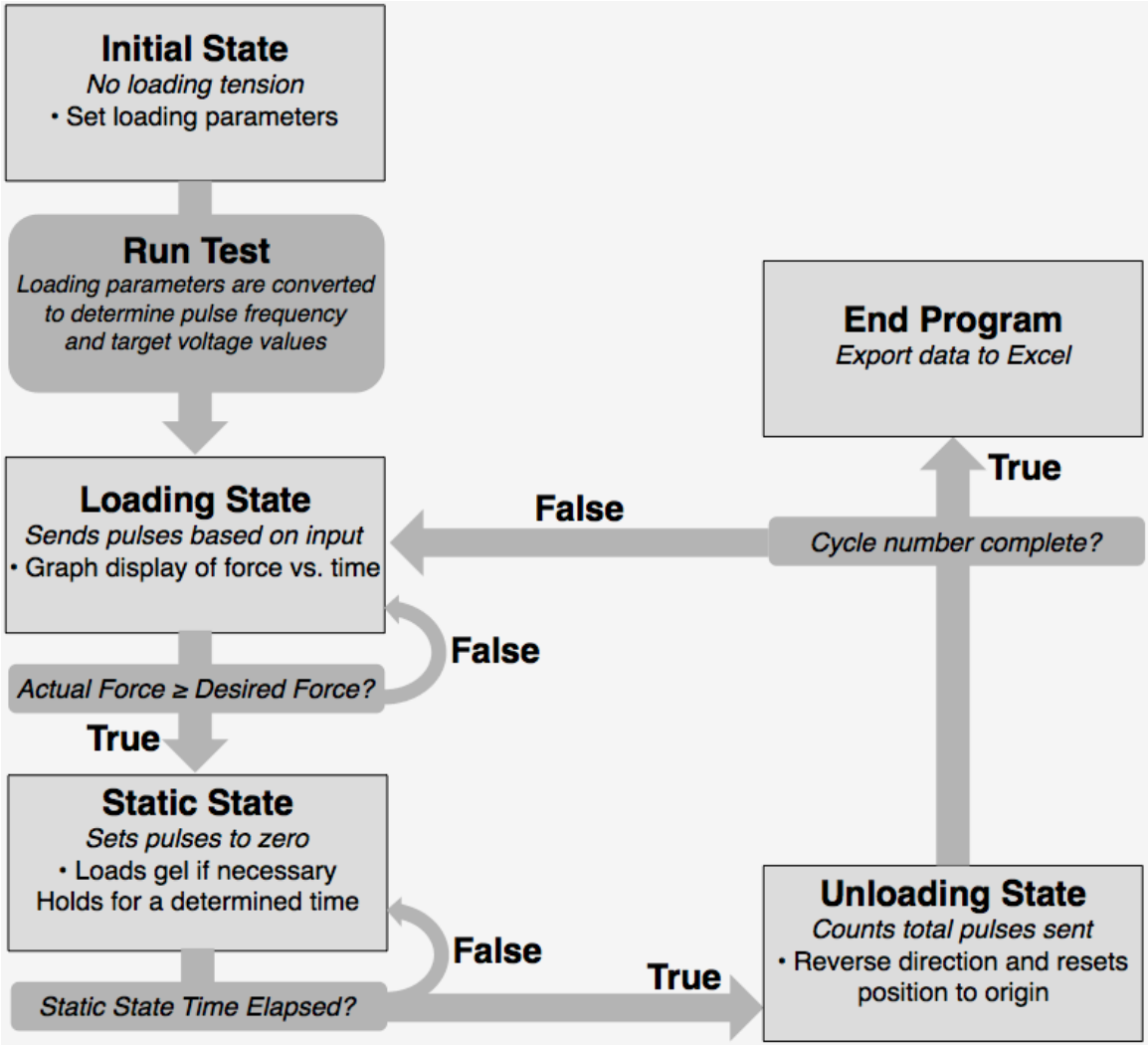

Figure 5.4: Logic Diagram of Tension Bioreactor Program. The programming logic flow chart outlines the comparisons made during each state and the Boolean output indicating if the program will enter the next state or continue in the current while loop.

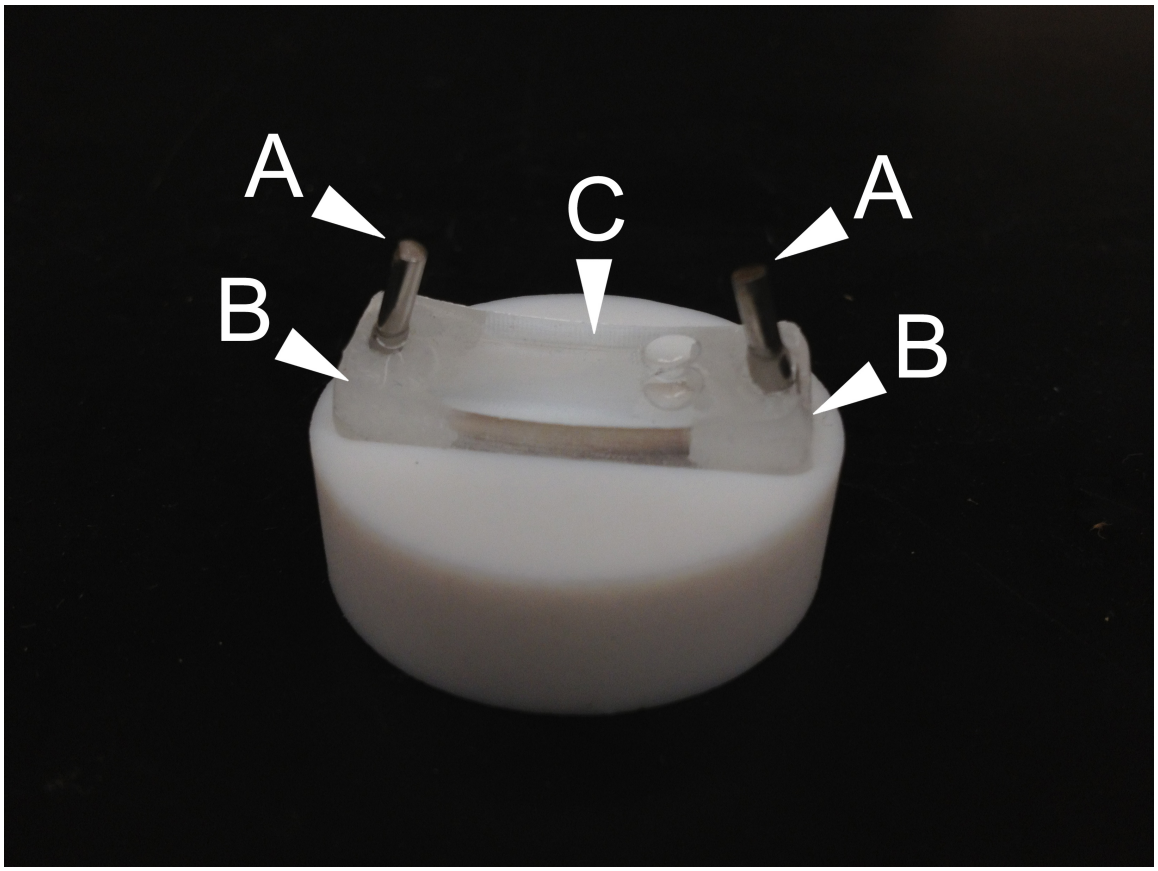

Figure 5.5: Teflon molds for hydrogel constructs. Small pins (A) with neodymium rare earth magnets (not pictured) are attached to porous Biovyon wafers (B) and filled with components for hydrogel formation in the rectangular insert (C).

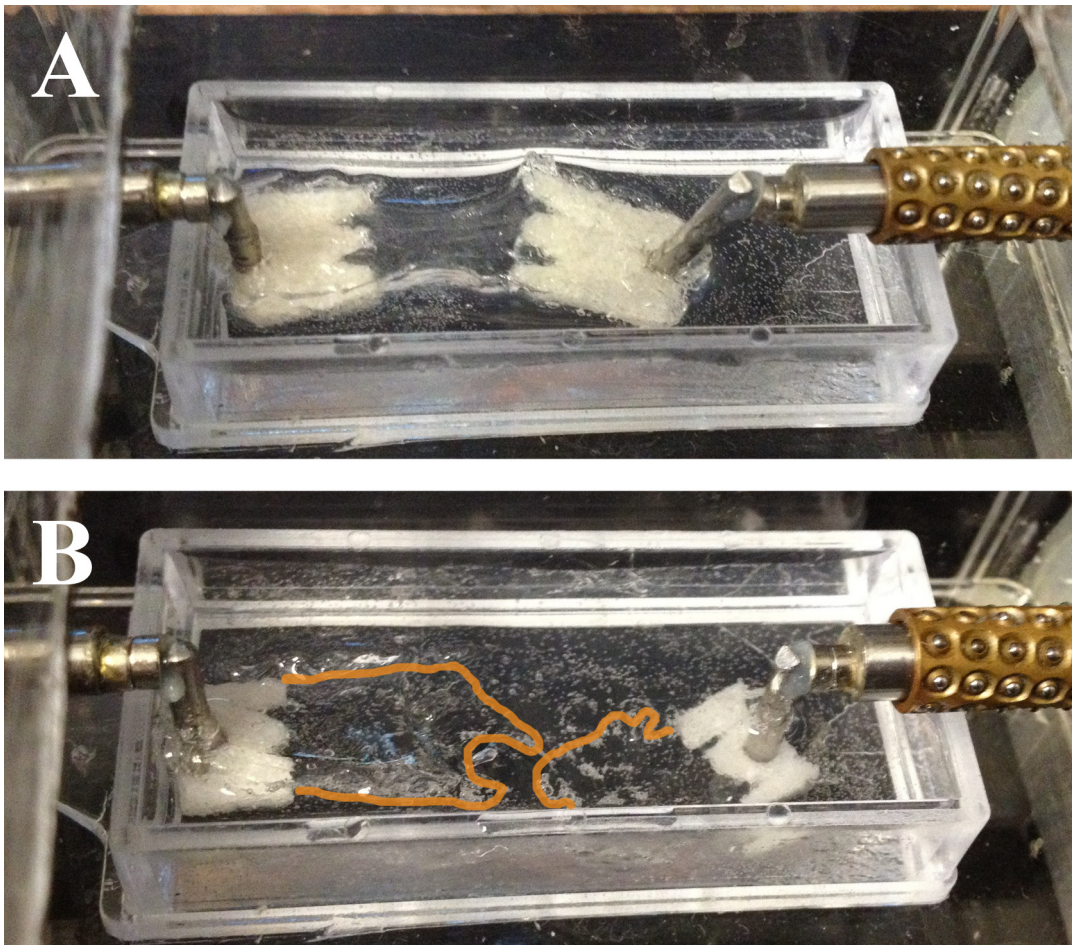

Figure 5.6: Gross examination of T1107 hybrid hydrogel during loading cycle.

Linear displacement of stepper motor applies force to hydrogel construct (A). Prior to reaching the desired force, the hydrogel construct separated due to failure during stretch. The orange highlight outlines the border of the hydrogel construct (B).

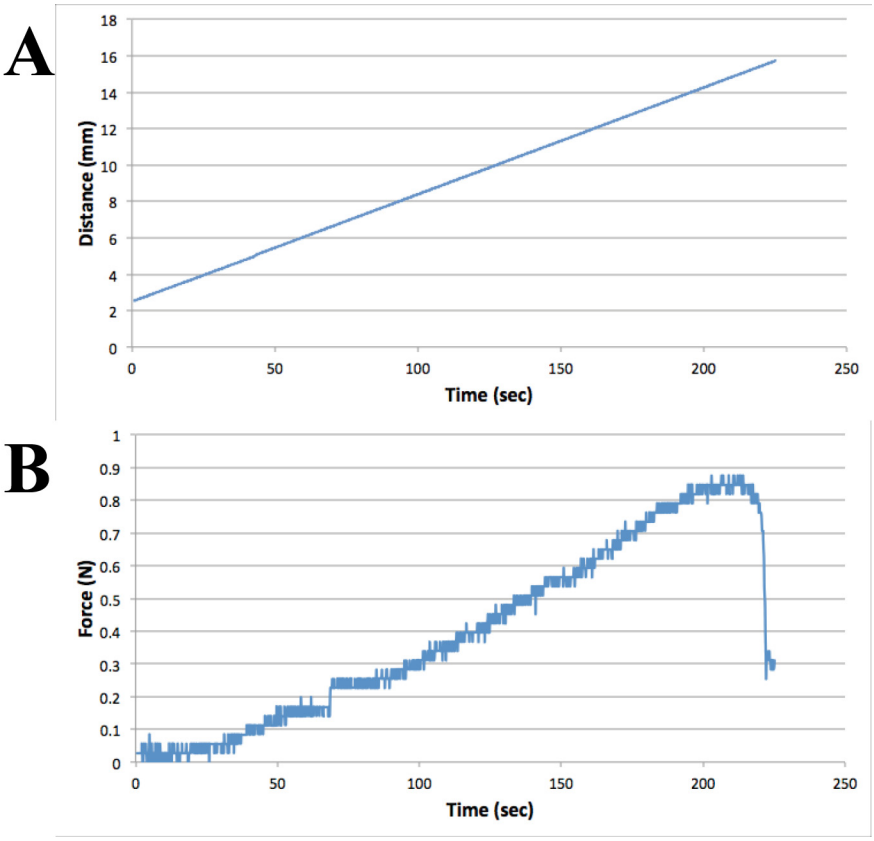

Figure 5.7: Distance and Force vs. Time Plots for T1107 Hybrid Hydrogel on Tension Bioreactor. Linear displacement of stepper motor shows load rate of 0.0625 mm/sec for the initial loading stage (A). At approximately 0.9 N of force and 14 mm of linear displacement, the T1107 hybrid hydrogel construct separated in the center and a drastic decrease in the force detected was observed.

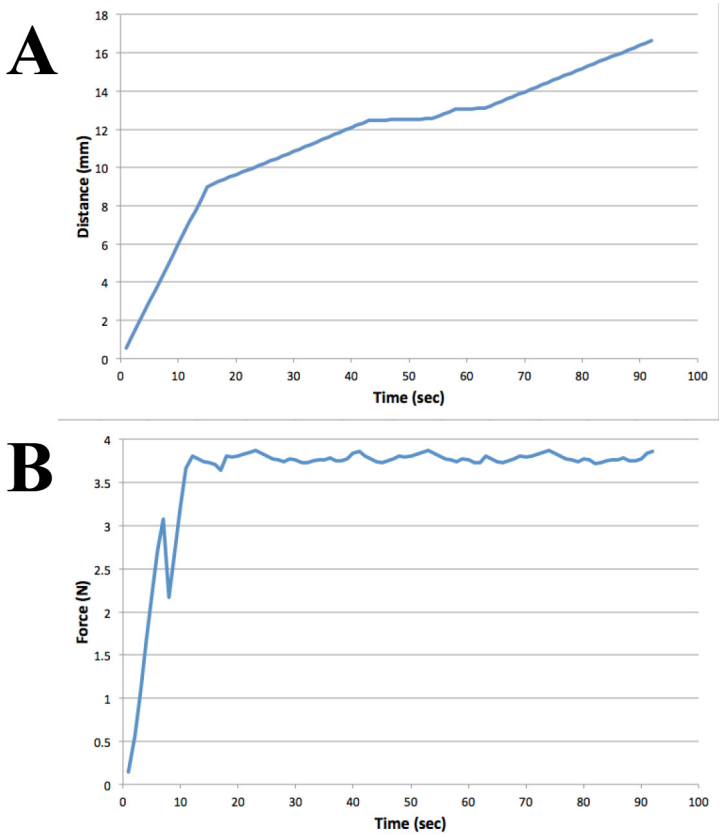

Figure 5.8: Distance and Force vs. Time Plots for Parafilm M on Tension Bioreactor. Linear displacement of stepper motor shows load rate of 0.2 mm/sec for the initial loading stage (A). After reaching the desired force of 4.0 N, the change in linear displacement reduces to a lower load rate in order to compensate for stress relaxation of Parafilm over the remainder of the test.

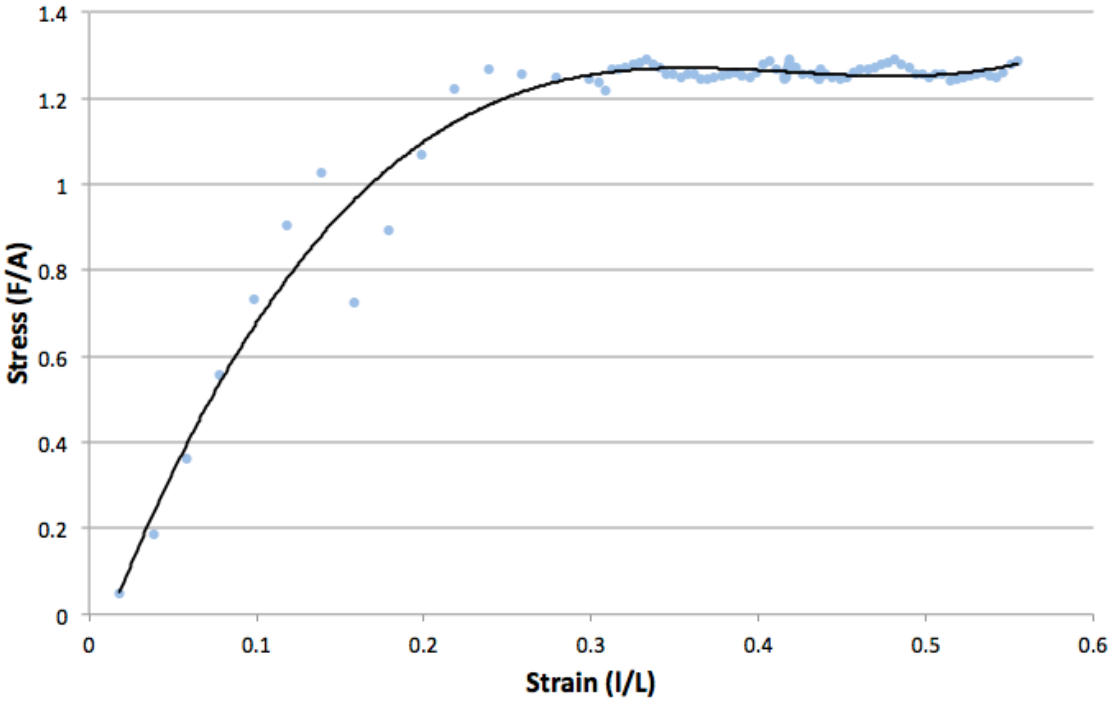

Figure 5.9: Stress/Strain Curve of Parafilm M. From the initial conditions of the experiment, a stress strain curve can be generated from the bioreactor output data in order to monitor material behavior during loading tests.

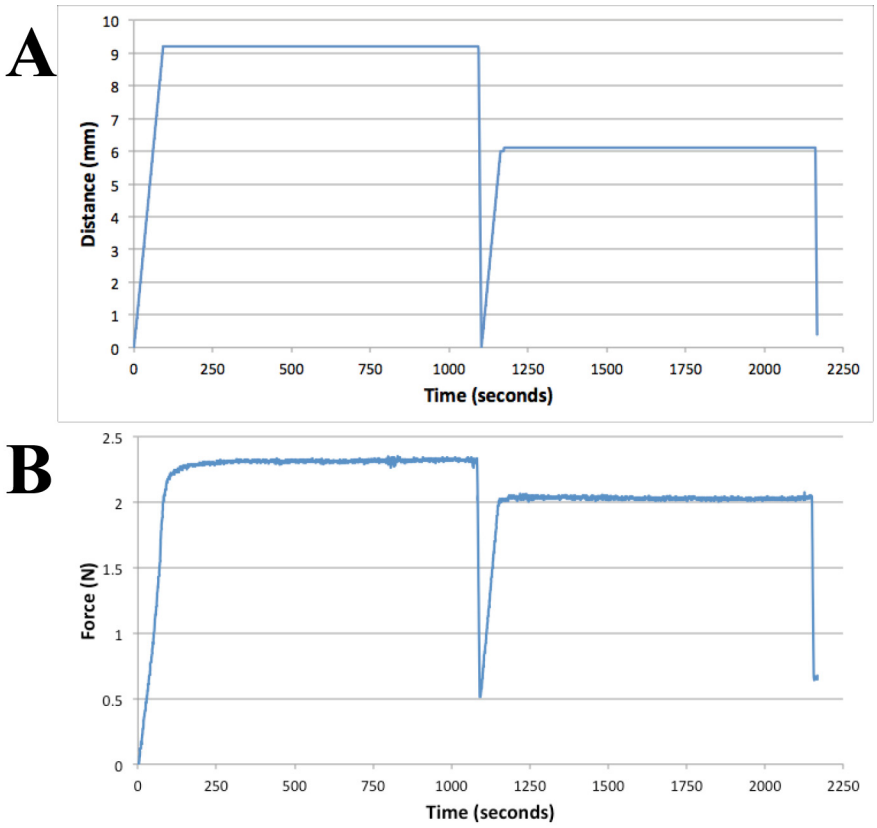

Figure 5.10: Distance and Force vs. Time Plots for PCUU Scaffold on Tension Bioreactor. Linear displacement of stepper motor shows load rate of 0.1 mm/sec for the initial loading stage (A). After reaching the desired force of 2.3 N for the first cycle and remaining static for 1000 seconds, the stepper motor returns to the origin and begins the second cycle (B). During the second cycle, the output force reaches 2.0 N and remains for 1000 seconds.

5.4. Discussion

The results of calibration provided evidence that the custom-designed tension bioreactor was capable of applying a static force to tissue engineering constructs for a

predetermined time period and number of cycles in a physiological environment. The bioreactor demonstrated variability in force and distance vs. time profiles based on the physical properties of the three test materials (parafilm, PCUU, and T1107 hybrid hydrogel).

The use of hydrogels for treating medical conditions involving urogenital organs at various stages of pre-clinical and clinical tests have begun to appear in new research in tissue engineering [35-37, 42, 47, 49, 56, 63-67]. The unique properties of hydrogels such as their viscoelasticity and capacity to fine-tune the mechanical properties have been key for their adaptation in many applications in tissue engineering [42, 47]. Recently, hydrogels prepared with chemically crosslinked Tetronic-acrylate (BASF Corporation) polymers have been explored for its potential use as a tissue scaffold in bladder applications. In particular, modified T1107-acrylate hydrogels combined with collagen type-I and hyaluronic acid have been studied for its mechanical properties and viability as a cellular scaffold *in vitro* [172]. In the present study, the T1107 hybrid hydrogel specimen failed structurally at 1 kPa peak stress and a peak stretch ratio of 1.5. In the previous study, acellular T1107 hybrid hydrogels were subjected to tension at 5 mm/min (0.083 mm/sec) until failure, and a peak stress of 4.1 ± 1.2 kPa and peak stretch of 1.21 ±1.23 were recorded [172]. Results in the present study are on the same order of magnitude to results obtained previously in uniaxial tensile testing on MTS Synergie 100 providing evidence for the reliability of the tension bioreactor results. The differences in the values between studies can be attributed to the differences in loading rate or the

orientation of the specimen during testing (vertical on MTS vs. horizontal in tension bioreactor).

When the parafilm was subjected to a constant tension on the bioreactor, the material was noted to surpass the yield point and plastic deformation was observed. Under the static tension state at 4.0 N, the parafilm strip continued to stretch (Figure 5.8). From these results, mechanical properties such as elastic modulus and yield point can be determined. In the present study, elastic modulus of the parafilm was 8.7 MPa in the initial section of the stress/strain curve with a yield point of approx. 1 MPa (Figure 5.9).

Electrospun, wet PCUU scaffolds have been demonstrated previously in our lab as a potential bladder tissue substitute scaffold because its mechanical behavior is similar to that of native human bladder with respect to maximum tension (PCUU: 0.43±0.029 N/mm; Native: 0.27±0.14 MPa), stretch ratio (PCUU: 2.43±0.26; Native: 1.69±0.17), and tension-stretch curve profiles [175, 176]. Moreover, using the bioreactor in the stretch-control mode [175] PCUU scaffolds seeded with BSMCs were subjected to 25% uniaxial stretch over a 3 hour period (1 hour in loading, static, and unloading states) resulting in an increase of cells exhibiting expression of smoothelin indicative of contractile smooth muscle phenotype compared to non-stretched groups. In the present study, the force-control mode was used to subject the PCUU scaffold to two cycles at the desired value of 2.5N. In contrast to the parafilm, the PCUU did not demonstrate plastic deformation during the loading cycles indicating that PCUU had not surpassed yield strength. Although a number of previous studies have demonstrated correlation between mechanical loads applied on cells and cellular/molecular responses such as ECM

production, growth factor secretion, and cell proliferation [177, 178], which type of stimuli (forces, tension vs. stretch, displacement) triggers these events is not well understood. Thus, the ability to apply mechanically loading to tissue engineering scaffolds both in a force-control and displacement-control manner is one of the unique features of our bioreactor and potentially useful for the study of functional tissue development. In the case of the bladder, where cells are constantly subjected to both wall tension and large deformation, it is critical to study the role of mechanical stimuli in cellular response and tissue development.

5.5. Conclusions

To date, the tension bioreactor has been designed to apply controlled mechanical force stimuli on soft biomaterials intended to reproduce the *in vivo* bladder filling and voiding cycles for the purpose of studying functional tissue engineering. Conditioning cells with cyclic mechanical stimulation may improve the overall tissue physiology, which might typically fail after implantation due to compliance mismatch or improper cellular ingrowth from the lack of mechanical preconditioning [174]. In addition, mechanical conditioning may play a role in the study of neurogenic bladder conditions, such as overactive bladder, which may arise during tissue development [63, 68, 84]. The tension bioreactor has potential to apply cyclic and static tension to tissue engineered scaffolds and soft biomaterials in a fashion that mimics native bladder cycling, which is essential to illuminate the mechanisms that are key in functional bladder tissue development and restoration.

CHAPTER 6

CONCLUSIONS AND RECOMMENDATIONS

6.1 Introduction

Bladder tissue engineering using synthetic and naturally derived materials has made significant progress in recent years, however those *in vitro* successes have fallen short in outperforming current gold standard surgical techniques [143-146]. Still, the body of knowledge for functional regeneration of smooth muscle and urothelial tissue layers continues to grow. The present dissertation research explored the effects of the chemical and physical microenvironments of cell culture on hADSC differentiation towards functional urothelial cells. First, the use of defined keratinocyte serum-free media and all-trans retinoic acid were explored to elucidate their effects on the expression of urothelial-specific markers in hADSCs (Chapter 3). Next, the differentiated hADSCs were cultured in a three-dimensional microenvironment using a layer-by-layer fibronectin/gelatin scaffold to test the hypothesis that urothelial morphology and marker expression could be dependent on the physical environment (Chapter 4). Furthermore, a tension bioreactor system capable of applying constant force in a sterile, physiological environment was developed to mimic native loading conditions and study force-dependent cellular activity (Chapter 5).

6.2 Expression of Urothelial Markers in hADSCs due to Defined KSFM Supplementation

One approach in tissue engineering is the use of adult stem cells to take advantage of their regenerative properties. Particularly, hADSCs has been shown to exhibit multi-

potency, immunosuppressive properties, and relative ease-of-harvest [110, 153]. Furthermore, in developing a system for restoration of urothelium in human patients, research indicates that the use of autologous urothelial cells [152] and serum-based media [156] should be avoided due to their potential complications when transferring to an *in vivo* environment. With these goals in mind, the effects of all-trans retinoic acid and defined keratinocyte serum free media with supplementation were investigated on urothelial differentiation of hADSCs in two-dimensional cell culture (Chapter 3). The mRNA expression profile of hADSCs (increase in CK-20, UPIb, UPII; decrease in CK-17, CD90, CD105) when cultured in defined KSFM after 14 days indicated differentiation away from the hADSCs phenotype and towards a urothelial cell phenotype. Western blot and immunofluorescence results confirmed corresponding protein translation of CK-17, CK-20, UPIb genes providing evidence that hADSCs differentiated towards the urothelial lineage in 2D culture partially shares a phenotypic profile with the superficial layer of native urothelium. In contrast, when hADSCs were cultured under KSFM in a 3D growth environment via collagen gel encapsulation, protein expression of CK-17 and CK-20 reversed compared to 2D and became closer to the basal/intermediate urothelial phenotype. The results of the present study show that ATRA affects cell morphology *in vitro* by causing a monolayer, contact-inhibited growth profile in hADSCs, but has a negligible effect on differentiation towards urothelial-specific cell phenotype in gene and protein expression. These experiments established a novel and reliable differentiation method to drive hADSCs towards a urothelial-like cell

lineage using serum-free media and without relying on multiple cell lines for supplementation.

6.3 Fibronectin/Gelatin Coating Effect on hADSC and UROtsa Multilayer Constructs

Ultimately, functional restoration of the urothelial layer requires pre-differentiated hADSCs grow in a 3D microenvironment. To ensure that changes in hADSC phenotype due to defined KSFM supplementation are preserved in 3D and thus facilitate development of a functional multilayer, the effects of layer-by-layer fibronectin/gelatin coatings to create three-dimensional constructs with hADSCs and UROtsa cells were explored (Chapter 4). Results indicated that hADSCs, which underwent changes in cell physiology under defined KSFM supplementation, aggregate under fibronectin/gelatin coating and differentiated conditions when seeding the cells in a 3D microenvironment. The present findings show that UROtsa cells, which were used to investigate if similar aggregation would occur in a urothelial-like cell population, do undergo some extent of cellular aggregation when coated in fibronectin/gelatin. However, use of the same coating method on the Transwell® membrane prior to UROtsa cell seeding improves multilayer formation, promotes urothelial protein expression, and decreases cellular aggregation after 24 hours. In addition to cell coating, fibronectin/gelatin coating of the Transwell® membrane could improve the formation of a multilayer in urothelial-differentiated hADSCs.

6.4 Barrier Function of hADSC and UROtsa Multilayer Constructs

Results from permeability experiments indicate that both hADSC and UROtsa multilayer constructs are not completely impermeable to passive transport of dextran molecules (Chapter 4). Since the presence of uroplakins and tight junction proteins in UROtsa cells with FNG-coating was confirmed, these results indicate that other components in providing a functional urothelial barrier may be missing from the model used in the present study. Studies have shown that glycosaminoglycan (GAG), particularly chondroitin sulfate, contributes to an increase in the transmembrane resistance (i.e. decrease in urothelial permeability) in native human and porcine bladder [130]. Alcian blue stain for acidic polysaccharides indicated that GAGs were absent in UROtsa and hADSC multilayer constructs after 24 hours of culture, which suggests that the short culture time was not enough for seeded cells to begin GAG production. Recent literature indicates that ATRA along with ActA (Activin-A) and BMP-7 (bone morphogenetic protein-7) contribute to production of tight junction proteins in ADSCs [169]. Though ATRA was excluded from these multilayer experiments due to the negligible effect it had on urothelial phenotypic expression, it is possible that ATRA could potentially contribute to the formation of a spread, umbrella layer as evidenced by the monolayer, contact-inhibition growth pattern.

6.5 The Development of a Tension Bioreactor System to Study Effects of Mechanical Stimulation in Sterile Environment

The custom-designed bioreactor has been calibrated to apply controlled mechanical force stimuli to cells seeded on various scaffolds and matrices to improve

overall bladder tissue development, which has been shown to fail after implantation from the lack of mechanical preconditioning [173]. The bioreactor's unique capability of applying a cyclic load representative of bladder cycling would be useful in studying the effect of mechanical stimuli on differentiated hADSCs within an *in vitro* model of multilayered urothelium (Chapter 4), which have only been studied in a static growth environment to date. Thus, the tension bioreactor has the distinct benefit of contributing to functional bladder restoration via mechanical preconditioning resembling bladder filling cycles on various materials used for bladder tissue engineering.

6.6 Summary

In the present study, the results provide novel evidence that, through a combination of physical and chemical factors, defined KSFM causes hADSCs to increase expression of urothelial-specific mRNA and protein markers of both superficial urothelial lineage and decrease expression of mesenchymal stem cell mRNA markers under 2D TCPS after 14 days in culture. Furthermore, administering the same culture regimen for 7 days in 3D collagen gel culture can induce the protein expression of CK-17 indicative of basal/intermediate urothelial-lineage. In UROtsa cells, the results of the present study have demonstrated that fibronectin/gelatin coating on both cells and growth membrane allow for the formation of multilayer constructs with cytokeratin, uroplakin, and tight-junction proteins indicative of *in vitro* urothelial formation. A tension bioreactor system has been calibrated to monitor cellular activity caused by mechanical stimuli, which can aid in expanding knowledge of tissue engineering for bladder tissue constructs *in vitro*.

Future experiments have been outlined below as potential avenues for exploration to provide new uses for hADSCs in bladder tissue engineering and regenerative medicine.

Recommendations for Future Studies

- Determine the phenotypic, morphological, and functional changes of both hADSC and UROtsa multilayer construct after an extended maturation period (longer than 24 hours)
- Determine the effects on cell phenotype and morphology of supplementing specific growth factors used in 2D urothelial pre-differentiation to undifferentiated hADSCs in 3D.
- Investigate the use of additional natural or synthetic polymers that may contribute to the impermeability of the multilayer construct
- Develop a testing model for the bioreactor to characterize the effects of mechanical stimuli on the multilayer construct, particularly focusing on the overall mechanical strength and stability.
- Investigate the response of urothelial-differentiated hADSCs in co-culture with native bladder SMCs or SMC-differentiated hADSCs to determine the efficacy of a complete *in vitro* bladder tissue construct.
- Investigate the behavior of urothelial-differentiated hADSCs on acellular synthetic polymers for bladder tissue regeneration.

APPENDICES

APPENDIX A

Human Adipose-derived Stem Cell Encapsulation in PMBV/PVA Polymer

After results were obtained showing differences in the phenotypic protein expression of urothelial markers in hADSCs grown in collagen gel and on TCPS, the use of gel-reversible PMBV/PVA hydrogel was explored to study the effects of a 3D microenvironment on differentiated and undifferentiated hADSCs *in vitro*.

Human Adipose Derived Stem Cell Culture

Human adipose derived stem cells (hADSCs) were purchased from Lonza (PT-5006) and expanded in low D-glucose (1000 mg/L) DMEM (Life Technologies) supplemented with 10% fetal bovine serum (FBS, Fisher), 1% GlutaMAX (Life Technologies), and 1% antibiotic/antimycotic solution (AB/AM; Life Technologies). HADSC between passages 3 and 7 were used in all experiments of the present study.

PMBV/PVA Hydrogel Preparation

PMBV and PVA (kindly donated by Dr. Kazuhiko Ishihara from University of Tokyo) polymer were dissolved separately into 1X PBS solution at 5% weight/volume solution. Approximately 1.0 x 10^6 human ADSCs were suspended in 200 μL of PMBV solution and mixed with 200 μL PVA solution to form the hydrogel and allowed to set for 5 minutes. Human ADSCs were pre-labeled with Celltracker Red CMPTX (Molecular Probes) prior to encapsulation in PMBV/PVA hydrogel. DMEM was added on top of the PMBV/PVA hydrogel and changed every 2 days over a 10-day period. Fluorescence imaging was taken to visualize cells within the PMBV/PVA hydrogel. Afterwards, 0.3 M D-sorbitol solution in PBS was gently pipetted onto the compound and

incubated in 37°C for 10 minutes with occasional pipetting to dissolve the PMBV/PVA hydrogel for protein and RNA extraction. After 10 minutes, the solution was filtered using a 40-µm mesh membrane and then centrifuged for 3 minutes at 1000 rpm. Both the TRIzol extraction method and Qiagen RNeasy Mini Kit were used to isolate total RNA from encapsulated hADSCs. Total RNA was quantified using Thermo Scientific Nanodrop 2000c UV-Vis Spectrophotometer.

RESULTS AND DISCUSSION

Fluorescence imaging of the hADSCs encapsulated in the PMBV/PVA hydrogel after 10 days show a spherical morphology and limited spreading of the cells indicating lack of attachment sites for cellular adhesion. Additionally, attempts with both TRIzol and RNeasy Mini Kit extraction methods yielded insufficient amounts of total RNA (TRIzol and RNeasy Mini Kit) and protein (TRIzol method only) to run further analysis. The PMBV/PVA hydrogel dissolution and cell extraction process was adapted from studies conducted on murine mesenchymal stem cells (C3H10T1/2), and further study will be necessary to adjust the extraction process to successfully remove hADSCs from the hydrogel microenvironment. Although the use of PMBV/PVA provides an inert environment with good cytocompatibility, the difficulty in reliably extracting the cells from the 3D microenvironment and lack of multilayer formation within the hydrogel prevents its use for as an *in vitro* model for urothelial-like tissue constructs.

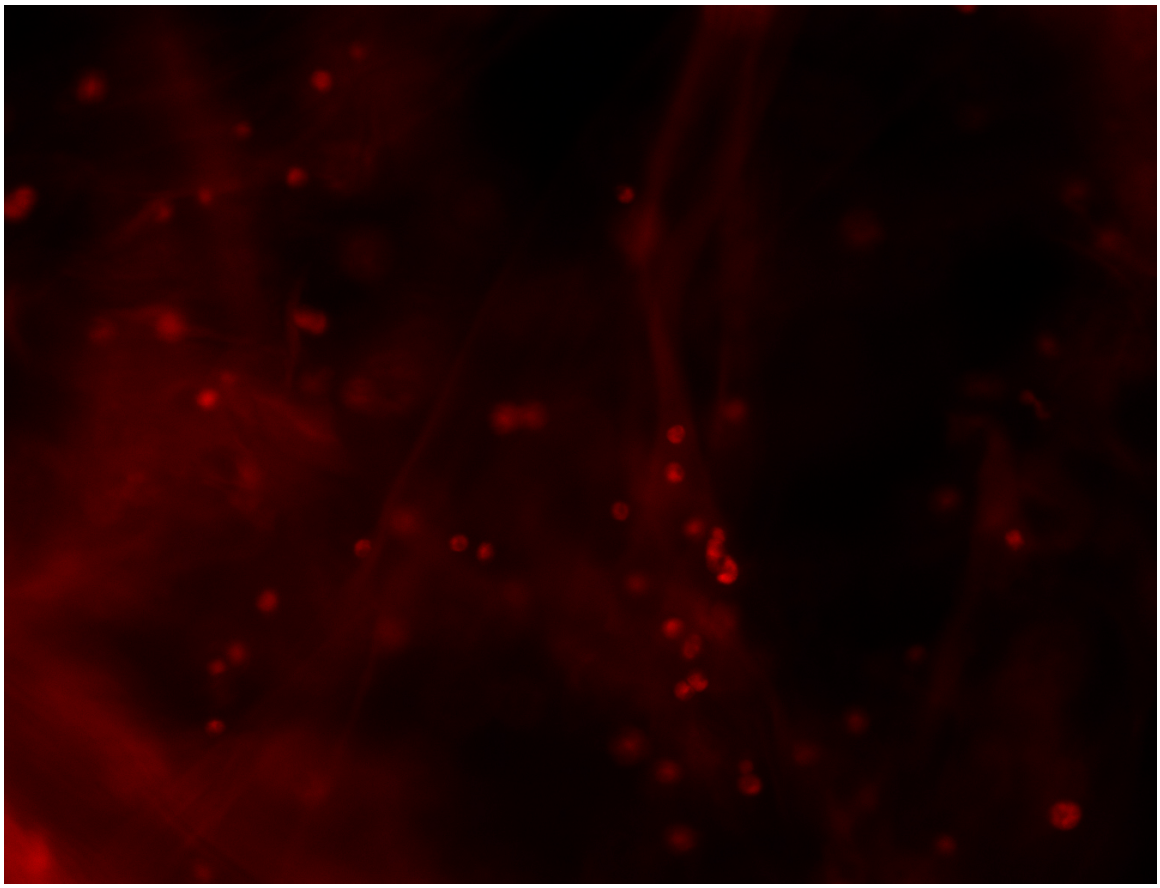

Figure A.1: Human ADSCs labeled with Celltracker Red within PMBV/PVA.

Fluorescence imaging shows spherical morphology and limited cell spreading for hADSCs within hydrogel microenvironment.

APPENDIX B

Tension Bioreactor Voltage-Force Calibration

Weights of measured mass were attached to the tension bioreactor load cells and allowed to hang. Forces were calculated from known masses and standard gravity. Voltage was recorded at each interval and a linear relationship was established.

Bioreactor Calibration			
Grams	Conv. Force (N)	Voltage1	Voltage2
0	0	0.034	0
16.76	0.1644156	0.337	0.057
31.85	0.3124485	0.683	0.106
46.04	0.4516524	0.84	0.144
61.5	0.603315	1.29	0.209
77.65	0.7617465	1.61	0.272
	Multiplier Values	0.478987481	2.826052693

Table B.1: Bioreactor Calibration Table.

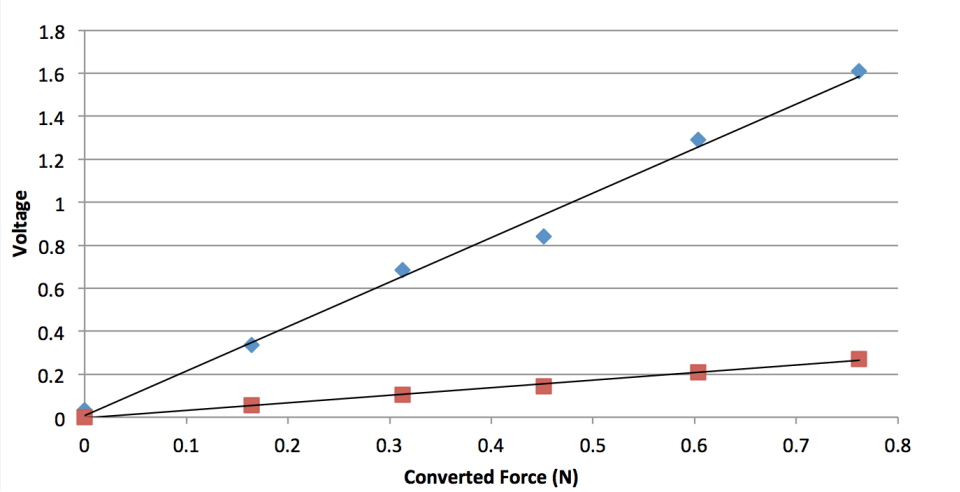

Figure B.1: Linear Bioreactor Calibration Chart. A linear relationship was established between calculated force values and the output voltage of the load cell on the two channels.

REFERENCES

[1] A. Staack, S. Hayward, L. Baskin, G. Cunha, Molecular, cellular and developmental biology of urothelium as a basis of bladder regeneration, Differentiation 73 (2005) 121–133.

[2] T. Hensle, G. Dean, Complications of urinary tract reconstruction. Urol Clin North Am 18 (1991) 755–764.

[3] R.D. Mills, U.E. Studer, Metabolic consequences of continent urinary diversion. J Urol 161 (1999) 1057–1066.

[4] E.W. Gerharz, W.H. Turner, T. Kalble, C.R. Woodhouse, Metabolic and functional consequences of urinary reconstruction with bowel. BJU Int 91 (2003) 143–149.

[5] W.C. de Groat, A neurologic basis for the overactive bladder. Urology 50(6A Suppl) (1997) 53–56.

[6] C.A. Maggi, The dual function of capsaicin-sensitive sensory nerves in the bladder and urethra. Ciba Found Symp 151 (1990) 77–90.

[7] L.A. Birder, W. C. de Groat. Mechanisms of disease: involvement of the urothelium in bladder dysfunction. Nature Clin Pract Urol 4 (2007) 46–54.

[8] J.I. Gillespie, M. Markerink-van Ittersum, J. de Vente, Sensory collaterals, intramural ganglia and motor nerves in the guinea-pig bladder: evidence for intramural neural circuits. Cell Tissue Res 235 (2006) 33–45.

[9] S. Barrick, et al., Receptors and channels: TRPV4 receptors in urinary bladder urothelium: involvement in urinary bladder function. The Journal of Pain 5(3, Supp.1) (2004) S10–S10.

[10] S. Du, I. Araki, Y. Mikami, Amiloride-Sensitive Ion Channels in Urinary Bladder Epithelium Involved in Mechanosensory Transduction by Modulating Stretch-Evoked Adenosine Triphosphate Release. Urology 69 (2007) 590–595.

[11] D. Ferguson, et al., ATP is released from rabbit urinary bladder epithelial cells by hydrostatic pressure changes -- a possible sensory mechanism? Journal of Physiology 505 (1997) 503–511.

[12] E.C. Wang, et al., ATP and purinergic receptor-dependent membrane traffic in bladder umbrella cells. J Clin Invest 115 (2005) 2412–2422.

[13] G. Apodaca, The Uroepithelium: Not Just a Passive Barrier. Traffic 5 (2004) 5(3) 117-128.

[14] P. Khandelwal, S. Abraham, and G. Apodaca, Cell biology and physiology of the uroepithelium, Am. J. Physiol Renal Physiol. 297 (2009) F1477-F1501

[15] O.J. Wiseman, C.J. Fowler, D.N. Landon, The role of the human bladder lamina propria myofibroblast. BJU Int 91 (2003) 89–93.

[16] J. Morrison, J. Wen, A. Kibble, Activation of pelvic afferent nerves from the rat bladder during filling. Scand. J. Urol. Nephrol. 201 (1999), 73–75.

[17] J.W. Downie, J.A. Armour, Mechanoreceptor afferent activity compared with receptor field dimensions and pressure changes in feline urinary bladder. Can. J. Physiol. Pharmacol. 70 (1992) 1457–1467.

[18] S.L. Chang, J. S. Chung, M. K. Yeung, P. S. Howard, E. J. Macarak, Roles of the Lamina Propria and the Detrusor in Tension Transfer during Bladder Filling. Scand. J. Urol. Nephrol. Suppl. 201 (1999) 38–45.

[19] K. Aitken, D. R. Bagli, The bladder extracellular matrix. Part I: architecture, development and disease. Nat. Rev. Urol. 6 (2009) 596-611.

[20] L. Baskin, P.S. Howard, E. Macarak, Effect of physical forces on bladder smooth muscle and urothelium. J. Urol. 150 (1993) 601–607.

[21] A. Liapis, P. Bakas, A. Pafiti, D. Hassiakos, M. Frangos-Plemenos, G. Creatsas, Changes in the quantity of collagen type I in women with genuine stress incontinence. Urol. Res. 28 (2000) 323–326.

[22] I. Araki, S. Du, H. Kobayashi, N. Sawada, T. Mochizuki, H. Zakoji, M. Takeda, Roles of mechanosensitive ion channels in bladder sensory transduction and overactive bladder. Int. J. Uro. 15 (2008) 681–687.

[23] N. Yoshimura, Bladder afferent pathway and spinal cord injury: Possible mechanisms inducing hyperreflexia of the urinary bladder. Progress in Neurobiology 57 (1999) 583–606.

[24] N. Lameire, W.V. Biesen, R. Vanholder, Acute renal failure. Lancet 365 (2005) 417–430.

[25] O. Pleniceanu, H.S. Orit, D. Benjamin. Concise review: Kidney stem/progenitor cells: differentiate, sort out, or reprogram? Stem Cells 28 (2010) 1649–1660.

[26] C. Sagrinati, E. Ronconi, E. Lazzeri, L. Lasagni, P. Romagnani, Stem-cell

approaches for kidney repair: choosing the right cells. Cell 14 (2006) 1471–1491.

[27] J. Gao, R. Liu, J. Wu, Z. Liu, J. Li, J. Zhou, T. Hao, Y. Wang, Z. Du, C. Duan, C. Wang, The use of chitosan based hydrogel for enhancing the therapeutic benefits of adipose-derived MSCs for acute kidney injury. Biomaterials 33 (2012) 3673–3681.

[28] J. Basu, et al. Functional Evaluation of Primary Renal Cell/Biomaterial Neo-Kidney Augment Prototypes for Renal Tissue Engineering. Cell Transplantation 20 (2011) 1771–1790.

[29] R.V. Clayman, L.R. Kavoussi, N.J. Soper, et al. Laparoscopic nephrectomy: initial case report. J. Urol. 146 (1991) 278–282.

[30] A. Weizer and J.S. Wolf Jr., in Complications of Urologic Surgery, Ed. S. S. Taneja (Saunders Elsevier, Philadelphia, 2010).

[31] J.E. Bernie, J. Ng, V. Bargman, T. Gardner, L. Cheng, C.P. Sundaram, Evaluation of hydrogel tissue sealant in porcine laparoscopic partial-nephrectomy model. J. Endourol. 19 (2005) 1122–1126.

[32] E.L. Park, J.B. Ulreich, K.M. Scott, et al. Evaluation of polyethylene glycol based hydrogel for tissue sealing after laparoscopic partial nephrectomy in a porcine model. J Urol 172 (2004) 2446–2450.

[33] S. Ramakumar, W.W. Roberts, O.E. Fugita, P. Colegrove, T.M. Nicol, T.W. Jarrett, L.R. Kavoussi, M.J. Slepian, Local hemostasis during laparoscopic partial nephrectomy using biodegradable hydrogels: initial porcine results. J. Endourol.16 (2002) 489–494.

[34] A. Breda, et al. Use of haemostatic agents and glues during laparoscopic partial nephrectomy: a multi-institutional survey from the United States and Europe of 1347 cases. European Urology 52 (2007) 798–803.

[35] T. John, A. Rajpurkar, G. Smith, M. Fairfax, J. Triest, Antibiotic Pretreatment of Hydrogel Ureteral Stent. Journal of Endourology 21 (2007) 1211–1216.

[36] M.M. Tunney, S.P. Gorman, Evaluation of a poly(vinyl pyrollidone)-coated biomaterial for urological use. Biomaterials 23 (2002) 4601–4608.

[37] S.P Gorman, M.M. Tunney, P.F. Keane, K. Van Bladel, B. Bley, Characterization and assessment of a novel poly(ethylene oxide)/polyurethane composite hydrogel (Aquavene) as a ureteral stent biomaterial. J. Biomed. Mat. Research 39 (1998) 642–649.

[38] L.M.D. Shortliffe, in Overcoming Bladder Disease: A Strategic Plan of Research, Report of the Bladder Research Progress Review Group, National Institute of Diabetes & Digestive & Kidney Diseases, National Institutes of Health, 2002.

[39] T.W. Hensle, S.M. Gilbert, A review of metabolic consequences and long-term complications of enterocystoplasty in children. Curr. Urol. Rep., 8 (2007) 157–162.

[40] G.C. Mingin, J.A. Stock, M.K. Hanna, Gastrocystoplasty: long-term complications in 22 patients. J. Urol., 162 (1999) 1122–1125.

[41] W.S. McDougal, Metabolic complications of urinary intestinal diversion, J Urol 147 (1992) 1199–1208.

[42] C. Adelöw, T. Segura, J.A. Hubbell, P. Frey, The effect of enzymatically degradable poly(ethylene glycol) hydrogels on smooth muscle cell phenotype. Biomaterials, 29 (2008) 314–326.

[43] T. Boland, T. Xu, B. Damon, X. Cui, Application of inkjet printing to tissue engineering. Biotechnol J 1 (2006) 910–917.

[44] T. Xu, C.A. Gregory, P. Molnar, X. Cui, S. Jalota, S.B. Bhaduri, T. Boland, Viability and electrophysiology of neural cell structures generated by the inkjet printing method. Biomaterials 27 (2006) 3580–3588.

[45] F. Xu, S.J. Moon, A.E. Emre, E.S. Turali, Y.S. Song, S.A. Hacking, J. Nagatomi, U. Demirci, A droplet-based building block approach for bladder smooth muscle cell (SMC) proliferation. Biofabrication 2 (2010) 014105.

[46] B.S. Kim, J. Nikolovski, J. Bonadio, D.J. Mooney, Cyclic mechanical strain regulates the development of engineered smooth muscle tissue. Nature Biotechnol. 17 (1999) 979–983.

[47] P.X. Ma, Scaffolds for tissue fabrication. Materials Today 7 (2004) 30–40.

[48] A.M. Turner, R. Subramaniam, D.F.M. Thomas, J. Southgate, in Tissue engineering using ceramics and polymers, Ed. A. R. Boccaccini and J. E. Gough (CRC Press, Boca Raton, 2007), p. 445.

[49] E.M. Engelhardt, L.A. Micol, S. Houis, F.M. Wurm, J. Hilborn, J.A. Hubbell, P. Frey, A collagen-poly(lactic acid-co-ε-caprolactone) hybrid scaffold for bladder tissue regeneration. Biomat. 32 (2011) 3969–3976.

[50] A. Remes, D.F. Williams, Immune response in biocompatibility. Biomat. 11 (1992) 731–743.

[51] K. Ceonzo, A. Gaynor, L. Shaffer, K. Kojima, C.A. Vacanti, G.L. Stahl. Polyglycolic acid-induced inflammation: role of hydrolysis and resulting complement activation. Tissue Eng. 12 (2006) 301–308.

[52] Y. Shiroyanagi, M. Yamato, Y. Yamazaki, H. Toma, T. Okano, Transplantable

Urothelial Cell Sheets Harvested Noninvasively from Temperature-Responsive Culture Surfaces by Reducing Temperature, Tissue Engineering 9 (2003) 1005–1012.

[53] Y. Shiroyanagi, M. Yamato, Y. Yamazaki, H. Toma, T. Okano, Urothelium regeneration using viable cultured urothelial cell sheets grafted on demucosalized gastric flaps, BJU Int. 93 (2004) 1069–1075.

[54] Z. Tang, Y. Akiyama, T. Okano, Temperature-Responsive Polymer Modified Surface for Cell Sheet Engineering. Polymers 4 (2012) 1478–1498.

[55] S. GuhaShakar, R. Banerjee, Intravesical drug delivery: Challenges, current status, opportunities and novel strategies. Journal of Controlled Release 148 (2010) 147–159.

[56] P. Tyagi, Z. Li, M. Chancellor, W.C. De Groat, N. Yoshimura, L. Huang, Sustained intravesical drug delivery using thermosensitive hydrogel. Pharm. Res. 21 (2004) 832–837.

[57] J.P. Chen, Y.L. Leu, C.L. Fang, C.H. Chen, J.Y. Fang, Thermosensitive hydrogels composed of hyaluronic acid and gelatin as carriers for the intravesical administration of cisplatin. J. Pharm. Sci. 100 (2011) 655–666.

[58] R.H. Schoenfeld, W.D. Belville, W.H. Jacob, A.S. Buck, M.L. Dresner, S.J. Insalaco, G.S. Ward, The effect of dimethyl sulfoxide on the uptake of cisplatin from the urinary bladder of the dog: a pilot study. J Am Osteopath Assoc 82 (1983) 570–573.

[59] B.A. Hadaschik, M.G. ter Borg, J. Jackson, R.D. Sowery, A.I. So, H.M. Burt, M.E. Gleave, Paclitaxel and cisplatin as intravesical agents against non-muscle-invasive bladder cancer. BJU Int 101 (2008) 1347–1355.

[60] S.L. Johansson, M. Fall, Clinical features and spectrum of light microscopic changes in interstitial cystitis. J. Urol. 143 (1990) 1118–1124.

[61] W.L. Lynes, S.D. Flynn, L.D. Shortliffe, T.A. Stamey, The histology of interstitial cystitis. Am. J. Surg. Pathol. 14 (1990) 969–976.

[62] C. H. Hsieh, W. C. Chang, M. C. Huang, T. H. Su, Y. T. Li, H. S. Chiang, Hydrodistention plus bladder training versus hydrodistention for the treatment of interstitial cystitis. Taiwanese Journal of Obstetrics & Gynecology 51 (2012). 591–595.

[63] A.C. Thompson, T.J. Christmas, Interstitial cystitis--an update. Br. J. Urol. 78 (1996) 813–820.

[64] J.J. Bade, M. Lasuer, A. Nieuwenburg, L.T. Van der Weele, H.J.A. Memsink, A placebo-controlled study of intravesical pentosanpolysulphate for the treatment of interstitial cystitis. Br. J. Urol. 79 (1997) 168–171.

[65] D. Porru, M. Cervigni, L. Nasta, F. Natale, R. Lo Voi, C. Tinelli, B. Gardella, A. Anghileri, A. Spinillo, B. Rovereto, Results of endovesical hyaluronic acid/chondroitin sulfate in the treatment of Interstitial Cystitis/Painful Bladder Syndrome. Rev Recent Clin Trials 3 (2008) 126–129.

[66] M. Cervigni, F. Natale, L. Nasta, A. Padoa, R. Lo Voi, D. Porru, A combined intravesical therapy with hyaluronic acid and chondroitin for refractory painful bladder syndrome/interstitial cystitis. Int Urogynecol J Pelvic Floor Dysfunct 19 (2008) 943–947.

[67] D. Porru, F. Leva, A. Parmigiani, D. Barletta, D. Choussos, B. Gardella, M. D. Dacco, R.E. Nappi, M. Allegri, C. Tinelli, C. M. Bianchi, A. Spinillo, B. Rovereto, Impact of intravesical hyaluronic acid and chondroitin sulfate on bladder pain syndrome/interstitial cystitis. Int. Urogynecol. J. 23 (2012) 1193–1199.

[68] S. Hunskaar, G. Lose, D. Sykes, S. Voss, The prevalence of urinary incontinence in women in four European countries. BJU Int, 93 (2004) 324–330.

[69] L.A. Kerr, Bulking agents in the treatment of stress urinary incontinence: history, outcomes, patient populations, and reimbursement profile. Rev. Urol., 7 (supp. 1) 2005 S3–S11.

[70] S. Mohr, M. Seigenthaler, M. Mueller, A. Kuhn, Bulking agents: an analysis of 500 cases and review of the literature. Int Urogynecol J 24 (2013) 241–247.

[71] N. Klarskov, G. Lose, Urethral injection therapy: What is the mechanism of action? Neurourology and Urodynamics 27 (2008) 789–792.

[72] J.P. Sumner, R.J. Hardie, J.N. Henningson, R. Drees, M.D. Markel, and D. Bjorling, Evaluation of Submucosally Injected Polyethylene Glycol-Based Hydrogel and Bovine Cross-Linked Collagen in the Canine Urethra using Cystoscopy, Magnetic Resonance Imaging and Histopathology. Veterinary Surgery 41 (2012) 655–663.

[73] H. Dolk, M. Loane, and E. Garne, The Prevalence of Congenital Anomalies in Europe. Adv Exp Med Biol, 686 (2010) 349–364.

[74] L.A. Micol, L.F.A. da Silva, P.J. Geutjes, E. Oosterwijk, J.A. Hubbell, W.F.J. Feitz, P. Frey, In-vivo performance of high-density collagen gel tubes for urethral regeneration in a rabbit model. Biomaterials, 33 (2012).

[75] W.T. Snodgrass, A. Lorenzo, Tubularized incised-plate urethroplasty for proximal hypospadias. BJU Int., 89 (2002).

[76] S.C. Gopal, A.N. Gangopadhyay, T.V. Mohan, V.D. Upadhyaya, A. Pandey, A. Upadhyaya, D.K. Gupta, Use of fibrin glue in preventing urethrocutaneous fistula after hypospadias repair. J. of Ped. Surg., 43 (2008) 1869–72.

[77] J. Hick, A.F. Morey, Initial experience with fibrin sealant in pendulous urethral reconstruction. Is early catheter removal possible? J. Urol., 171 (2004) 1547–9.

[78] G. Barbagli, S. De Stefani, M.C. Sighinolfi, Bulbar urethroplasty with dorsal onlay buccal mucosal graft and fibrin glue. Eur. Urol. 50 (2006) 467–474.

[79] K.D. Park, Y.S. Kim, D.K. Han, Y.H. Kim, E.H. Lee, H. Suh, K.S. Choi, Bacterial adhesion on PEG modified polyurethane surfaces. Biomaterials 19 (1998) 851–859.

[80] J.M. Schierholz, N. Yucel, A.F. Rump, J. Beuth, G. Pulverer, Antiinfective and encrustation-inhibiting materials--myth and facts. Int J Antimicrob Agents 19 (2002) 511–516.

[81] P.F. Keane, M.C. Bonner, S.R. Johnston, A. Zafar, S.P. Gorman, Characterization of biofilm and encrustation on ureteric stents in vivo. Br J Urol 73 (1994) 687–691.

[82] P. Francois, P. Vaudaux, N. Nurdin, H. J. Mathieu, P. Descouts, D.P. Lew, Physical and biological effects of a surface coating procedure on polyurethane catheters. Biomaterials 17 (1996) 667–678.

[83] S.H. Yang, Y.S. J. Lee, F.H. Lin, J.M. Yang, K.S. Chen, Chitosan/poly(vinyl alcohol) blending hydrogel coating improves the surface characteristics of segmented polyurethane urethral catheters. J. Biomed. Mat. Res. Part B 83B (2007) 304–313.

[84] G. Apodaca, E. Balestreire, L.A. Birder, The Uroepithelial-associated sensory web. Kidney International 72 (2007) 1057-1064.

[85] A. Atala, H. Hendren, S. Bauer, A. Retik. The effect of augmentation on bladder function. J Urol 149 (1993) 1099-1102.

[86] M. Kaefer, M. Tobin, H. Hendren et al. Continent urinary diversion: The Children's Hospital experience. J Urol 157 (1997) 1394-1399.

[87] M. Kaefer, H. Hendren, S. Bauer, et al. Reservoir calculi: a comparison of reservoirs constructed from stomach and other enteric segments. J Urol 160 (1998) 2187-2190.

[88] H. Hauner, P. Schmid, E.F. Pfeiffer, Glucocorticoids and insulin promote the differentiation of human adipocyte precursor cells into fat cells. J. Clin. Endocrinol. Metabol. 64 (1987) 832.

[89] A. Grigoradis, J.N.M. Heersche, J. Aubin, Differentiation of muscle fat, cartilage and bone from progenitor cells present in a bone-derived clonal cell population: effect of dexamethasone. J. Cell Biol. 106 (1988) 2139.

[90] S. Wakitani, T. Saito, A.I. Caplan, Myogenic cells derived from rat bone marrow mesenchymal stem cells exposed to 5-azacytidine. Muscle Nerve 18 (1995) 1417.

[91] G. Ferrari, G. Cusella-De Angelis, M. Coletta, E. Paolucci, A. Stornaiuolo, G. Cossu, F. Mavilio, Muscle regeneration by bone marrow-derived myogenic progenitors. Science 279 (1998) 1528.

[92] B. Johnstone, T.M. Hering, A.I. Caplan, V.M. Goldberg, J.U. Yoo, In vitro chondrogenesis of bone marrow-derived mesenchymal progenitor cells. Exp. Cell Res. 238 (1998) 265.

[93] M.F. Pittenger, A.M. Mackay, S.C. Beck, R.K. Jaiswal, R. Douglas, J.D. Mosca, M.A. Moorman, D.W. Simonetti, S. Craig, D.R. Marshak, Multilineage potential of adult human mesenchymal stem cells. Science 284 (1999) 143.

[94] P. Zuk, et al., Multilineage Cells from Human Adipose Tissue: Implications for Cell-Based Therapies. Tissue Engineering Vol. 7, No. 2 (2001) 211–228.

[95] P. Zuk, et al., Human Adipose Tissue is a Source of Multipotent Stem Cells. Molecular Biology of the Cell Vol. 13 (2002) 4279–4295.

[96] A.M. Rodriguez, et al. Transplantation of a multipotent cell population from human adipose tissue induces dystrophin expression in the immunocompetent mdx mouse. J. Exp. Med. 201 (2005) 1397–1405

[97] H. Mizuno, et al. Myogenic differentiation by human processed lipoaspirate cells. Plast. Reconstr. Surg. 109 (2002) 199–209.

[98] Bacou, F. et al. (2004) Transplantation of adipose tissue-derived stromal cells increases mass and functional capacity of damaged skeletal muscle. Cell Transplant. 13, 103–111.

[99] S. Rangappa, et al., Transformation of adult mesenchymal stem cells isolated from the fatty tissue into cardiomyocytes. Ann. Thorac. Surg. 75 (2003) 775–779.

[100] K.G. Gaustad, et al., Differentiation of human adipose tissue stem cells using extracts of rat cardiomyocytes. Biochem. Biophys. Res. Commun. 314 (2004) 420–427.

[101] V. Planat-Benard, et al. Spontaneous cardiomyocyte differentiation from adipose tissue stroma cells. Circ. Res. 94 (2004) 223–229.

[102] P.H. Ashjian, et al., In vitro differentiation of human processed lipoaspirate cells into early neural progenitors. Plast. Reconstr. Surg. 111 (2003) 1922–1931.

[103] S.K. Kang, et al., Improvement of neurological deficits by intracerebral transplantation of human adipose tissue-derived stromal cells after cerebral ischemia in rats. Exp. Neurol. 183 (2003) 355–366

[104] K.M. Safford, et al., Neurogenic differentiation of murine and human adipose-

derived stromal cells. Biochem. Biophys. Res. Commun. 294 (2002) 371–379.

[105] B. Cousin, et al., Reconstitution of lethally irradiated mice by cells isolated from adipose tissue. Biochem. Biophys. Res. Commun. 301 (2003) 1016–1022.

[106] A. Miranville, et al., Improvement of postnatal neovascularization by human adipose tissue-derived stem cells. Circulation 110 (2004) 349–355.

[107] M.J. Seo, et al., Differentiation of human adipose stromal cells into hepatic lineage in vitro and in vivo. Biochem. Biophys. Res. Commun. 328 (2005) 258–264.

[108] C.S. Lin, Z.C. Xin, Z. Wang, C. Deng, Y.C. Huang, G. Lin, T.F. Lue, Stem cell therapy for erectile dysfunction: a critical review. Stem Cells Dev 21 (2012) 343–351.

[109] C. S. Lin, T.F. Lue., Stem cell therapy for stress urinary incontinence: a critical review. Stem Cells Dev 21 (2012) 834–843.

[110] B. Puissant, et al. Immunomodulatory effect of human adipose tissue-derived adult stem cells: comparison with bone marrow mesenchymal stem cells. Br J Haematol 129 (2005) 118–129.

[111] S. Wolbank, et al., Dose-dependent immunomodulatory effect of human stem cells from amniotic membrane: a comparison with human mesenchymal stem cells from adipose tissue. Tissue Eng 13 (2007) 1173–1183.

[112] L. Cui, S. Yin, W. Liu, N. Li, W. Zhang Y. Cao, Expanded adipose-derived stem cells suppress mixed lymphocyte reaction by secretion of prostaglandin E2. Tissue Eng 13 (2007) 1185–1195.

[113] J.W. Kang, K.S. Kang, H.C. Koo, J.R. Park, E.W. Choi and Y.H. Park. Soluble factors-mediated immunomodulatory effects of canine adipose tissue-derived mesenchymal stem cells. Stem Cells Dev 17 (2008) 681–693.

[114] M. Najar, et al., Mesenchymal stromal cells use PGE2 to modulate activation and proliferation of lymphocyte subsets: Combined comparison of adipose tissue, Wharton's Jelly and bone marrow sources. Cell Immunol 264 (2010) 171–179.

[115] R. Yanez, A. Oviedo, M. Aldea, J.A. Bueren, M.L. Lamana. Prostaglandin E2 plays a key role in the immuno-suppressive properties of adipose and bone marrow tissue-derived mesenchymal stromal cells. Exp Cell Res 316 (2010) 3109–3123.

[116] V. Paunescu, E. Deak, D. Herman, I.R. Siska, G. Tanasie, C. Bunu, S. Anghel, C.A. Tatu, T.I. Oprea, R. Henschler, B. Ruster, R. Bistrian, E. Seifried, In vitro differentiation of human mesenchymal stem cells to epithelial lineage. J Cell Mol Med 11 (2007) 502.

[117] B.V. Popov, V.B. Serikov, N.S. Petrov, T.V. Izusova, N. Gupta, M.A. Matthay, Lung epithelial cells induce endodermal differentiation in mouse mesenchymal bone marrow stem cells by paracrine mechanism. Tissue Eng 13 (2007) 2441.

[118] S. Gu, C. Xing, J. Han, M.O. Tso, J. Hong, Differentiation of rabbit bone marrow mesenchymal stem cells into corneal epithelial cells in vivo and ex vivo. Mol Vis 15 (2009) 99.

[119] K. Ma, F. Laco, S. Ramakrishna, S. Liao, C.K. Chan, Differentiation of bone marrow-derived mesenchymal stem cells into multi-layered epidermis-like cells in 3D organotypic coculture. Biomaterials 30 (2009) 3251.

[120] H. Gronemeyer, R. Miturski, Molecular mechanisms of retinoid action, Cellular and Molecular Biology Letters 6 (2001) 3–52.

[121] M. Brzoska, H. Geiger, S. Gauer, P. Baer, Epithelial differentiation of human adipose tissue-derived adult stem cells. Biochem Biophys Res Commun 330 (2005) 42.

[122] J.L. Long, P. Zuk, G.S. Berke, D.K. Chhetri, Epithelial differentiation of adipose-derived stem cells for laryngeal tissue engineering. Laryngoscope 120 (2010) 125.

[123] T.A. Beyer, S. Werner, C. Dickson, R. Grose, Fibroblast growth factor 22 and its potential role during skin development and repair. Exp Cell Res 287 (2003) 228.

[124] P. Castagnino, M.V. Lorenzi, J. Yeh, D. Breckenridge, H. Sakata, B. Munz, S. Werner, D.P. Bottaro, Neudifferentiation factor/heregulin induction by hepatocyte and keratinocyte growth factors. Oncogene 19 (2000) 640.

[125] Fujiyama, C., Masaki, Z., and Sugihara, H. Reconstruction of the urinary bladder mucosa in three-dimensional colla- gen gel culture: Fibroblast–extracellular matrix interactions on the differentiation of transitional epithelial cells. J. Urol. 153 (1995) 2060.

[126] Sugasi, S., Lesbros, Y., Bisson, I., Zhang, Y.Y., Kucera, P., and Frey, P. In vitro engineering of human stratified urothelium: Analysis of its morphology and function. J. Urol. 164 (2000) 951.

[127] Tash, J.A., David, S.G., Vaughan, E.E., and Herzlinger, D.A. Fibroblast growth factor-7 regulates stratification of the bladder urothelium. J. Urol. 166 (2001) 2536.

[128] K. Matter, M.S. Balda, Functional analysis of tight junctions. Methods 30 (2003) 228–234.

[129] A. Hoffmann, J. Bredno, M. Wendland, N. Derugin, P. Ohara, M. Wintermark, High and Low Molecular Weight Fluorescein Isothiocyanate (FITC)–Dextrans to Assess Blood-Brain Barrier Disruption: Technical Considerations. Trans. Stroke Res. 2 (2011)

106–111.

[130] D. Janssen, X. van Wijk, K. Jansen, T. van Kuppevelt, J. Heesakkers, J. Schalken, The Distribution and Function of Chondroitin Sulfate and Other Sulfated Glycosaminoglycans in the Human Bladder and Their Contribution to the Protective Bladder Barrier. J. Urol. 189 (2013) 336–342.

[131] A. Matsuzawa, M. Matsusaki, M. Akashi, Effectiveness of Nanometer-Sized Extracellular Matrix Layer-by-Layer Assembled Films for a Cell Membrane Coating Protecting Cells from Physical Stress. Langmuir 29 (2013) 7362–7368.

[132] K.Y. Lee, D.J. Mooney, Hydrogels for tissue engineering. Chem Rev 101 (2001) 1869–1879.

[133] R.O. Hynes, Fibronectins; Springer-Verlag: New York, 1990.

[134] K. Kadowaki, M. Matsusaki, M. Akashi, Control of Cell Surface and Functions by Layer-by-Layer Nanofilms. Langmuir 26 (2010) 5670−5678.

[135] K. Kadowaki, M. Matsusaki, M. Akashi, Three-Dimensional Constructs Induce High Cellular Activity: Structural Stability and the Specific Production of Proteins and Cytokines. Biochem. Biophys. Res. Commun. 402 (2010) 153−157.

[136] J. Ning, C. Li, H. Li, J. Chang, Bone marrow mesenchymal stem cells differentiate into urothelial cells and the implications for reconstructing urinary bladder mucosa, Cytotechnology 63 (2011) 531-539.

[137] J. Liu, J. Huang, T. Lin, C. Zhang, X. Yin, Cell-to-cell contact induces human adipose tissue-derived stromal cells to differentiate into urothelium-like cells in vitro, Biochem. Biophys. Res. Commun. 390 (2009) 931-936.

[138] J.G. Shi, W.J. Fu, X.X. Wang, Y.D. Xu, G. Li, B.F. Hong, K. Hu, F.Z. Cui, Y. Wang, X. Zhang, Transdifferentiation of human adipose-derived stem cells into urothelial cells: potential for urinary tract tissue engineering, Cell. Tiss. Res. 347 (2012) 737-746.

[139] M. Zhang, Y. Peng, Z. Zhou, J. Zhou, Z. Wang, M. Lu, Differentiation of Human Adipose-derived Stem Cells Co-cultured With Urothelium Cell Line Toward a Urothelium-like Phenotype in a Nude Murine Model, Urology 81 (2013) 465.e15-465.e22.

[140] Oberpenning, F., Meng, J., Yoo, J.J., Atala, A. De novo reconstitution of a functional mammalian urinary bladder by tissue engineering, Nat. Biotechnol. 17 (1999) 149–155.

[141] W. Kim, Cellular signaling in tissue regeneration. Yonsei Med. J. 41 (2000) 692–

703.

[142] K. Yabroff, C. Bradley, A. Mariotto, M. Brown, E. Feuer, Estimates and projections of value of life lost from cancer deaths in the United States, J Natl Cancer Inst 100 (2008) 1755–62.

[143] D. Wood, J. Southgate, Current status of tissue engineering in urology, Curr. Opin. Urol. 18 (2008) 564–569.

[144] K. Sievert, B. Amend, A. Stenzl, Tissue Engineering for the Lower Urinary Tract: A Review of a State of the Art Approach, Eur. Uro. 52 (2007) 1580–1589.

[145] A. Atala, Tissue engineering of human bladder, Br. Med. Bull. 97 (2011) 81–104.

[146] Pariente JL, Kim BS, Atala A. In vitro biocompatibility assessment of naturally derived and synthetic biomaterials using normal human urothelial cells. J Biomed Mater Res 2001;55:33 – 9.

[147] D. Eberli, J.J. Yoo, A. Atala, A novel composite scaffold promotes the formation of normal bladder tissue, Urologe A 46 (2007) S32.

[148] A.K. Sharma, P.V. Hota, D.J. Matoka, N.J. Fuller, D. Jandali, H. Thaker, G.A. Ameer, E.Y. Cheng, Urinary bladder smooth muscle regeneration utilizing bone marrow derived mesenchymal stem cell seeded elastomeric poly(1,8-octanediol-co-citrate) based thin films, Biomaterials 31 (24) (2010) 6207–62178 Epub 2010 May 21.

[149] Y. Xu, W. Fu, G. Li, J. Shi, H. Tan, K. Hu, F. Cui, Q. Lin, X. Zhang, Autologous urothelial cells transplantation onto a prefabricated capsular stent for tissue engineered ureteral reconstruction, J. Mater. Sci: Mater. Med. 23 (2012) 1119–1128.

[150] J. Seibold, C. Selent, G. Feil, J. Wiedemann, D. Colleselli, J. Mundhenk, G. Gakis, K.D. Sievert, C. Schwentner, A. Stenzl, Development of a porcine animal model for urethral stricture repair using autologous urothelial cells, J. Ped. Uro. 8 (2012) 194–200.

[151] H. Orabi, T. AbouShwareb, Y. Zhang, J. J. Yoo, A. Atala, Cell-Seeded Tubularized Scaffolds for Reconstruction of Long Urethral Defects: A Preclinical Study, Eur. Uro. 63 (2013) 531–538.

[152] T. Drewa, J. Adamowicz, A. Sharma, Tissue engineering for the oncologic urinary bladder, Nat. Rev. Urol. 9 (2012) 561–572.

[153] P. Zuk, M. Zhu, P. Ashjian, D. A. De Ugarte, J. Huang, H. Mizuno, Z. Alfonso, J. Fraser,‡ P. Benhaim, and M Hedrick, Human Adipose Tissue Is a Source of Multipotent Stem Cells, Mol. Bio. Cell 13 (2002) 4279-95.

[154] J. Fraser, I. Wulur, Z. Alfonso and M. Hedrick, Fat tissue: an underappreciated

source of stem cells for biotechnology, Trends in Biotech. 24 (2006) 150-154.

[155] C.S. Lin, G. Lin, and T.F. Lue, Allogeneic and Xenogeneic Transplantation of Adipose-Derived Stem Cells in Immunocompetent Recipients Without Immunosuppressants, Stem Cells and Dev. 21 (2012) 2770-2778.

[156] J. van der Valk, D. Brunner, K. De Smet, A. Fex Svenningsen, P. Honegger, L.E. Knudsen, T. Lindl, J. Noraberg, A. Price, M.L. Scarino, G. Gstraunthaler, Optimization of chemically defined cell culture media – Replacing fetal bovine serum in mammalian in vitro methods, Toxicology in Vitro 24 (2010) 1053–1063.

[157] U. Nagele, S. Maurer, G. Feil, C. Bock, J. Krug, K.D. Sievert, A. Stenzl, In vitro investigations of tissue-engineered multilayered urothelium established from bladder washings, Eur. Urol. 54 (2008), 1414–1422.

[158] G. Feil, S. Maurer, U. Nagele, J. Krug, C. Bock, K.D. Sievert, A. Stenzl, Immunoreactivity of p63 in monolayered and in vitro stratified human urothelial cell cultures compared with native urothelial tissue, Eur. Urol. 53 (2008) 1066–1073.

[159] N. Sangha, Isolation of urothelial cells from bladder tissue, Met. Mol. Biol. 1001 (2013) 21–33.

[160] S. Sivaraman, R. Ostendorff, B. Fleishmann, J. Nagatomi, Tetronic((R))-based composite hydrogel scaffolds seeded with rat bladder smooth muscle cells for urinary bladder tissue engineering applications, J. Biomat. Sci. Polymer 26 (2015) 196-210.

[161] P. Veranic, K. Jezernik, The cytokeratins of urinary bladder epithelial cells. *Asian J Cell Biol* 1 (2006) 1–8.

[162] R. Romih, K. Jezernik, A. Masera, Uroplakins and cytokeratins in the regenerating rat urothelium after sodium saccharin treatment, Histochem Cell Biol 109 (1998) 263–269.

[163] X. Wu, X. Kong, A. Pellicer, G. Kreibich, T.T. Sun, Uroplakins in urothelial biology, function and disease, Kidney Int. 75 (2009) 1153-1165.

[164] J. Olsburgh, P. Harnden, R. Weeks, B. Smith, A. Joyce, G. Hall, R. Poulsom, P. Selby, J. Southgate, Uroplakin gene expression in normal human tissues and locally advanced bladder cancer, J. Pathol 199 (2003) 41-49.

[165] L.M. De Luca, Retinoids and their receptors in differentiation, embryogenesis, and neoplasia, FASEB 5 (1991) 2924-2933.

[166] C. Metallo, L. Ji, J. De Pablo, S. Palecek, Retinoic acid and bone morphogenetic protein signaling synergize to efficiently direct epithelial differentiation of human

embryonic stem cells, Stem Cells 26 (2008) 372-380.

[167] R. Romih, P. Veranic, K. Jezernik, Actin filaments during terminal differentiation of urothelial cells in the rat urinary bladder, Histochem Cell Biol 112 (1999) 375-380.

[168] H. Oda, T. Konno, K. Ishihara, The use of the mechanical microenvironment of phospholipid polymer hydrogels to control cell behavior, Biomaterials 34 (2013) 5891–5896.

[169] A. Atala, S.B. Bauer, S. Soker, et al., Tissue-engineered autologous bladders for patients needing cystoplasty, Lancet 367 (2006) 1241–6.

[170] T. Roby, S. Olsen, J. Nagatomi, Effect of sustained tension on bladder smooth muscle cells in three-dimensional culture. Ann Biomed Eng. 36 (2008) 1744-51.

[171] T. Mochizuki et al., The TRPV4 Cation Channel Mediates Stretch-evoked Ca2+ Influx and ATP Release in Primary Urothelial Cell Cultures, J. Bio. Chem. 284 (2009) 21257-21264.

[172] S. Sivaraman, R. Ostendorff, B. Fleishman, J. Nagatomi, Tetronic®-based composite hydrogel scaffolds seeded with rat bladder smooth muscle cells for urinary bladder tissue engineering applications, J. Biomat. Sci., Polymer Edition. 26 (2015) 196-210.

[173] E. Seltzer, M. Tillinger, M.J. Jayo, T.A. Bertram, Role of biomechanical stimulation (cycling) in neo-bladder regeneration-translational basis for clinical outcomes, J Urol 181 (2009) 282

[174] S. Korossis, F. Bolland, E. Ingham, J. Fisher, J. Kearney, J. Southgate, Tissue Engineering of the Urinary Bladder: Considering Structure-Function Relationships and the Role of Mechanotransduction, Tissue Engineering 12 (2006) 635-644.

[175] S. Sivaraman, Investigating Polymer based Scaffolds for Urinary Bladder Tissue Engineering, All Dissertations (2015) Clemson University.

[176] S.E. Dahms, H.J. Piechota, R. Dahiya, T.F. Lue, E.A. Tanagho, Composition and biomechanical properties of the bladder acellular matrix graft: comparative analysis in rat, pig and human, Br J Urol. 82 (1998) 411-419.

[177] D.L. Butler, S.A. Goldstein, R.E. Guldberg, X.E. Guo, R. Kamm, C.T. Laurencin, L.V. McIntire, V.C. Mow, R.M. Nerem, R.L. Sah, L.J. Soslowsky, R.L. Spilker, and R.T. Tranquillo, The Impact of Biomechanics in Tissue Engineering and Regenerative Medicine, Tissue Engineering Part B: Reviews 15 (2009) 477-484.

[178] P.A. Janmey, C.A. McCulloch, Cell mechanics: integrating cell responses to

mechanical stimuli, Annu Rev Biomed Eng 9 (2007) 1-34.

[179] H. Li, Y. Xu, Q. Fu, C. Li, Effects of Multiple Agents on Epithelial Differentiation of Rabbit Adipose-Derived Stem Cells in 3D Culture, Tis. Eng. Part A 18 (2012) 1760–1770.